LIQUID PHASE SINTERING OF T15 AND T42 GRADE HIGH SPEED STEEL COMPOSITES CONTAINNING TiB_2 OR Ti(C,N) PARTICLES

by

BHASKAR PRASAD SAHA

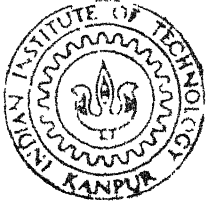

DEPARTMENT OF METALLURGICAL ENGINEERING
INDIAN INSTITUTE OF TECHNOLOGY KANPUR
September, 1991

LIQUID PHASE SINTERING OF T15 AND T42 GRADE HIGH SPEED STEEL COMPOSITES CONTAINNING TiB_2 OR Ti(C,N) PARTICLES

A Thesis Submitted
in Partial Fulfilment of the Requirements
for the Degree of

MASTER OF TECHNOLOGY

by

BHASKAR PRASAD SAHA

to the

DEPARTMENT OF METALLURGICAL ENGINEERING
INDIAN INSTITUTE OF TECHNOLOGY KANPUR
September, 1991

CERTIFICATE

It is certified that the work contained in the thesis entitled "LIQUID PHASE SINTERING OF T15 AND T42 GRADE HIGH SPEED STEEL COMPOSITES CONTAINING TiB_2 OR Ti(C,N) PARTICLES", by Mr. Bhasker Prasad Saha, has been carried out under my supervision and that this work has not been submitted elsewhere for a degree.

6th Sept 1991

SEPTEMBER, 1991

G. S. UPADHYAYA
Professor
Department of Metallurgical Engineering
Indian Institute of Technology
Kanpur, India

To

My Parents

ACKNOWLEDGEMENTS

I am very pleased to acknowledge with gratitude the generous help, invaluable guidance and constant inspiration at every stage tendered to me by Prof. G.S. Upadhyaya throughout the course of this work.

I specially thank M/s S.C. Soni and K.P. Mukherjee for their help and cooperation in the experimental work.

I express my appreciation to all my research colleagues, namely, Pradipta, Subir, Hamid and Prasanta who were ever-ready to help and made the working in the Powder Metallurgy Laboratory a pleasure.

I am thankful to the management of M/s British India Steels, Ahmedabad, India for allowing me to utilize some of their facilities and to their staff for extending all the help and cooperation.

I am also thankful to the Head, ACMS for allowing me to utilize some of their laboratory facilities in ACMS.

Finally, I congratulate M/s R.N. Srivastava and A.K. Ganguly for excellent typing and tracing work respectively.

- B.P. Saha

TABLE OF CONTENTS

			Page
LIST OF TABLES			vii
LIST OF FIGURES			viii
ABSTRACT			xi
CHAPTER I	LITERATURE REVIEW		1
I.1.	Introduction		1
I.2.	Various P/M Routes of HSS Production		5
I.3.	Liquid Phase Sintered HSS and Their Properties		7
	I.3.1.	Supersolidus Sintering of HSS	7
	I.3.2.	Phase Diagram Characteristics	10
	I.3.3.	The Effect of Processing Variables	11
	I.3.4.	Mechanical Properties of Liquid Phase Sintered HSS	22
I.4.	HSS Based Particulate Composite through P/M Route		24
I.5.	Scope of the Present Investigation		29
CHAPTER II	EXPERIMENTAL PROCEDURE		31
II.1.	Powders and Their Characteristics		31
II.2.	Powder Mix Preparation and Room Temperature Compaction		33
II.3.	Sintering		34
	II.3.1.	Sintered Density Measurement	35
II.4.	Heat Treatment		35
	II.4.1.	Determination of Critical Temperature for Heat Treatment	36

II.4.2. Hardening 37

II.4.3. Tempering 37

II.5. Mechanical Tests 37

II.5.1. Hardness 37

II.5.2. Transverse Rupture Strength 38

II.6. Microstructural Studies 38

II.6.1. Qualitative Optical Metallography 39

II.6.2. SEM, EDX and X-ray Mapping Studies 39

CHAPTER III EXPERIMENTAL RESULTS 40

III.1. T15 and T42 Grade HSS Sintered in Vacuum 40

III.1.1. Densification 40

III.1.2. Critical Temperature for Transformation Annealing 40

III.1.3. Hardness 43

III.1.4. Transverse Rupture Strength 45

III.1.5. Microstructural Analysis 45

III.2. HSS Composites Containing TiB_2 53

III.2.1. Densification 53

III.2.1A. Densification Behaviour of Vacuum Sintered HSS Composites Containing TiB_2 53

III.2.1B. Densification Behaviour of T15 HSS Composites Containing TiB_2 Sintered in Hydrogen at 1210°C 54

III.2.2. Hardness 59

III.2.3. Microstructural Analysis 63

III.3. HSS Composites Containing Ti(C,N) 67

III.3.1. Densification 67

III.3.2. Hardness 74

III.3.3. Transverse Rupture Strength 77

III.3.4. Microstructural Analysis 80

CHAPTER IV DISCUSSION 88

IV.1. Introduction 88

IV.2. T15 and T42 Grade HSS 91

IV.2.1. Densification 91

IV.2.2. Heat Treatment, Mechanical Properties and Microstructural Aspects 93

IV.3. TiB_2 Containing Composites 98

IV.3.1. Densification 98

IV.3.2. Mechanical Properties and Microstructural Aspects 100

IV.4. Ti(C,N) Containing Composites 101

IV.4.1. Densification 101

IV.4.2. Mechanical Properties and Microstructural Aspects 102

CHAPTER V CONCLUSIONS 106

REFERENCES 108

LIST OF TABLES

Number	Title	Page
I.1.	Mechanical properties of HSS processed through direct sintering route	25
I.2.	Hardness and melting temperature of various refractory compounds as candidate additives to HSS	28
III.1.	EDX analysis of various phases in T15 and T42 HSS	49
III.2.	EDX analysis of various phases in T15-2TiB_2 and T15-8TiB_2 composites	66
III.3.	EDX analysis of various phases in T15 and T42 HSS and their 6 mass % Ti(C,N) containing composites	84

LIST OF FIGURES

Number	Title	Page
1.1.	Phase diagram of Fe-W-Cr-C system at W = 18%, Cr = 4%, showing the region with liquid phase and the supersolidus sintering temperature range	12
1.2.	Density and green strength of different sized fractions of water atomised and annealed M2 HSS	14
1.3.	Sintering response of high speed steels (schematic)	19
1.4.	Microstructure of as-sintered P/M HSS (schematic)	23
3.1.	Effect of sintering temperature on properties of T15 HSS (a) sintered density (b) Vickers hardness	41
3.2.	Effect of sintering temperature on (a) sintered density and (b) sintered hardness of T42 HSS	42
3.3.	Critical temperature for transformation annealing as determined from DTA	44
3.4.	Optical and SEM microstructures of as-sintered and triple tempered T15 and T42 HSS	47
3.5.	SEM microstructures of triple tempered T15 and T42 HSS showing different phases	48
3.6.	SEM fractographs of T15 and T42 HSS in triple tempered condition	50
3.7.	X-ray mapping analysis of vacuum sintered and triple tempered T15 HSS	51
3.8.	X-ray mapping analysis of vacuum sintered and triple tempered T42 HSS	52
3.9.	Effect of TiB_2 addition on (a) density, (b) total porosity and (c) Vickers hardness of T15 HSS vacuum sintered at different temperatures	55
3.10.	Effect of sintering temperature on % theoretical density of vacuum sintered T42-TiB_2 composites	56

3.11.	Total porosity variation of vacuum sintered T42-TiB_2 composites with respect to sintering temperatures	57
3.12.	Effect of TiB_2 addition on (a) % theoretical density and (b) total porosity of hydrogen sintered T15 HSS (sintered at 1210°C for 1.5 hrs)	58
3.13.	Effect of sintering temperature on Vickers hardness of T42-TiB_2 composites	60
3.14.	Vickers hardness variation of T15-TiB_2 composites sintered in hydrogen at 1210°C for 1.5 hrs	61
3.15.	Variation of (a) total porosity and (b) Vickers hardness of T15-TiB_2 composites sintered in vacuum at 1220°C for 1.5 hrs	62
3.16.	Optical microstructures of vacuum sintered T15-TiB_2 composites	64
3.17.	Optical microstructures of vacuum sintered T42-TiB_2 composites in as-sintered condition	65
3.18.	Optical and SEM microstructures of hydrogen sintered T15-TiB_2 composites	68
3.19.	X-ray mapping analysis of triple tempered T15-2TiB_2 composite (hydrogen sintered at 1210°C)	69
3.20.	X-ray mapping analysis of triple tempered T15-8TiB_2 composite (hydrogen sintered at 1210°C)	70
3.21.	Sintered density variation of T15-Ti(C,N) composites hydrogen sintered at different temperatures	71
3.22.	Effect of Ti(C,N) addition on (a) sintered density and (b) optimum sintering temperature to achieve full density for hydrogen sintered T15 HSS	72
3.23.	Sintered density variation of T42-Ti(C,N) composites hydrogen sintered at different temperatures	73
3.24.	Effect of Ti(C,N) addition on (a) sintered density and (b) optimum sintering temperature to achieve full density for hydrogen sintered T42 HSS	75
3.25.	Effect of Ti(C,N) addition on Vickers hardness of T15 HSS after hydrogen sintering and various heat treatments	76

3.26. Effect of Ti(C,N) addition on Vickers hardness of T42 HSS after hydrogen sintering and various heat treatments 78

3.27. Effect of Ti(C,N) addition on triple tempered TRS after hydrogen sintering (a) T15 HSS and its Ti(C,N) containing composites (b) T42 HSS and its Ti(C,N) containing composites 79

3.28. SEM microstructures of T15 and T42 HSS in sintered and heat treated conditions 81

3.29. SEM microstructures of T15-6Ti(C,N) composite in sintered and heat treated conditions 82

3.30. SEM microstructures of T42-6Ti(C,N) composite in sintered and heat treated conditions 83

3.31. X-ray mapping analysis of hydrogen sintered and triple tempered T15-6Ti(C,N) composite 86

3.32. SEM fractographs of T15 and T42 HSS and their 6 mass % Ti(C,N) containing composites 87

ABSTRACT

In the present investigation liquid phase sintering of T15 and T42 grade High Speed Steels (HSS) and their composites containing TiB_2 or Ti(C,N) has been studied. Compacts with different mass fractions of refractory TiB_2 and Ti(C,N) (0-8%) were prepared by blending their respective proportions with the water atomised HSS powder followed by cold compacting. Compacts were then sintered in vacuum and hydrogen atmosphere. Sintered pellets were then subjected to heat treatment operations viz. annealing, hardening and tempering. Characterization of sintered as well as tempered HSS consisted of measurement of sintered density, Vickers hardness and TRS. Microstructural study and analysis were performed using both optical microscope and SEM. It was seen that temperature required to achieve full density for vacuum sintered T15 or T42 HSS was higher than that required for hydrogen sintering, the highest being in case of vacuum sintered T15 HSS. Hardness was found to be maximum after triple tempered condition. Optimum sintering temperature was found to increase with the increase in the amount of refractory compounds in the composites. TiB_2 containing composites showed lower hardness value than its straight grade as it decomposed at the sintering temperature. Ti(C,N) containing composites

showed higher hardness values as compared to the respective straight grades. The triple tempered TRS of T15 HSS was higher than the sintered one, whereas the reverse was true in case of T42 HSS. Triple tempered TRS was found to increase with the increase in Ti(C,N) content in T15 HSS whereas the reverse was true in case of T42 HSS.

CHAPTER I

LITERATURE REVIEW

I.1. INTRODUCTION:

High speed steels (HSS) have been known for about a century, during which time there have been many developments to keep pace with increasing demands on properties and with advances in basic metallurgical understanding. These are amongst the most important engineering materials in todays life. It takes its name from its capacity to retain a high level of hardness while cutting metals at high speed. It is also appropriately named in view of more recent applications such as bearings for aircraft jet engines and for space vehicle components besides for cutting, shaping, forming and blanking of materials at either ordinary or elevated temperature. In either event the important factor is that the steel can be hardened to a level upto 1000 HV and that no appreciable softening takes place until about a temperature range of 500-600^{o}C is reached [1].

Despite the inroads made by competitive cutting tool materials such as cast cobalt alloys, cemented carbides, ceramics and cermets, HSS tools have continued to be of importance in industry for about a century. The superior toughness combined with high hardness of HSS guarantees its place as a cutting tool material [2, 3].

High speed steels are a range of highly alloyed steels which have been developed to possess a desirable blend of the following properties [4]: (a) High hot-hardness, (b) wear resistance and (c) toughness. These properties are best achieved by an alloy consisting of uniform dispersion of fine, hard stable particles, such as carbides in a tough matrix. In HSS, this has been achieved by alloying with high carbon steels with several of the elements W, Mo, Cr, V, Co to give a dispersion of hard alloy carbides in a relatively tough tempered alloy martensitic matrix [5, 6].

HSS can be classified in to three basic groups such as: (1) Tungsten HSS, (2) Molybdenum HSS and (3) Tungsten-Molybdenum HSS. The earliest composition of HSS, T1 (18% W, 4% Cr, 1% V) is still in use since 1900. Vanadium content in HSS was increased for improving wear resistance but it was limited to 5% owing to the difficulty in hot working. To get the full benefit of the vanadium addition the carbon content was correspondingly increased. For improving the red-hardness and secondary hardening characteristics cobalt was added to the basic T1 grade during the first world war period. But the increased addition of cobalt to HSS results in the strengthening of the matrix which impairs the hot workability in ingot metallurgy products [1, 45]. Since cobalt has less diffusivity it is very difficult to produce high Co content HSS through casting which calls for the use of powder metallurgy technique where diffusion distance is very less.

Due to the scarcity of tungsten and also from economic point of view, it was found that molybdenum could be used in addition to or in place of tungsten in HSS. In comparing tungsten and molybdenum high speed steels, it is well known fact that, Mo having approximately one half the atomic weight of tungsten, supplies about twice as many atoms of alloying element to the steel when added in equal weight percentage. Because molybdenum and tungsten atoms have similar atomic radii and form similar carbides in HSS, replacement of 1.6 to 2% W with only 1% (by weight) has resulted in a marked similarity in structure and properties [3, 7].

In addition to the selection of the best chemical composition, optimum heat treatment is important to achieve the required end properties. Annealing is the first step in heat treatment. This operation is necessary in many respects. Because of air hardening properties of the steels, HSS is almost inevitably found in a hard condition when cooled to room temperature from the previous manufacturing step. Internal stresses may be high, and the ductility of HSS in as sintered condition is very low: thus relief of these stresses is important before additional stresses are imposed by any means. Annealing is also necessary to facilitate further processing, particularly the final machining if required, during the processing cycle.

A further feature is that annealing before a hardening operation, particularly if the specimen has already been hardened, is necessary in order to provide austenitic grain size in the hardened sample. Without such annealing, excessive grain growth can occur to give the so called "fish scale" fracture. During the process of austenitization, the carbides get progressively [1, 8] dissolved into austenite. Therefore, the hardened HSS contains highly alloyed retained austenite (15-30%) and undissolved M_6C and MC carbides (5-15%). The steel in this condition is hard, highly stressed, brittle and dimensionally unstable [1, 5, 9, 10]. During multiple tempering, the room temperature as well as red-hardness is further enhanced due to the transformation of the retained austenite to martensite and secondary hardening due to the precipitation of very fine, stable alloy carbides in the martensite. Techniques for hardening and tempering have been refined considerably over the years to counteract the problems of decarburisation during austenitizing, distortion during quenching and the uniformity of hardening response throughout the cross section. Vacuum heat treatment is the recent advancement in the HSS tool manufacture [42, 43].

P/M technique for the production of HSS overcomes the problem those arise in conventional HSS production method. Grain growth and carbide banding are always encountered in conventional HSS structures. The segregation of hard, brittle carbide regions in final large tool steel

sections results in undesirable characteristics which affect the performance of tools both directly and indirectly. Therefore the powder metallurgy (P/M) processing of HSS was developed commercially since seventies. P/M route provides a means of making new alloys and composites of tool steels which cannot be made by conventional melting, casting and hot extrusion methods. In addition to providing a method for making new alloys, the P/M process provides a means of significantly improving the properties of existing tool steels. The other advantages of P/M processed products over their conventionally produced counterparts are [3, 10-12, 21, 22]:

- Superior grindability in the hardened condition
- Improved toughness of tools in service
- Isotropic mechanical properties
- Faster response to hardening treatment
- More uniform size change as a result of hardening heat treatment
- Greater cross-sectional uniformity of hardness
- Near net-shape processing requiring minimal finishing operations for making finished tools
- Greater metal yield from the melt.

1.2. VARIOUS P/M ROUTES OF HSS PRODUCTION:

The problems encountered in the earlier premix route for the manufacture of HSS by P/M technique were compaction and homogenisation difficulties. These were

overcomed by using prealloyed powder. There are various commercial methods for manufacture of P/M HSS, the main intention of which is to produce a fully dense material with a fine and uniform microstructure giving performance equal or superior to conventional HSS [12]. P/M steels are much better than conventional steels on large sections in higher alloys.

Following are the methods for manufacture of P/M HSS:

1. Hot isostatic pressing (HIP) of gas atomised powders.
2. The P/M extrusion process.
3. Powder forging/sinter hot work.
4. P/M nearnet shape processing.
5. Sinter HIP.
6. CAP (consolidation by atomospheric pressure) process.

In the HIP process though 100% dense compact is obtained but because of its high process cost it could take a relatively small share of the HSS market. HIP route is best suited for the production of large sections [13]. Powder forging/ sinter hot work process consist of sintering followed by forging or rolling which calls for a higher cost of tooling for both cold compaction and hot working. P/M near net shape processing consist of pressing the annealed water atomised powder having good compressibility into parts followed by super solidus sintering. 100% theoretical density can be achieved by this technique. However this process is limited to parts which may be die pressed and

are hence required in large numbers. Post sinter hipping in sinter hip process gives finer and more uniform carbide distribution with no residual porosity. These products are required in aerospace industry where reliability of the product is important than its cost effectiveness. Main shaft bearings for aero-gas turbine engines is one of the example of this type of products [14, 15, 17]. In CAP process densification occurs due to combine effect of chemical treatment which enhances diffusion operation and isostatic atmospheric pressure. The primary advantage of this process is its economy [16].

I.3. LIQUID PHASE SINTERED HSS AND THEIR PROPERTIES:

The most critical step in the P/M production of near-net shape HSS parts is the liquid phase sintering. Achievement or full density (>98% Th.) during the sintering process is very important from the technological as well as economic point of view [11].

I.3.1. Super Solidus Sintering of HSS:

The liquid phase sintering of HSS pertains to super solidus category where solid and liquid phases have similar composition. Sintering is generally very rapid in the presence of a liquid phase. It has been estimated that 70% by weight and 90% by value of sintered metallic products are made using some form of liquid phase sintering [17]. In super solidus liquid phase sintering (SLPS) a prealloyed

powder which is heated to a temperature between the liquidus and solidus to attain partial melting. At a temperature intermediate between the liquidus and solidus for the alloy, the particles form a liquid phase at the grain boundaries that causes them to become mushy. Densification occurs by capilary induced rearrangement and solution-reprecipitation in the partially liquid particles. The sintering temperature and alloy composition are the most important process variables since these dictate the volume fraction of liquid.

The concept of SLPS was first introduced by Lund [18] who tried to sinter a loose powder mass of Fe containing 0.95% carbon. He has shown that if the amount of liquid present is restricted by temperature, the porosity remaining between powder clusters would be continuous. Under these conditions, an increase in sintering time will cause some decrease in the size of voids, but they will tend to remain continuous for long time. In contrast, if the sintering temperature is increased to produce enough liquid phase, the clustering of particles and the subsequent closing of pores proceeds very rapidly. The original powder particle surfaces totally loose their identity which is evident from the granular fractured surface consistent with grain boundaries but not spherical surface boundaries. Increasing the sintering time at a given temperature results in the growth of the larger pores at the expense of the smaller ones [17, 18]. On the basis of sintering studies on M2 HSS, Takajo [19] concludes that before the liquid phase appears, powder

particles are sintered in solid phase to form a skeleton which gets disintegrated by the penetrating liquid to the individual solid grains corroborates the findings of Lund. The grains rearrange their configuration and a rapid densification follows. The solid grains grow by a solution reprecipitation process in which the material transport occurs through the liquid phase. The austenite grain size after cooling is almost determined by the solid grain size at the end of liquid phase sintering. During cooling the liquid phase decomposes into austenite and carbide phases, which are mainly present along grain boundaries. Additional carbide precipitation from the austenite phase is characterised by finer carbides inside the grain.

On the basis of another set of experiments, using water atomised, annealed M2 and T15 HSS powder, Kulkarni [20, 21] has reported different set of findings regarding the densification during supersolidus sintering of HSS. According to his findings a very limited amount of densification occurs through solid state diffusion till the temperature is within a few degrees of the optimum sintering temperature range. In the optimum sintering temperature range, fine particles melt preferentially to form a small quantity of liquid phase. Melting also occurs over the surfaces of the larger particles and to some extent at grain boundaries within particles. Due to the high viscosity of the liquid phase it does not move over large

distances. The densification very likely occurs through rearrangement with substantial contribution by particle deformation as the matrix is very low in strength at this temperature. According to Kulkarni [21], the solution-reprecipitation stage does not play any significant role in the densification of HSS by supersolidus sintering owing to the high viscosity of the liquid phase.

I.3.2. Phase Diagram Characteristics:

In SLPS, densification is clearly linked with the temperature of liquid formation. Thus, the solidus and liquidus temperatures are important phase diagram characteristics. However, the actual temperature of first liquid formation will differ from the equilibrium phase diagram since the particles solidify in a nonequilibrium manner during atomization. Additionally, the phase chemistry and quantity of liquid will typically change after initial liquid formation as the system establishes equilibrium. As a first principle, a high concentration of alloying additions is desirable. This generally gives greater separation of the liquidus and solidus temperatures. Such separation aids in process control since the liquid volume fraction dependence on temperature is proportionate to the inverse of this separation. To minimise the sensitivity to normal compositional fluctuations in the alloy, it is desirable to have a moderately large compositional difference. However too large a difference may prove detrimental to liquid

wetting of the solid. Wetting is better with compositional similarity. Finally temperature control is less critical if the volume fraction of liquid does not change rapidly with temperature fluctuations. Eutectic systems are candidates for SLPS. At the eutectic temperature a sudden and discontinuous amount of liquid will form. If this quantity of liquid is large then there will be problems with process control. Phase diagrams are satisfactory to predict the level of sensitivity to sintering temperature, but cannot predict the optimal sintering temperature.

I.3.3. The Effect of Processing Variables:

Optimal sintering occurs on heating within a narrow temperature range located within the austenite, carbide and liquid phase field i.e. sinter gate [15, 87]. This sinter gate depends on the composition of the particular steel. The sinter gate for M2 is $<5^{o}C$ whereas for T1 (and other T grades) it is of the order of $20^{o}C$. For this reason the sintering of M2 is more difficult than T1 or any other T grades of HSS. Once the composition is selected, there are other controllable sintering variables which determine the properties of the sintered product. Figure 1.1 indicates the sintering temperature range for T1 grade HSS.

Powder Production Method: For liquid phase sintering of HSS, a powder compact having high green density, high green strength and low oxygen content produces excellent

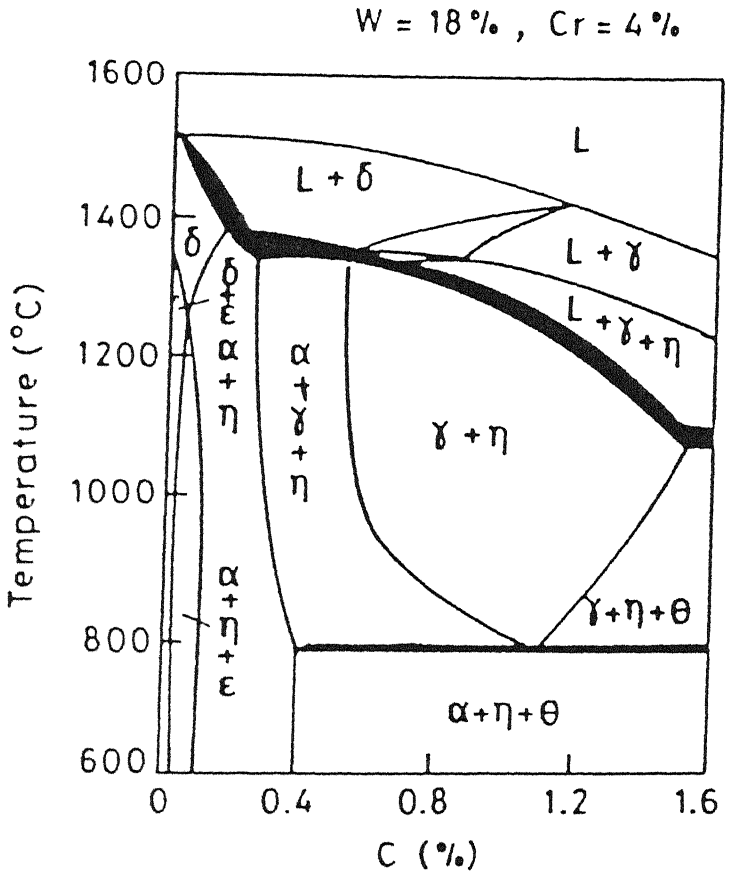

Figure 1.1. Phase diagram of Fe-W-Cr-C system at W = 18%, Cr = 4%, showing the region with liquid phase and the supersolidus sintering temperature range [19].

sintered properties. A broad particle size distribution will increase the packing density and coordination, thereby speeding densification while reducing the net dimensional change. Typically the small particles control the initial bonding. Thus, their presence is beneficial in widening the temperature range over which SLPS can be practiced. Gas atomised powders have less oxygen content but result in very poor green strength owing to their round shape. Attempts have been made to consolidate gas atomised powders by cold compaction and sintering but the high temperature required for effective densification destroys the fine carbide distribution. Finely milled powders could be densified to 99% of theoretical density at relatively low temperature [14] without carbide coarsening or by double pressing and double sintering. Water atomised powders after reduction anneal either in H_2 or in vacuum give green strength, green density and low oxygen content required for achieving the optimum sintered properties [11].

Powder Characteristics and Compaction Pressure:

Green and sintered densities for M2 and T15 grades are studied by Kulkarni [21]. The study shows that the green density for the finest fraction is somewhat higher than the coarse fractions (Figure 1.2). The difference in density persists for the samples compacted at lower compaction pressure and sintered at higher temperature, with the coarser fractions showing some large residual pores. Thus, to get full density

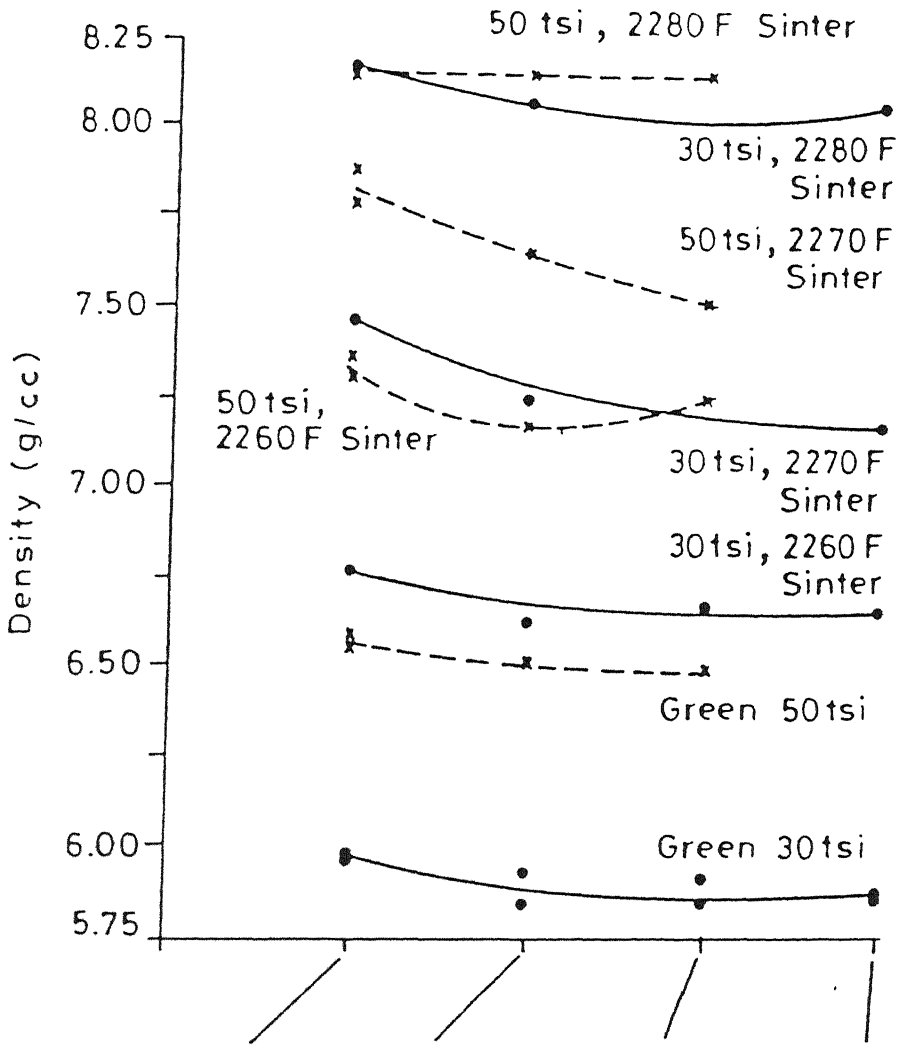

mesh	-400	325/400	270/325	200/270
microns	-37	44/37	53/44	74/53
	Green Strength of 30 tsi (414 MPa) Compacts			
ksi	2.33	3.95	3.89	3.79
MPa	16.1	27.2	26.8	26.1
	Green Strength of 50 tsi (690 MPa) Compacts			
ksi	4.54	7.42	7.66	
MPa	31.3	51.2	52.8	

Figure 1.2. Density and green strength of different sized fractions of water atomised and annealed M2 HSS [21].

and satisfactory microstructure, it is important to have a reasonable amount of particle of fine size say, less than 45 μm.

Powder Surface Chemistry: Once formed, the powder has a composition gradient from the surface to the interior because of surface nucleated solidification. This gradient will affect SLPS. Also, surface contamination can be a problem, especially if the contaminant can alter the temperature where the liquid forms. Surface oxides on metallic particles are detrimental since they alter the liquid wetting and spreading characteristics. In HSS, a surface oxide will decarburize the alloy. This depletion of carbon raises the temperature for optimal sintering [17].

Particle Shape: The sintering temperature and conditions mentioned for very fine milled powder which are equiaxed [22] and for water atomised powders which are irregular in shape [21] are remarkably similar.

Internal Powder Microstructure: In gas atomized powders some of the atomization gas can be trapped in the particles as spherical pores. These gas filled pores prove difficult to eliminate during sintering. Consequently, it is desirable to start with void-free particles so that all of the porosity is located between particles. Homogeneous liquid formation throughout the compact is most desirable for densification and shape retention. Transient melting

occurs first during heating in the regions out of equilibrium, but this can be eliminated by anneals prior to sintering. In atomized powder, the first liquid can be detected up to 25 K below the solidus temperature. After liquid formation the diffusion rates are high and equilibrium is established.

Green Density: As the compaction pressure increases, the green density increases. This higher green density of compacts helps in achieving greater sintered density at the given sintering conditions [21]. Green density in excess of approximately 85% will trap gas in the pores. Also, higher green densities have an adverse effect on capillarly flow of the liquid and hinder final densification. In practice, a green density of about 70-75% results in effective densification. Density gradients in the green compact is a source of distortion during sintering [17].

Heating Rate: The heating rate is dictated by the furnace capabilities and a need to reduce surface oxides prior to significant densification. Faster heating gives faster densification in the supersolidus liquid phase sintering or HSS since less homogenization occurs. With slow heating, the compositional gradient in the powder are reduced, giving less densification at temperatures below the optimal sintering temperature. When the powder is heated slowly or annealed prior to supersolidus sintering the volume of liquid becomes invariant with sintering time. Typical

heating rates in practice are between 0.5°C and 10°C/min [17].

Sintering Atmosphere: Vacuum sintering is usually the best choice for supersolidus sintering. At low temperatures where radiant heating is poor, a process gas can aid temperature control. Alternatively, at high temperatures vapourization kinetics can be suppressed by a process gas. However, the use of vacuum avoids the trapping of gas in the pores in the final stage of densification. The pores become closed at approximately 90 to 92% density. In the final stage of sintering the environmental gas becomes trapped in the pores thereby limiting the final density. An inert gas gives a limiting density of approximately 94 to 96% of the theoretical. Hydrogen is soluble in most metals, so the limiting density is higher. Near the optimal sintering temperature vacuum gives superior densification and hardness. Indeed, at high sintering temperatures the trapped gas can cause swelling since the pore pressure increases in proportion with the absolute temperatures [17]. Investigation carried out by Grinder et al. [22] indicates that samples sintered in argon or hydrogen contained as a rule relatively large amounts of pores. The pore size decreased with increase in the compaction pressure, but the pore volume seemed to be virtually unaffected. The pores were rounded and fairly evenly distributed in the specimen which led to assumption that they were gas pores. Palma et al. [23]

have reported that while sintering T42 HSS in the gas atmosphere (mixture of N_2-H_2-CH_4), over sintering by up to 40°C did not significantly modify the microstructure and did not produce a continuous film of eutectic phase but 10°C over sintering was enough to produce such a film in vacuum. The sintering in the gas atmosphere gave rise to nitrogenation of the steel and allowed a reduction of 20-30°C in the optimum sintering temperature.

Sintering Temperature: Liquid formation is the first dictate in the supersolidus sintering. The process temperature must exceed the solidus temperature to induce densification. When sufficient liquid forms there is rapid densification [17, 18, 19]. For each alloy, there is an optimal maximum sintering temperature that relates to the volume fraction of liquid. At temperatures lower than the optimum, pores are not eliminated even with prolonged durations at these temperatures [24]. Temperatures in excess of the optimal range result in grain growth, swelling, slumping or sweating of the liquid out of the compact. Thus, temperature control is essential for good densification, minimum microstructural coarsening and compact distortion.

The temperature range required for sintering to full density is extremely narrow, necessitating uniform temperature distribution in the furnace [17, 19]. Figure 1.3 schematically represents the effect of sintering temperature on carbide size and sintered density, from which, the optimum working range is established [25].

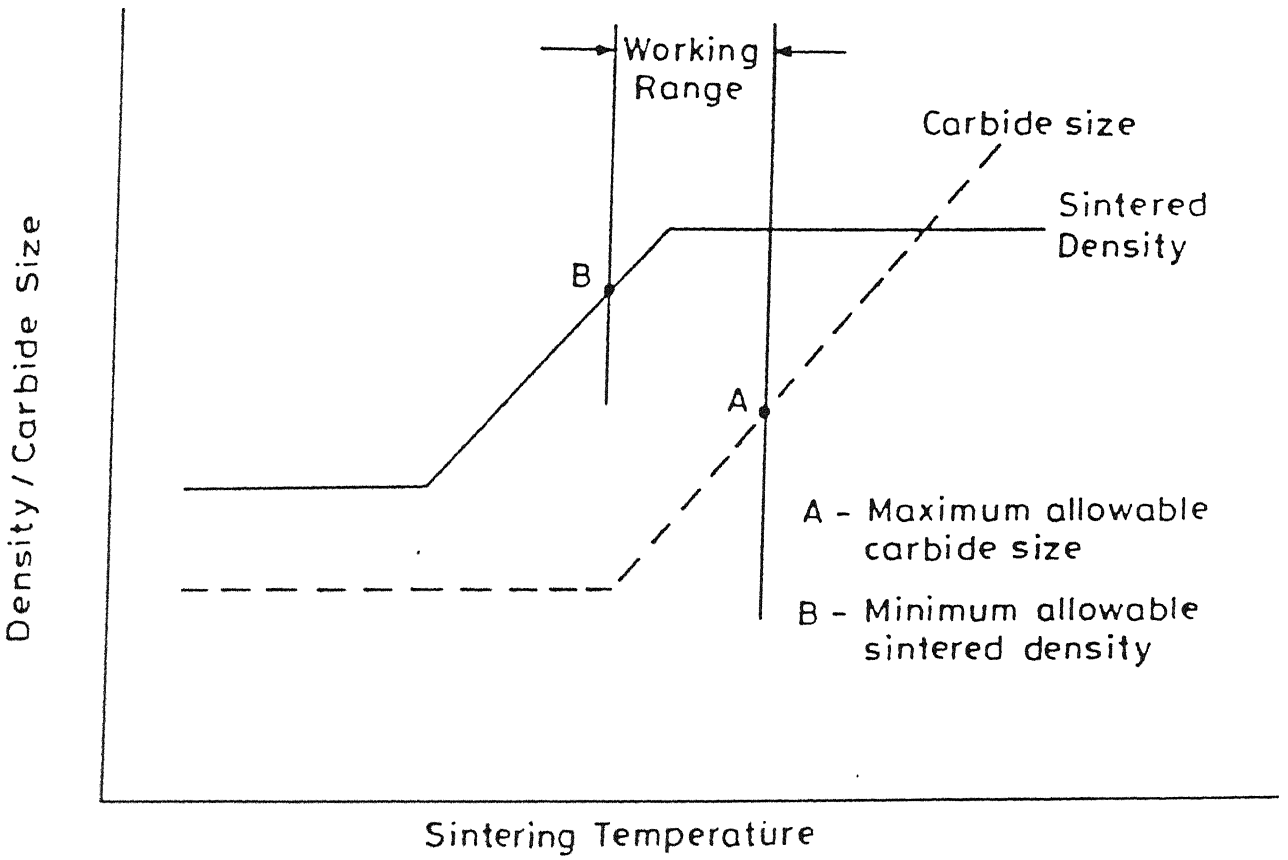

Figure 1.3. Sintering response of high speed steels (schematic) [25].

Sintering Time: At the optimum sintering temperature, full density is obtained within reasonable sintering period [17, 18, 19]. Prolong holds give relatively minor benefits and often cause property or density decrements. One consideration would be the increased homogeneity achieved with prolonged holds, but this may come at the expense of microstructural coarsening.

Cooling Rate: The microstructure and properties observed after sintering depend on the cooling rate [17, 19, 26, 27]. Additionally, phase transformations can take place during cooling which affect the properties. There is danger in very rapid cooling because solidification pores may form. Holds at temperatures just above the solidus during cooling increases the final density by minimising solidification porosity. During slow cooling, the grain boundary films that were liquid at the sintering temperature will decompose. This can be beneficial to the mechanical properties but adds expense to the sintering cycle.

Effect of Oxygen Content: Oxygen affects the sintering of HSS by reducing carbon content during sintering. Oxygen from the annealed powder reacts with carbon during sintering to form carbon monoxide. About 0.01% C is lost in the atmosphere for every 0.01% of oxygen present in the annealed powder. This reaction reduces the oxygen to less than 200 ppm during vacuum sintering [26, 30, 44].

Role of Carbon Addition: Given the total carbon content, Kulkarni et al. [28] have studied the effect of graphite addition on the sinterability between powder that is fully prealloyed and powder which has a small quantity of graphite added to it. It was observed that the free graphite may enhance sinterability by retaining lower melting eutectic phase at the interfaces with the powder particles. The addition of carbon was found to promote [23, 24, 29] sintering in several ways as well as bringing the final composition upto the specified value. The residual porosity with carbon addition was eliminated, the temperature range extended over which maximum density was achieved and the microstructure at the optimum sintering temperature improved. Kulkarni et al. [28] have proposed an empirical formula for the quantity of carbon to be added to get the optimum carbon content, which is:

$$\text{Carbon to be added} = 0.0326(W'-W) + 0.0625(Mo'-Mo) + 0.2353(V'-V) + 7.5 \times 10^{-5}(O'-O)$$

where, W', Mo', V' indicate the wt. % of elements in powder and O' in ppm of O_2 in powder. W, Mo, V are the wt. % and O in ppm in the compact desired.

Role of Sintering Aids: Similar to the beneficial effects of carbon addition in improving the sinterability of HSS, other additives in smaller quantities have been tried which lower the sintering temperature, increase the liquid volume % resulting in rapid and uniform densification and

microstructure. Carbon is an integral part of the HSS composition and does not result in unwanted phases, but the use of any other additive such as boron [12, 30], Cu-P [31, 32] result in newer phases. The effect of these additives has negligible effect in the carbide morphology and mechanical properties of the sintered products.

I.3.4. Mechanical Properties of Liquid Phase Sintered HSS:

The mechanical properties are dependent on the residual porosity and sintered microstructure. Figure 1.4 schematically shows the as sintered microstructure in P/M tool steels. Sintered HSS can suffer from three major strength reducing microstructural defects viz. (i) Metallic/non-metallic inclusions caused by contamination during powder processing, (ii) Porosity, if the sintering time or temperature are chosen too low, (iii) Carbide/grain coarsening, if the sintering temperature or time are too high [33, 34]. Porosity of 1% reduces the toughness in terms of TRS (Transverse Rupture Strength) more than 10% for M35 and 25% for 3% porosity. Over sintering due to excessive temperature or time yields a coarse carbide structure again causing unfavourable TRS. The decrease in TRS is of the order of 10-25% for slight to excessively overheated case. P/M HSS is always used after a suitable hardening treatment and the starting point in achieving optimum end properties is an optimum sintering in terms of full density with a sound and uniform microstructure. Table I.1 gives a survey of mechanical

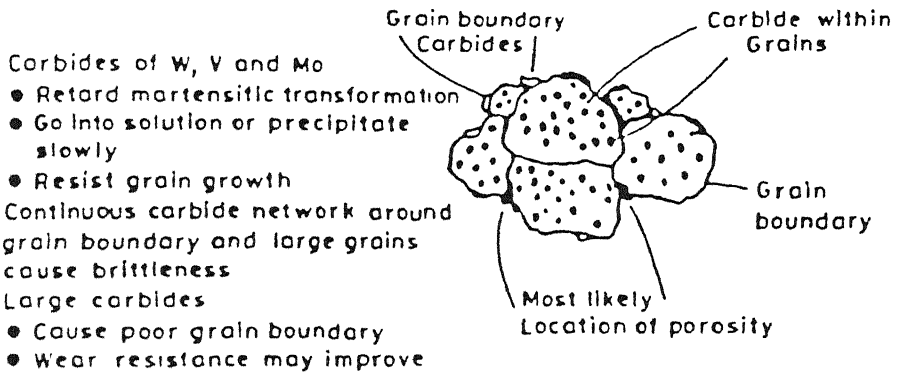

Figure 1.4. Microstructure of as-sintered P/M HSS (schematic) [26].

properties as reported by various workers while processing various grades of P/M HSS through direct sintering route.

I.4. HSS BASED PARTICULATE COMPOSITES THROUGH P/M ROUTE:

The hardness and wear resistance of any grade of HSS depend on the volume fraction of the hard phases in the matrix and the matrix hardness itself. The superiority of any grade of cutting tool material depends on the high temperature stability of the different phases, for which the hot compressive yield strength can be an indicator [1-4].

The wear resistance of HSS is directly related [2, 10, 16] to the volume fraction of the primary carbides (MC + M_6C types) in the matrix. It has been reported [35, 36] that the wear resistance can be linearly related to the volume fraction of MC type of carbides. Through alloy addition, it is possible to reach a very high primary carbide content in HSS. The high vanadium, high carbon grade of M2 HSS is an example. But, indefinite increase in vanadium and carbon is not practicable in wrought processing due to difficulties in hot working [1, 36]. Through P/M route it is possible to get a HSS with higher volume fractions of hard phase by enriching the HSS composition with hard, refractory oxides/nitrides/carbonitrides/carbides/borides. The hardness and melting temperature of the various candidate additives is given in Table I.2. This process of enrichment of HSS with hard particles to form a composite

Table I.1. Mechanical properties of high speed steels processed through direct sintering route.

Grade	Processing conditions	Mechanical properties	Author/s	Reference No.
M2	Vacuum sintered at 1245°C, Oil quenched from 1200°C, Triple tempered at 550°C, 45 min	Triple tempered, Hardness = 820 HV Impact strength = 10 J/cm^2	I. Kvasnicka	83
M3/2	Vacuum sintered at 1150°C, Cu-P alloy used as sinter aid	Sintered hardness = 730 HV_{10} Sintered TRS = 1595 MPa	I.M. Martins, M.M. Oliveira and H. Carvalhinhos	41
M3	Vacuum sintered at 1220°C, 1 hr Hardened and triple tempered (conditions not mentioned)	Triple tempered, Hardness = 53 HRc TRS = 2100 MPa	R.A. Queeney, J.L. Miller, R.J. Beltz and J.D. Dankoff	37
M35	Vacuum sintered to full density, Hardened and triple tempered (temperatures not mentioned)	Triple tempered, Hardness = 65 HRc TRS = 2400 MPa	P. Beiss, R. Wahling and D. Duda	33
T15	Vacuum sintered to full density, hardened and triple tempered	Triple tempered Hardness = 67.7 HRc TRS = 1550 MPa	P. Beiss, R. Wahling and D. Duda	33
T15	Vacuum sintered at: (i) 1260°C, 1 hr (ii) 1270°C, 15 min (iii) 1270°C, 1 hr All samples austenitized in salt bath at 1220°C and oil quenched, triple tempered at 520°C, 1 hr	(i) Sintered hardness -HV_{30} = 589; Triple tempered hardness = 885; Triple tempered TRS, MPa = 2027 (ii) 602; 877; 2001 (iii) 599; 883; 1850	M. Santos, I.M. Martins, M.M. Oliveira and H. Carvalhinhos	14

contd...

Table I.1 (continued)

Grade	Processing conditions	Mechanical properties	Author/s	Refere No.
T42	Vacuum sintered at 1245°C, salt bath heat treated. Austenitized at 1175°C, triple tempered at 525°C	Hardness: HV_{50}-1000	C.S. Wright, A.S. Wronski and M.M. Rebbeck	82
Steel 12-8-10, W = 12%, Mo = 8%, V = 10%, Co = 10%	Vacuum sintered at 1180°C, quenched from 1200°C, triple tempered at 550°C, 1 hr	Triple tempered, Hardness = 70.3 HRc TRS = 1800 MPa	N. Uchida and H. Nakamura	81
Steel 13-11-8 W = 13%, Mo = 11%, V = 8%, Co = 8%	- do -	Triple tempered, Hardness = 71.6 HRc TRS = 2100 MPa	- do -	81
Steel 19-14-6 W = 19%, Mo = 14%, V = 6.5%, Co = 8%	Vacuum sintered at 1180°C, quenched from 1220°C, triple tempered at 550°C, 1 hr	Triple tempered, Hardness = 72.1 HRc TRS = 1700 MPa	- do -	81

for greater wear resistance is still in research stage and there has been no report of its commercial adoption.

The potential carbides which have been investigated as additives were VC, TiC, TaC, NbC, SiC, WC, Mo_2C, HfC, ZrC and Cr_2C_2. Wilson and Jackson [39] showed that VC/TiC addition to M2 HSS increase the sintering temperature to achieve full density. Kieffer et al. [12] observed that VC, TiC, NbC, TaC, HfC and ZrC addition to M2 HSS increase the cutting tool life or cutting speed of the composite. The effect of VC (upto 30 mass %) addition on the mechanical properties of sintered HSS of PX 16 grade (nearest AISI equivalent grade T15) made from water atomised powder has been reported by Yamada, Kohzuki and Okuno. They reported that though there was increase in the Vickers hardness with the increased addition of VC, the TRS decreased. Also, with increased addition of VC, higher sintering temperature was required for full density and this resulted in increased carbide grain size. The wetting and interfacial bonding during sintering associated with limited solubility lead to the essential carbide additive being retained as a dispersed phase which improves the wear resistance.

Addition of Ti(C,N) (upto 10%) to T1 HSS were studied by Kiparisov et al. [40]. Their finding indicates that the Ti(C,N) particles increases the sintering temperature and addition upto 10% can be made without hampering sinterability. As found with TiC addition, Ti(C,N) remained

Table I.2. Hardness and melting points of various refractory compounds as candidate additives to HSS.

Refractory compound	Melting point, ^{o}C	Room temperature hardness, HV Kg/mm^2
Al_2O_3	2015	2600
AlN	2235	1225 (Knoop 100 gm)
BN	3000	10600
TiN	2900	1770 (Knoop 100 gm)
TiC	3180	2900
VC	2810	2800
NbC	3500	2400
TaC	3877	1800
HfC	3887	2913
WC	2867	2400
Mo_2C	2687	2000
SiC	2500	3000
ZrC	3532	2600
Cr_3C_2	1890	1300
$Cr_{23}C_6$	3532	2600
TiB_2	2790	3370

unaffected at the sintering temperature and their presence enhanced the tempered hardness as well as wear resistance.

Queeney et al. [37] and Martins et al. [41] reported the work on enrichment of M3 and M3/2 grades of HSS respectively by Al_2O_3. Al_2O_3 is hard (HV 24 GPa) and stable at high temperatures. Composites with 5 wt. % Al_2O_3 could be vacuum sintered to full density. Even though there was enhancement of wear resistance properties, the toughness decreased. The wear resistance was directly proportional to the Al_2O_3 content. It is explained that due to lack of interaction between the Al_2O_3 particles and the matrix, porosity is frequently observed which leads to poor toughness of the composite.

Arai and Komatsu [38] have reported the effect of AlN, TiN and BN addition to M2 HSS. They have shown, beyond 5% nitride addition, the hardness as well as wear resistance of the composites deteriorated due to the lack of densification.

I.5. SCOPE OF THE PRESENT INVESTIGATION

Through P/M route processing it is possible to get a HSS with high volume fractions of hard phase by enriching the HSS composition with hard, refractory oxides/nitrides/carbonitrides/carbides/borides. Such a composite will have greater wear resistance and improved cutting ability. Through near-net shape processing route, a semi-precision part is obtainable which needs only finish grinding.

In the present investigation two refractory titanium based compounds viz. TiB_2 and Ti(C,N) have been used as dispersoids in T15 and T42 based HSS. Among various P/M processing routes, the present investigation singularly focusses on liquid phase sintering route, as the process is less capital intensive and could be easily adopted in a plant processing conventional sintered products.

The sintering study of HSS enriched with refractory TiB_2/Ti(C,N) compounds necessitated the selection of the composition of the high speed steels which offer wider 'sinter gate' as in this case the precise temperature control is less critical. The tungsten grades of HSS have relatively wider 'sinter gates' ($20^{o}C$) as compared to molybdenum grades ($<5^{o}C$). T15 and T42 grades are well known as wear resistant cutting tool materials owing to their high contents of carbide forming elements like W and V. In addition, T42 has a higher cobalt content (10%) as compared to T15 (5%). The matrix strengthening effect of cobalt combined with enhanced resistance to tempering enables T42 tools to be used for various purposes.

CHAPTER II

EXPERIMENTAL PROCEDURE

The detailed experimental procedures carried out in the present investigation are presented in this chapter.

II.1. POWDERS AND THEIR CHARACTERISTICS:

High Speed Steel Powders: The HSS powders used in this investigation were prealloyed, water atomised and annealed. T15 HSS powder and T42 HSS powder had the following composition and physical characteristics as furnished by the suppliers.

i) T15 HSS Powder:

Source: M/s British India Steels, Ahmedabad

Chemical Composition, mass %		
Carbon	-	1.60
Chromium	-	4.12
Cobalt	-	4.95
Manganese	-	0.40
Molybdenum	-	1.31
Tungsten	-	12.30
Vanadium	-	5.26
Sulphur	-	0.04 max
Phosphorous	-	0.04
Oxygen	-	1400 ppm

Physical Characteristics

A.D. = 2.49 gm/cc

Flow rate = 41 sec/50 gms

Compressibility = 5.54 gm/cc (at 30 Tsi)

Sieve Analysis

mesh	% cumulative mass fractions
+100	0.09
+150	9.15
+200	27.95
+350	68.15
-350	31.85

ii) T42 HSS Powder:

Source: M/s British India Steels, Ahmedabad

Chemical Composition, mass %			Physical Characteristics
Carbon	-	1.38	A.D. = 2.42 gm/cc
Chromium	-	3.96	Flow rate = 43.3 sec/50 gms
Cobalt	-	10.60	Compressibility = 5.58 gm/cc (at 30 Tsi)
Manganese	-	0.22	
Molybdenum	-	4.01	
Tungsten	-	9.70	
Vanadium	-	2.39	
Sulphur	-	0.044	
Phosphorous	-	0.044	
Oxygen	-	700 ppm	

Refractory Compounds:

i) TiB_2 Powder:

Source: Hermann C. Starck, Berlin, Germany

Chemical Composition, mass %

Boron	-	30.3%
Carbon	-	0.3%
O_2	-	0.25%
N_2	-	0.39%

Av.Particle size - 9.5 μm (FSSS)

ii) Ti(C,N) Powder:

Source: Treibacher, Austria

Ti(C,N)	-	50 : 50
C(total)	-	9.87%
C(free)	-	0.04%
Fe	-	0.12%
O	-	0.70%
N	-	11.0%

Av. particle size (FSSS) - 2.10 μm

II.2. POWDER MIX PREPARATION AND ROOM TEMPERATURE COMPACTION:

0.7 mass % magnesium-stearate as a solid lubricant was blended with the as received T15 and T42 powders respectively for 30 minutes using a laboratory double cone blender of Netzsch-Feinmahltechnik, Gmbh make.

For the composite composition, 2, 4, 6 and 8 mass % of TiB_2 and 2, 4 and 6 mass % of Ti(C,N) refractory compounds respectively and 0.7 mass % Mg-stearate were added to T15 and T42 HSS powder and blended for one hour. The uniformity of mixing was checked under an illuminated magnifying lens.

The blended powder was pressed into green compacts in the shape of tool bits of dimensions 7.00 X 11.00 X 76.70 mm^3 on an automatic mechanical press of 200 Tons capacity of 'Dorst', Germany make. These green dimensions were derived in to achieve the specified sintered dimension of 6.5 X 9.5 X 75.0 mm^3.

Compaction pressure used was fixed at 850 MPa for straight composition and in the range of 850-900 MPa for the composite compositions to ensure a constant green porosity of 24-26%. Green porosity was calculated on the basis of dimensional measurements.

From each of these green tool bits, smaller samples of approximately 10 mm length were cut using a fine HSS hack-shaw blade for sintering study. For the sintering of the TRS samples, three samples of approximately 25 mm length each were cut.

II.3. SINTERING:

Sintering experiments were carried out in a SiC resistance heated tubular furnace. The furnace of 4.4 cm internal diameter had a constant temperature zone of 7 cms length. The sintering was carried out in vacuum for TiB_2 containing composites and in H_2 atmosphere for Ti(C,N) containing composites. During vacuum sintering a dynamic vacuum of the order of 5×10^{-2} m bar was maintained. The sintered pellets were then cooled down to room temperature before opening the vacuum or hydrogen system to air. Green samples were placed on a fused alumina tile, which in turn was kept on a graphite boat within the constant temperature zone. The furnace temperature was controlled within $\pm 2.5^{\circ}C$ using a proportional temperature controller.

The sintering temperature was varied from $1200^{\circ}C$ to $1280^{\circ}C$ for T15 HSS based composites and from $1160^{\circ}C$ to $1250^{\circ}C$ for T42 HSS based composites in steps of $10^{\circ}C$. Pre-sintering soak [44], at $90^{\circ}C$ less than the selected sintering temperature was given for 2 hours to all the samples after which faster heating to the sintering temperature was done. The holding period at the sintering temperature was maintained uniformly for 90 minutes for all the samples. Then natural cooling to room temperature from respective sintering temperature followed.

II.3.1. Sintered Density Measurement:

The sintered densities of the samples were measured using water displacement method described by Arthur [46]. The sintered samples were impregnated with xylene in vacuum and the following formula was used to calculate the sintered density:

$$\text{Density} = \frac{\text{Weight of compact in air}}{\text{Wt. of xylene impregnated compact in air} - \text{Wt. of xylene impregnated compact in water}}$$

The samples which achieved densities in excess of 98% theoretical density were considered to be fully dense. The theoretical density for the composites were calculated using the rule of mixture. The sintering temperature at which the maximum density was obtained, was taken as the optimum sintering temperature for any composite.

II.4. HEAT TREATMENT:

For heat treatment different types of samples were chosen for two types of composites. Since TiB_2 containing composites could not attain full density except 2 mass % containing composites. Hence for TiB_2 containing composites a set of samples which attained maximum density was chosen for further heat treatment. On the other hand since Ti(C,N) containing composites attained full density, all fully dense ($\geq$98% Theoretical) samples were taken for further heat treatment. The critical temperature for transformation annealing was determined initially.

All the heat treatment operations such as transformation-annealing, austenitizing and oil quenching and tempering were done in air. To prevent the samples from decarburization, they were wrapped in a special graphite coated foil (sinter cast protec tool wrap of stainless steel) before introducing into the heat treatment furnace.

II.4.1. Determination of Critical Temperature for Heat Treatment:

Due to scant informations on the critical transformation temperatures of P/M grade of T15 and T42 HSS, the AC_1 and AC_m temperatures were determined. For this purpose a DTA of linseis, Germany make was used. Heating rate during the test was $5^{\circ}C$/min to $1100^{\circ}C$ from room temperature after which cooling was done at the same rate to the room temperature. The temperature at which an endothermic reaction peak appeared indicated the AC_m temperature during heating and the temperature at which the exothermic reaction peak ends during cooling indicated the AC_1 temperature. On the basis of this information, the transformation annealing temperatures were determined.

The purpose of the transformation annealing was to relieve the internal stresses developed in the sintered compacts during cooling from the sintering temperature and to provide a refined grain structure prior to further hardening and tempering treatments. Samples were held at $900^{\circ}C$ for 1 hour and at $760^{\circ}C$ for 4 hours. From $760^{\circ}C$, the samples were air cooled to room temperature.

II.4.2. Hardening:

An uniform austenitization temperature of 1195°C was selected for both the grades of HSS i.e. T15 and T42 and their based composites. Each batch of annealed samples was heated in the same furnace as was used for sintering. During austenitization, samples were slowly heated to 850°C and soaked for 60 minutes after which faster heating was done to 1195°C. Holding time at the austenitization temperature was kept as 10-15 minutes. One set of T15-TiB_2 particulate composites after sintering in hydrogen for 1.5 hours was also heat treated as described above. From austenitization temperature samples were quenched in mineral oil to room temperature.

II.4.3. Tempering:

Oil quenched samples were subsequently triple tempered isothermally in still air. The tempering time was kept uniform for 1 hour during each tempering. Tempering temperature selected for such grades of HSS was 550°C, as per optimised by Kar and Upadhyaya [47, 48]. Samples for mechanical property evaluation such as TRS were tempered at optimum temperature of 550°C prior to the tests.

II.5. MECHANICAL TESTS:

Hardness and transverse rupture strength tests were carried out at room temperature.

II.5.1. Hardness:

Hardness of the sintered as well as heat-treated

samples after every steps of heat treatment viz. hardening and tempering, were measured on Vickers hardness testing machine Model HPO 250 of "Fritz Heckert", Leipzig make, using a load of 10 Kg (98 N). At least 5 indentations were taken on each specimen and the average value reported.

II.5.2. TRS (Transverse Rupture Strength):

For the measurement of TRS, samples sintered at the optimum sintering temperature and heat treated as per schedule described earlier were used. Samples having approximate dimensions of 6.5 X 10.0 X 22.0 mm^3 were positioned in the standard TRS test fixture (ASTM B406-81). The tests were carried out at room temperature on the MTS-810 material testing machine at a cross head speed of 0.5 mm/min. The transverse rupture strength (TRS) was calculated according to ASTM Standard B528-76, as follows:

$$\text{TRS in MPa} = \frac{3PL}{2t^2W}$$

where P is the force in Newtons required to rupture the specimen, L is the distance between the bottom supports in meters, W and t are the width and thickness of the specimen in meters respectively. The average result of 3-specimens from each condition were taken as the TRS value.

II.6. MICROSTRUCTURAL STUDIES:

Microstructural studies included qualitative optical metallography, SEM and EDX studies, SEM fractography and X-ray mapping studies.

II.6.1. Qualitative Optical Metallography:

Samples for metallographic studies were selected after every stage of processing such as sintering, oil quenching and every stage of tempering. Microstructure was prepared using the conventional process starting from the belt grinding followed by wet polishing on 'Lunn Major' unit over 120, 400, 600 and 1000 grit size SiC coated paper successively. This was followed by disc polishing (Struers DAP-2 unit) using diamond paste of 7 μm and 1 μm grit size successively. Polished samples were then etched according to the features required to be examined.

II.6.2. SEM and EDX and X-ray Mapping Studies:

For SEM and EDX studies, samples were prepared using the same procedure as was followed for optical metallography. Both etched and unetched samples were observed under 'JEOL' JSM-840A scanning electron microscope fitted with Kevex EDX analyser for the chemical analysis of the observed phases.

The fracture surfaces of the TRS broken pieces in triple tempered condition were observed under 'JEOL', JSM-840A scanning electron microscope. The same microscope was used to see the distribution of different elements in the structure by using X-ray mapping method.

CHAPTER III

EXPERIMENTAL RESULTS

III.1. T15 AND T42 GRADE HSS SINTERED IN VACUUM:

III.1.1. Densification

The densification behaviour of vacuum sintered straight T15 and T42 HSS is shown in Figure 3.1a and 3.2a respectively. Sintered density of vacuum sintered T15 HSS increased with the increase in sintering temperature from about 87% of theoretical density at 1250°C to 98% at 1270°C, which was the optimum sintering temperature for this grade. Similarly, the sintered density of T42 HSS increased from 85% at 1220°C to 98.5% at 1230°C, which was the optimum sintering temperature for this grade when sintered in vacuum. When the sintering temperature was increased beyond optimum temperature, the sintered density either remained constant or decreased a little for either of the HSS.

III.1.2. Critical Temperature for Transformation Annealing:

Figure 3.3 shows the result of DTA study on the sintered stress relieved T15 and T42 HSS samples for the determination of the upper and lower critical temperatures. The start of $\alpha - \gamma$ transformation during heating is noticed from the appearance of the endothermic peak. For T15 HSS, this peak (indicating AC_m temperature) appeared at a temperature of 850°C whereas for T42 HSS, it is at 860°C. During cooling, the completion of the $\gamma \longrightarrow \alpha$ transformation is

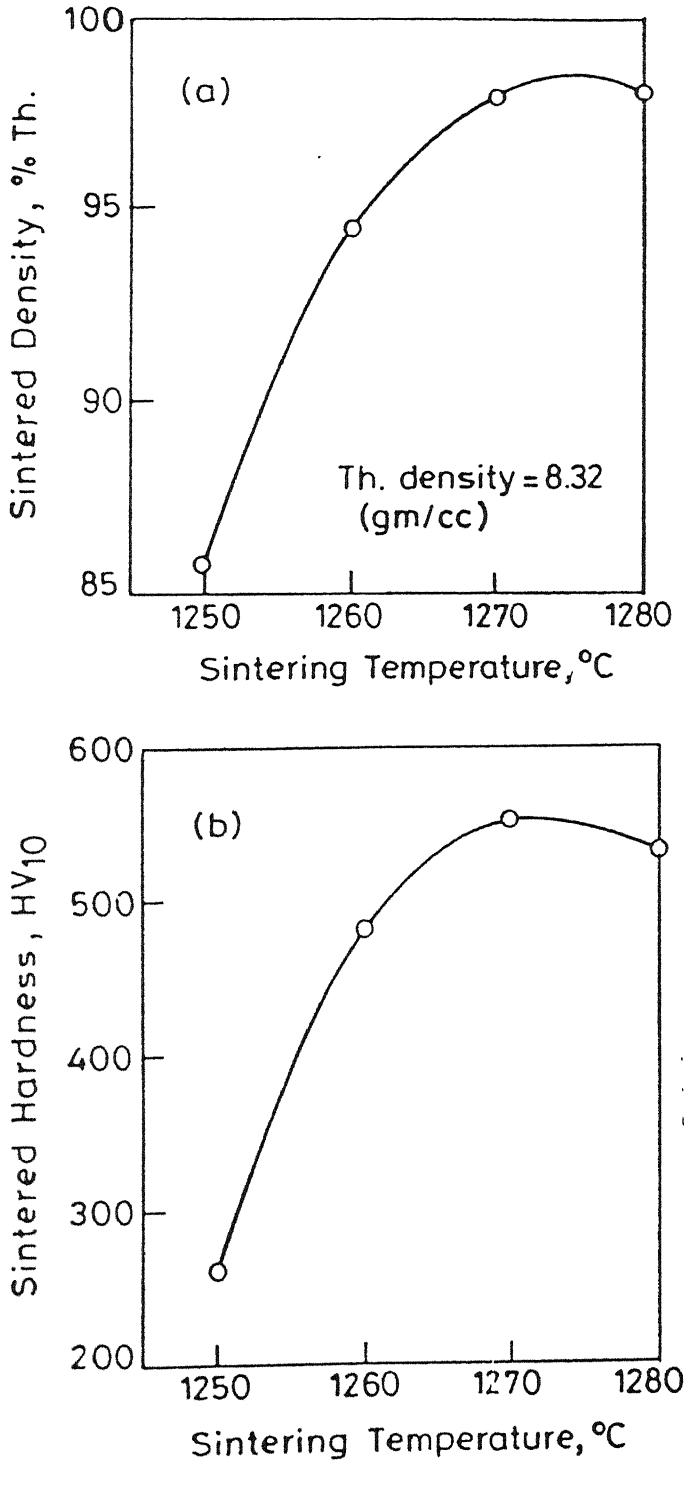

Fig. 3.1 Effect of sintering temperature on properties of T15HSS
(a) Sintered density (b) Vickers hardness

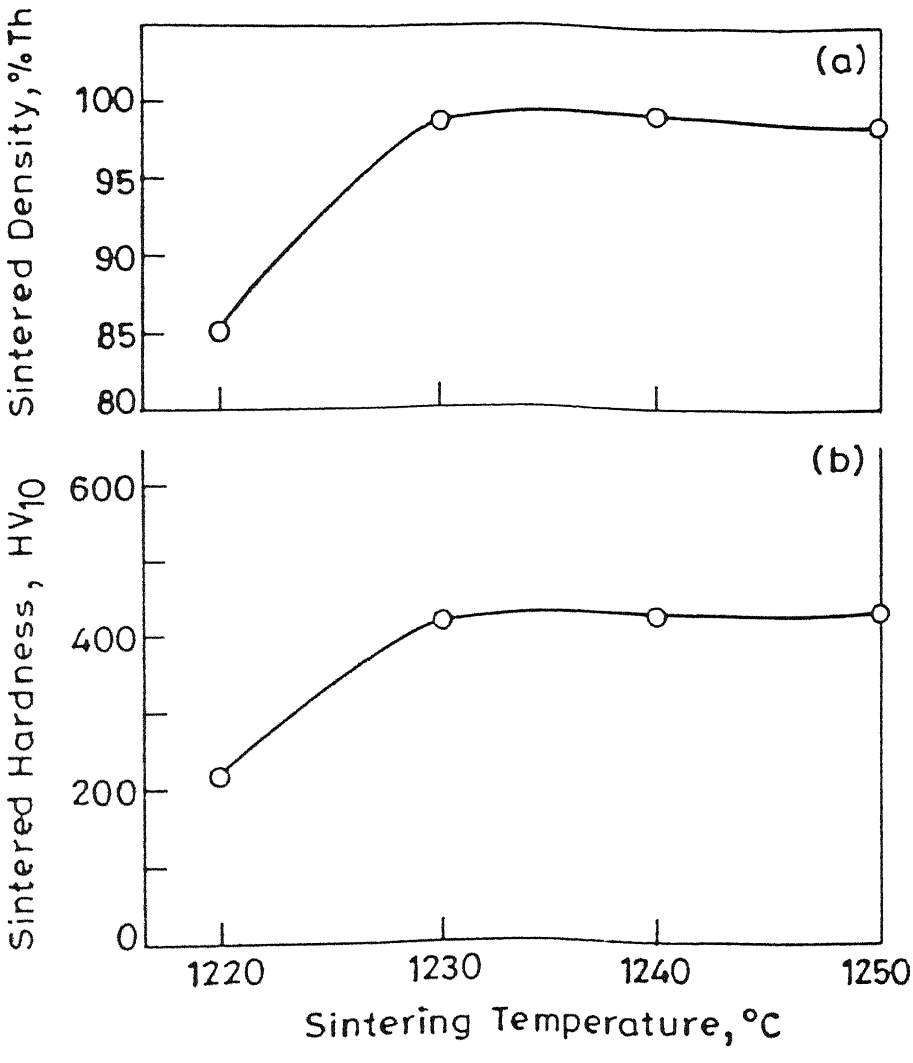

Fig.3.2 Effect of sintering temperature on: (a) Sintered density and (b) Sintered hardness of T42. HSS

seen from the end of the exothermic peak (indicating AC_1 temperature) at 780°C for T15, 770°C for T42 HSS. Above the AC_m temperature, the structure contains γ plus carbides and below the AC_1 temperature, the structure contains ferrite plus carbides. On the basis of these two temperatures, the isothermal heating conditions required for transformation annealing was determined. In the present investigation, the first and second hold temperatures for transformation annealing were fixed as 900°C and 760°C respectively for either grade of HSS.

III.1.3. Hardness:

The sintered hardness variation of vacuum sintered T15 and T42 HSS with respect to sintering temperature is shown in Figure 3.1b and Figure 3.2b respectively. The plot follows a similar trend to that observed for densification with respect to the sintering temperature. The as sintered hardness of T15 HSS sintered at the optimum temperature (1270°C) was 550 HV_{10}, which was higher than the corresponding hardness of T42 HSS sintered at 1230°C. The as quenched hardness also followed a similar trend to that of densification with respect to temperature. The triple tempered hardness obtained for T15 grade was 900 HV_{10} corresponding to the sintering temperature of 1270°C. On the other hand triple tempered hardness of T42 HSS was 960 HV_{10} corresponding to the sintering temperature of 1230°C. Tempering temperature was kept fixed at 550°C as already optimised by Kar and Upadhyaya [48].

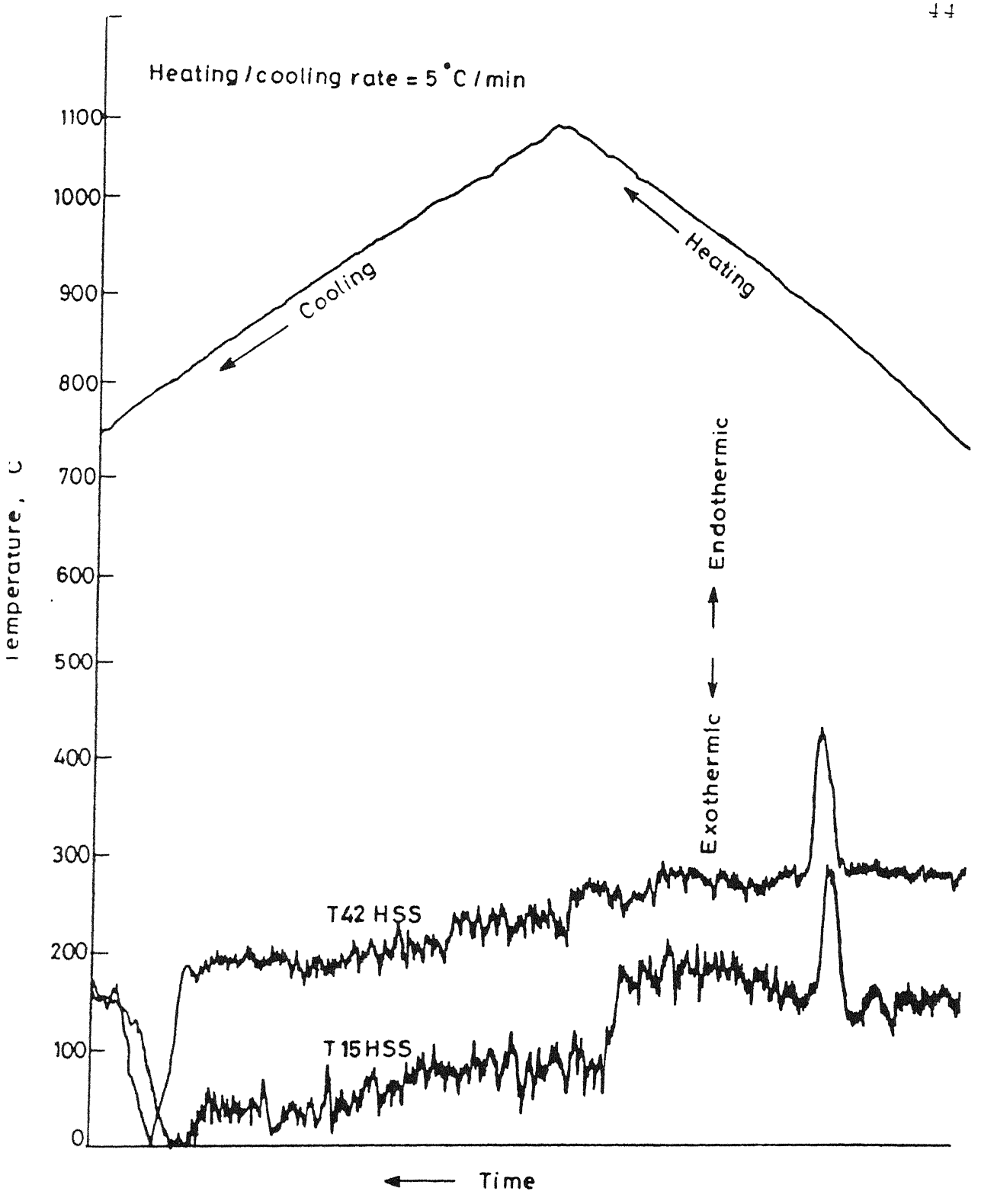

Fig 3.3 Critical temperatures for transformation annealing as determined from DTA.

III.1.4. Transverse Rupture Strength (TRS):

The as sintered TRS of T15 and T42 HSS were 1500 MPa and 1800 MPa respectively and the TRS in triple tempered condition for T15 and T42 which were vacuum sintered at the respective optimum sintering temperature were 1950 MPa and 1300 MPa respectively. The sintered TRS of T15 was lower than that of T42 whereas the reverse was true in case of the triple tempered TRS.

III.1.5. Microstructural Analysis:

The optical and SEM microstructures of T15 HSS sintered at the optimum sintering temperature i.e. 1270°C [Figure 3.4a and b) are well developed with fine grain matrix and carbides. The as sintered microstructures of T42 HSS sintered at optimum temperature i.e. 1230°C are shown in Figure 3.4d and e which show uniform microstructures with few isolated pores. Figure 3.5 show the triple tempered micrographs of T15 and T42 HSS. It is observed from Figures 3.4 and 3.5 that the sintered and triple tempered microstructures of T15 grade are coarser as compared to ones of T42 HSS. As sintered SEM micrograph of T15 HSS revealed that the structure consisted of primary carbides along the grain boundary and within the grains (Figure 3.4b). The white phase was M_6C carbide and the grey phase was MC carbide as confirmed from EDX analysis. In the triple tempered condition (Figure 3.5), the microstructure consisted of carbides in a tempered martensite matrix. Only the

primary carbides present over the surface and within the prior austenite grains could be observed as the secondary carbides for example, $Cr_{23}C_6$ could not get resolved on SEM. Here again, the two types of carbides viz. MC and M_6C could be distinguished from their colours.

T42 HSS also showed a structure [Figure 3.4d, e and 3.5] similar to that of T15 HSS.

Figure 3.5 shows the different phases in triple tempered T15 and T42 HSS and Table III.1 gives the chemical composition of various phases as determined by the SEM-EDX analysis for T15 and T42 HSS. In both the cases the grey phase was MC type carbide which was rich in vanadium, while the white phase, M_6C type carbide was rich in tungsten and iron. The matrix was naturally rich in elements which did not participate in the formation of primary carbides i.e. Fe and Co.

Figure 3.6 shows the SEM fractographs taken on the fracture surfaces of the broken TRS test pieces of T15 and T42 HSS. Both T15 and T42 HSS showed similar nature of crack propagation.

Figures 3.7 and 3.8 show the X-ray mapping analysis of triple tempered T15 and T42 HSS samples respectively. Comparing both the two figures it can be concluded that concentration of Co in the matrix is more in case of T42 HSS as compared to T15 HSS, which confirms the analysis of such steels. On the other hand vanadium concentration is more in T15 HSS as compared to T42 HSS which forms MC

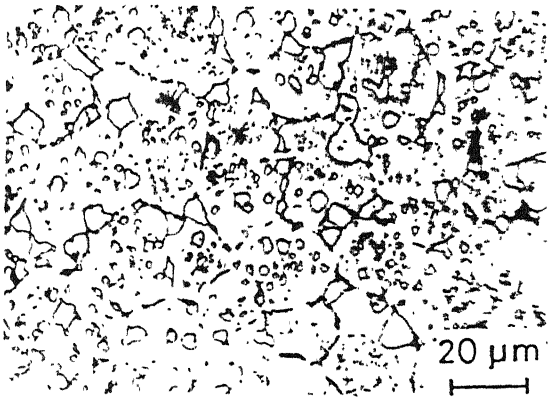

(a) Sintered (optical)

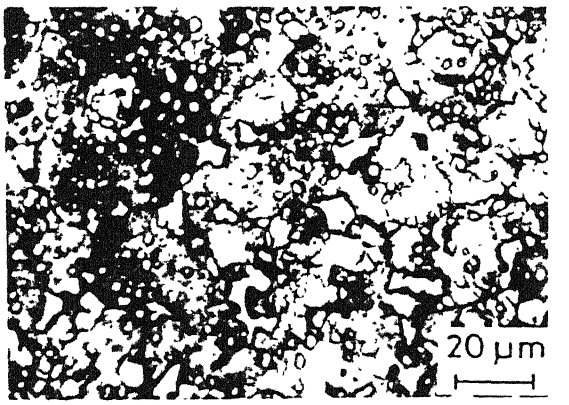

(d) Sintered (optical)

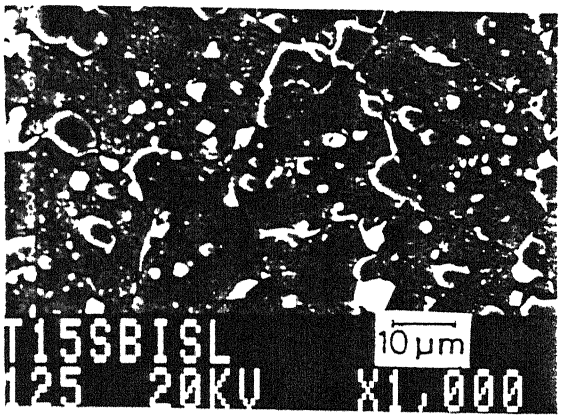

(b) Sintered (SEM)

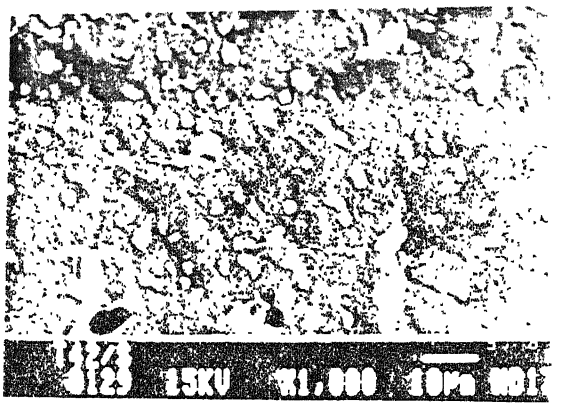

(e) Sintered (SEM)

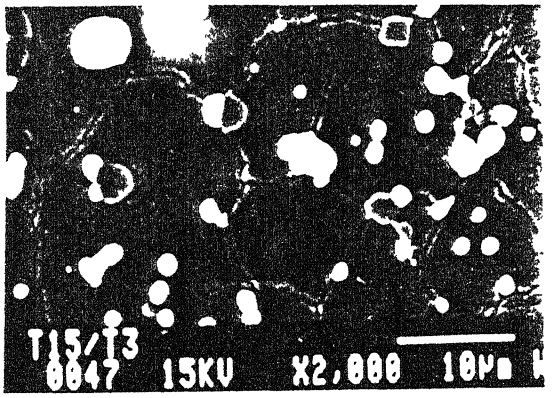

(c) Triple tempered (SEM)

T15

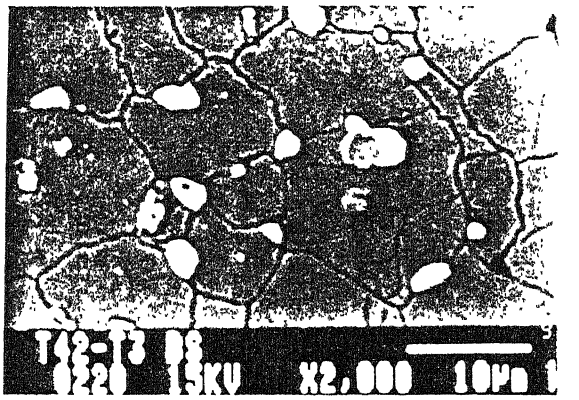

(f) Triple tempered (SEM)

T42

Figure 3.4. Optical and SEM microstructures of as sintered and triple tempered T15 and T42 HSS.

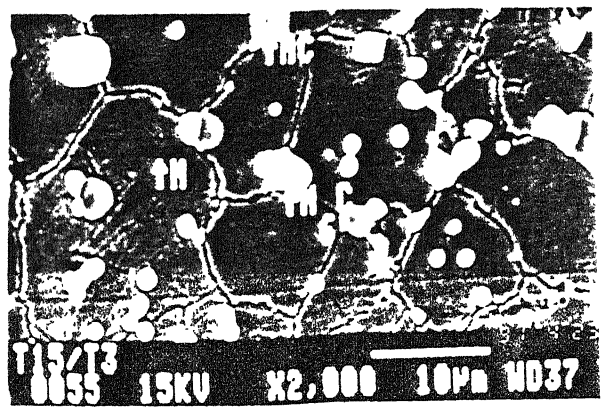

T15

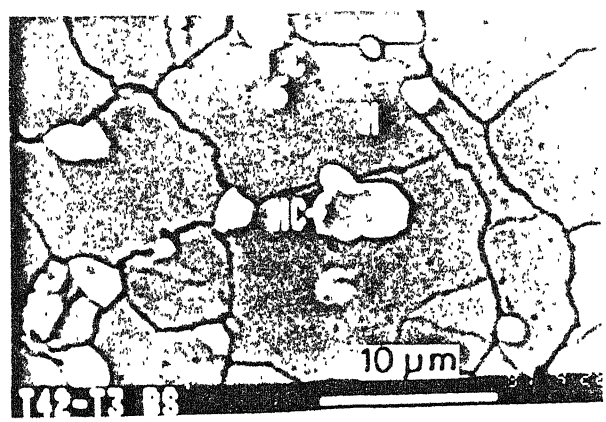

T42

Figure 3.5. SEM microstructures of triple tempered T15 and T42 HSS showing different phases.

Table III.1. EDX analysis of various phases in T15 and T42 HSS.

HSS grade	Description of phase	Mass % chemical analysis						Assigned phase
		Fe	Cr	Co	Mo	V	W	
T15 HSS (sintered)	Matrix	79.31	3.97	4.80	0.41	2.78	8.73	Matrix
	Grey phase	19.18	-	-	-	48.80	32.02	MC type carbide
	White phase	31.62	-	-	-	-	68.37	M_6C type carbide
T15 HSS (triple tempered)	Matrix	83.02	4.32	8.95	-	1.80	1.93	Matrix
	Grey phase	4.82	12.10	1.34	2.66	52.28	26.80	MC type carbide
	White phase	35.23	5.41	4.21	4.15	6.64	44.37	M_6C type carbide
T42 HSS (sintered)	Matrix	74.69	5.08	13.36	0.77	0.83	5.27	Matrix
	White phase	35.42	5.66	6.90	13.55	3.80	34.67	M_6C type carbide
T42 HSS (triple tempered)	Matrix	73.47	4.25	11.22	4.02	1.62	5.42	Matrix
	Grey phase	3.49	9.72	0.11	1.88	54.16	30.64	MC type carbide
	White phase	34.46	4.96	3.38	1.48	7.21	48.50	M_6C type carbide

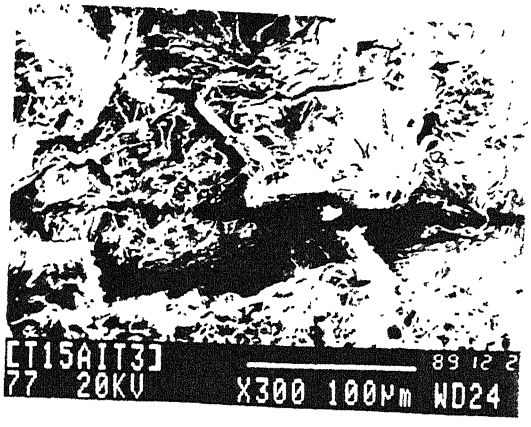

T15

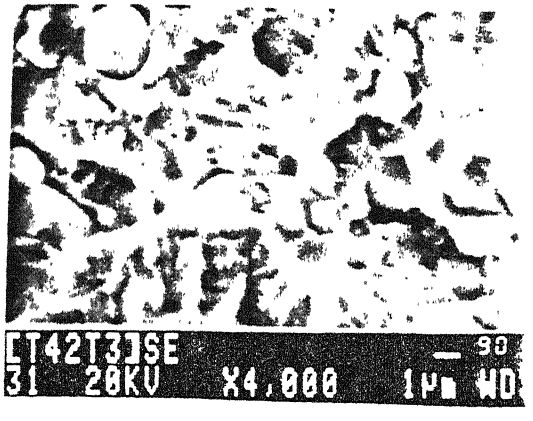

T42

Figure 3.6. SEM fractographs of T15 and T42 HSS in triple tempered condition.

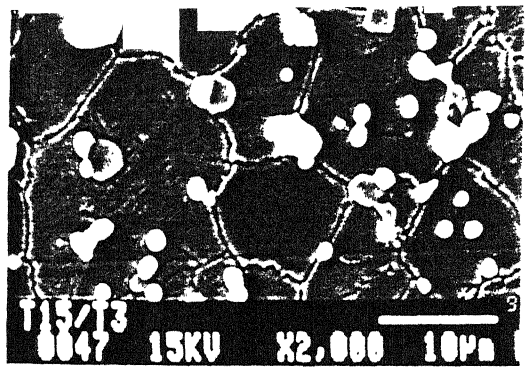

Image

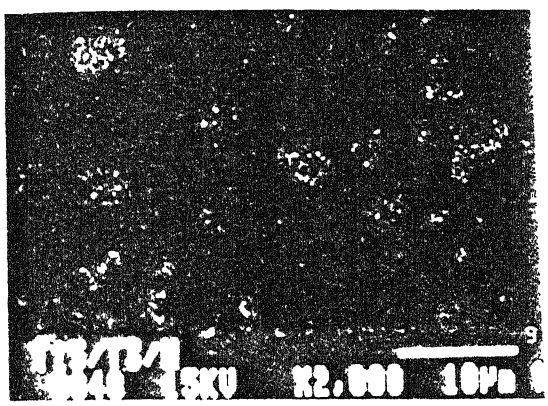

W

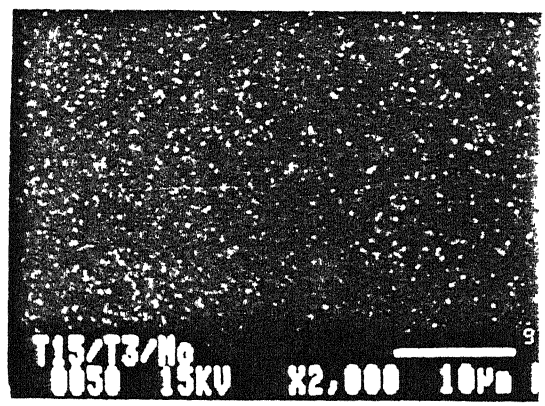

Mo

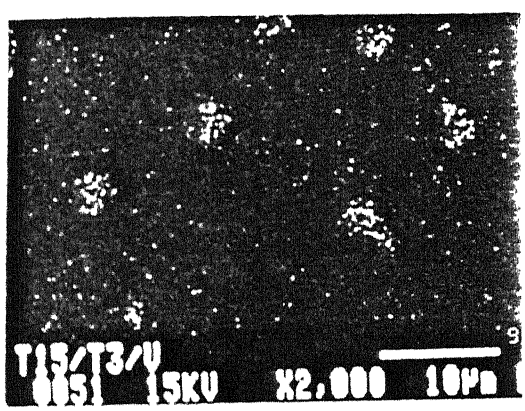

V

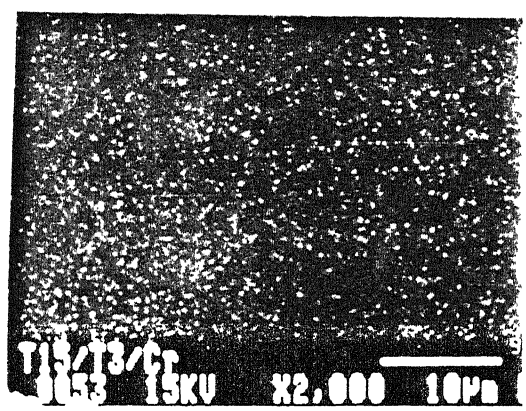

Cr

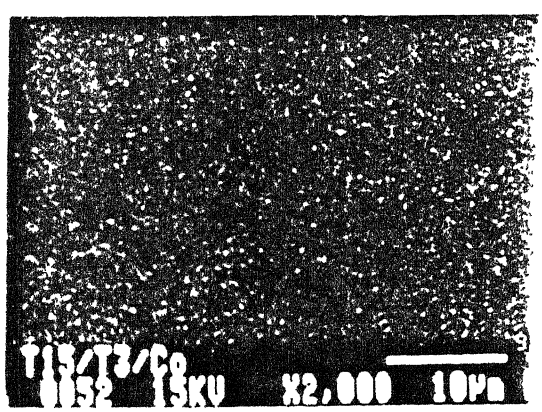

Co

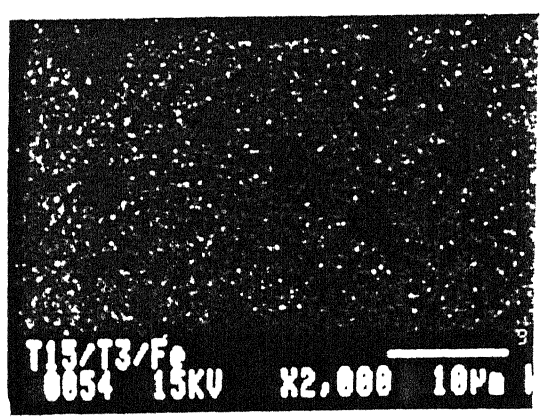

Fe

Figure 3.7. X-ray mapping analysis of vacuum sintered and triple tempered T15 HSS.

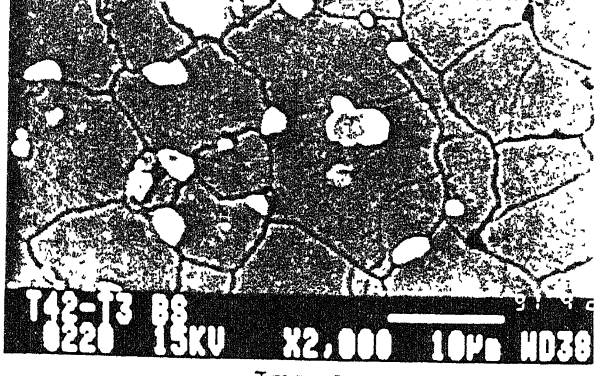

Image

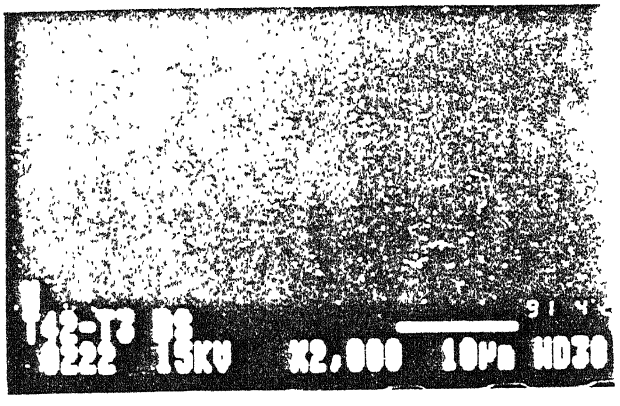

W

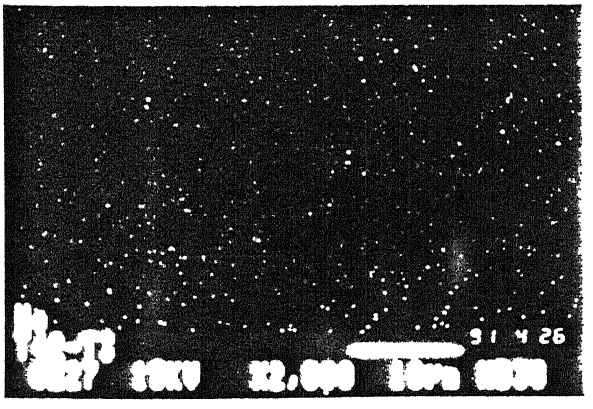

Mo

V

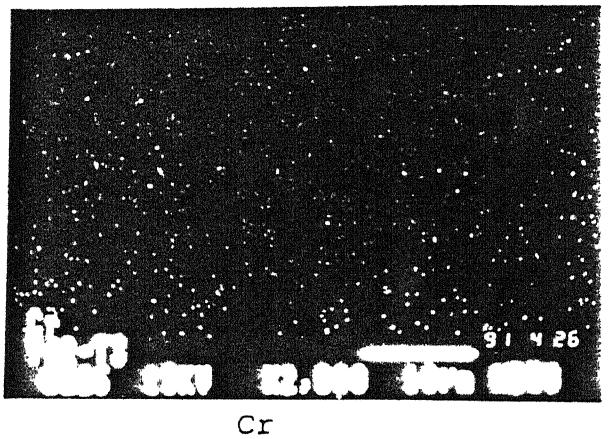

Cr

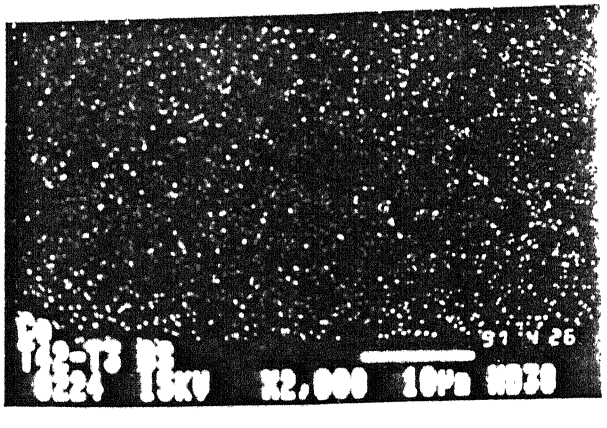

Co

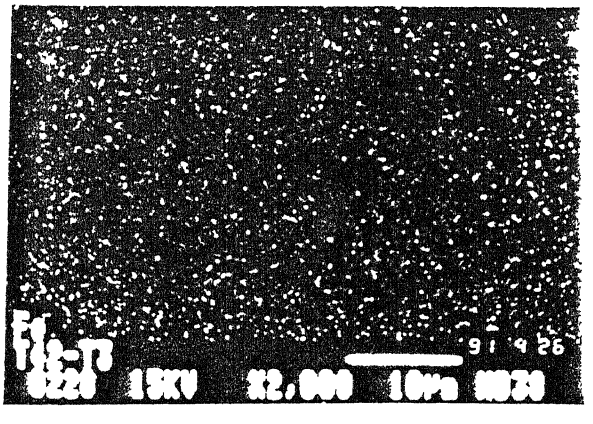

Fe

Figure 3.8. X-ray mapping analysis of vacuum sintered and triple tempered T42 HSS.

carbide. It was also confirmed from qualitative microstructural analysis that amount of MC type of carbide was more in T15 HSS than T42 HSS.

III.2. HSS COMPOSITES CONTAINING TiB_2:

III.2.1. Densification:

Two types of experiments were performed with TiB_2 containing composites. In one set of experiments T15 and T42 composites containing 2 to 8 mass % TiB_2 as dispersoids have been sintered in vacuum and in another set, T15 HSS based composites were sintered in hydrogen. The densification behaviour in both the sets of experiments are discussed separately.

III.2.1A. Densification Behaviour of Vacuum Sintered HSS Composites Containing TiB_2:

The densification behaviour of vacuum sintered T15 HSS containing 2 to 8 mass % TiB_2 is shown in Figure 3.9. Except 2 mass % TiB_2 containing composite, none of the remaining composites could achieve full density after 1220°C. After 1220°C sintering, densities achieved by the composites containing more than 2 mass % TiB_2 were lower than the remaining composites. Beyond 1220°C, T15 HSS samples containing more than 4 mass % TiB_2 got grossly distorted. Figure 3.9b shows the total porosity variation in the composites at various sintering temperatures. In general with the increase in TiB_2 content the optimum sintering temperature had to be

raised to achieve maximum density. For further experiments only those TiB_2 containing composites (sintered at 1220°C) were chosen, which achieved maximum density.

Figure 3.10 shows the densification behaviour of T42 HSS containing 2 to 8 mass % of TiB_2. Similar to T15-TiB_2 composites, except 2 mass % TiB_2 containing composite, none other could achieve full density. After 1190°C sintering, 2 and 4 mass % TiB_2 containing composites achieved maximum density. Beyond 1190°C, with further increase in temperature the densities of 2 and 4 mass % TiB_2 containing T42 HSS remained more or less constant. 6 and 8 mass % TiB_2 containing composites of such series achieved maximum density at 1200°C, beyond which they got grossly distorted. In general, optimum sintering temperature increased with the increase in TiB_2 content to achieve maximum density [Figure 3.10]. Similar to T15 HSS maximum dense composites (sintered at 1200°C) were selected for further experiments. Figure 3.11 shows the total porosity variation of T42-TiB_2 composites with respect to the sintering temperature.

III.2.1b. Densification Behaviour of T15 HSS Composites Containing TiB_2 Sintered in Hydrogen at 1210°C:

The densification behaviour of T15 HSS containing 2 to 8 mass % TiB_2 is shown in Figure 3.12. It was noticed that with the increase in TiB_2 content sintered density decreased. Neither of the above composites could achieve full density after sintering.

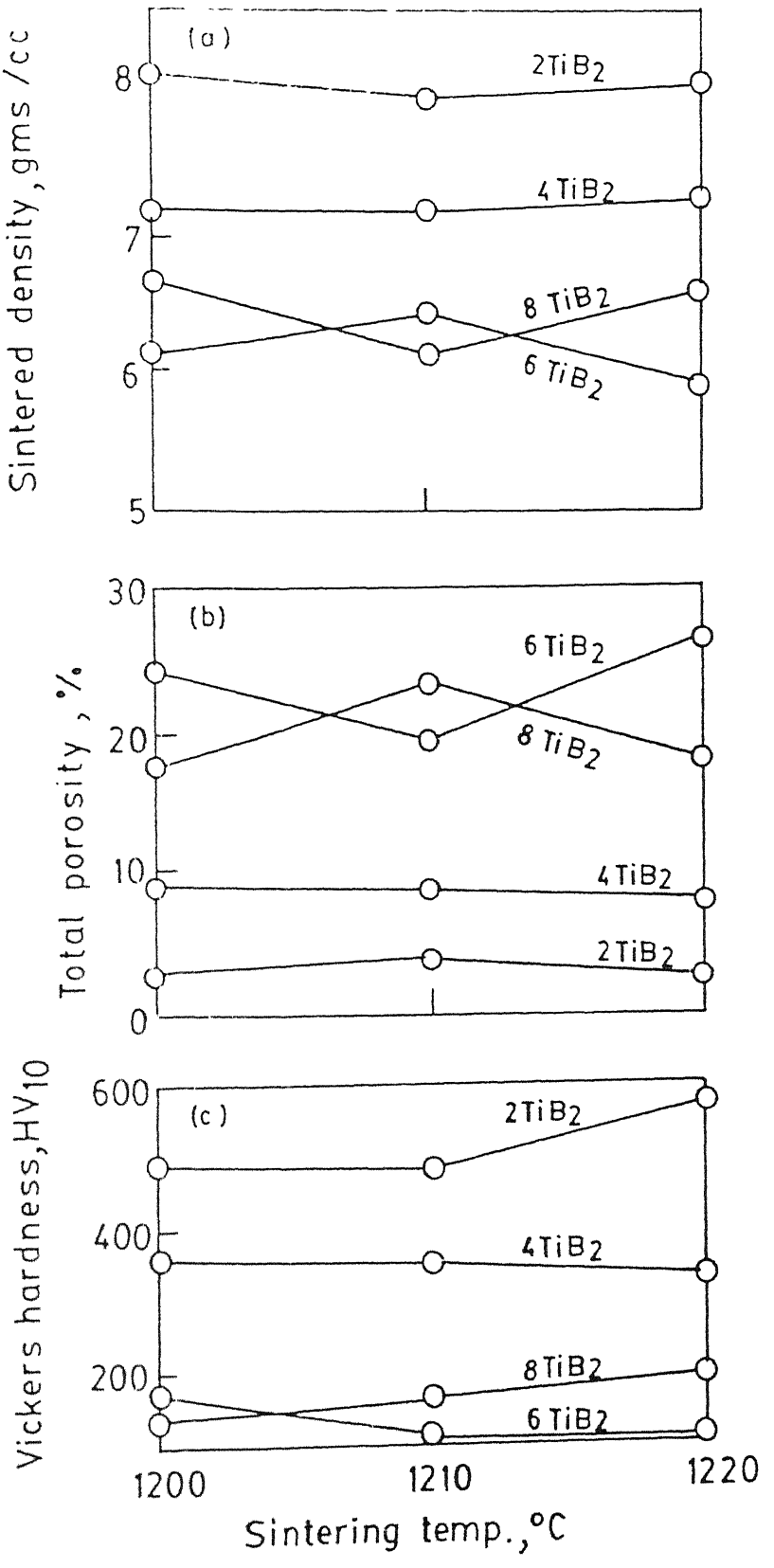

Fig. 3.9 Effect of TiB_2 addition on (a) density (b) Total porosity and (c) Vickers hardness of T 15 HSS vacuum sintered at different temperatures

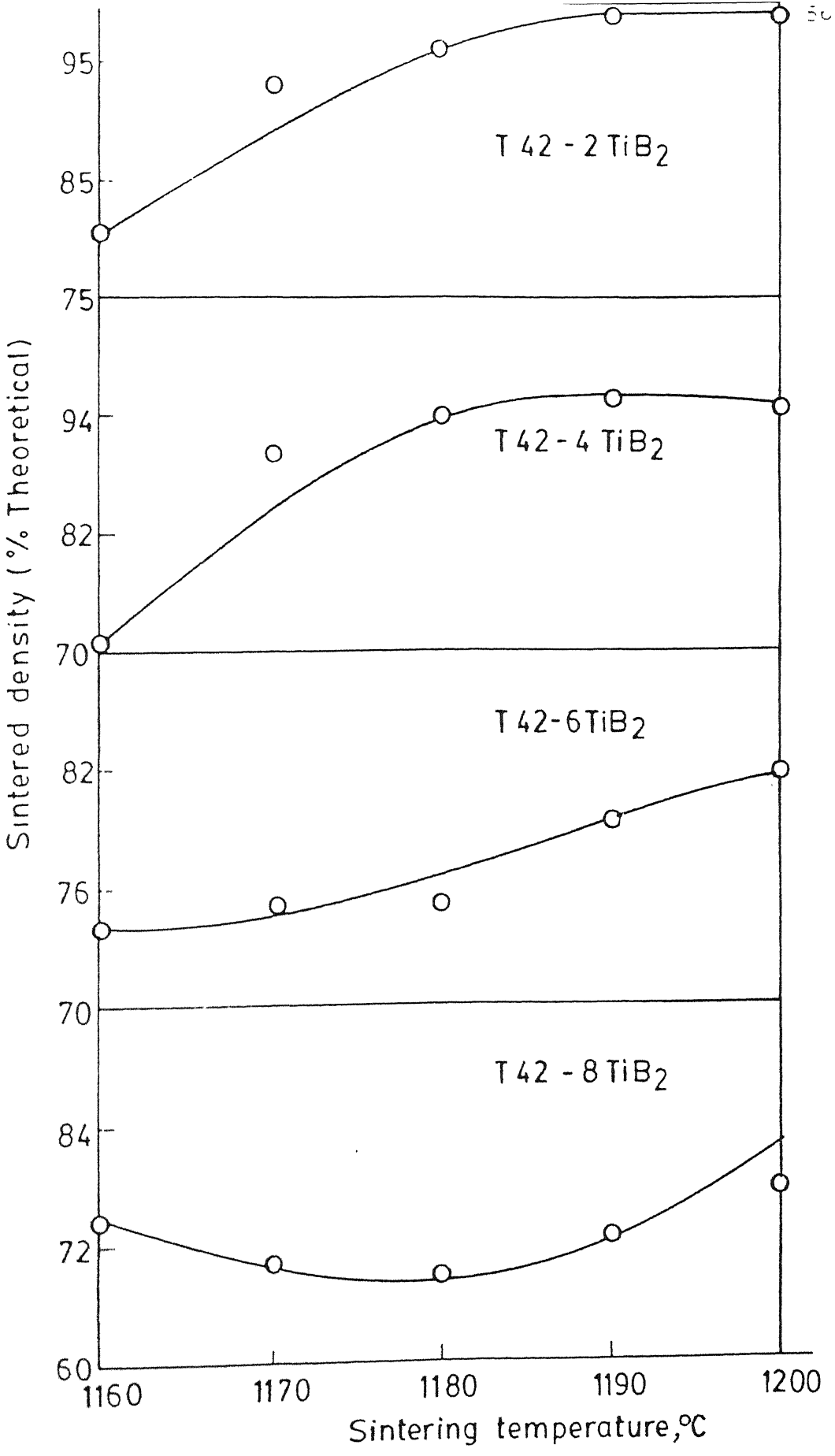

Fig. 3.10 Effect of sintering temperature on % theoretical

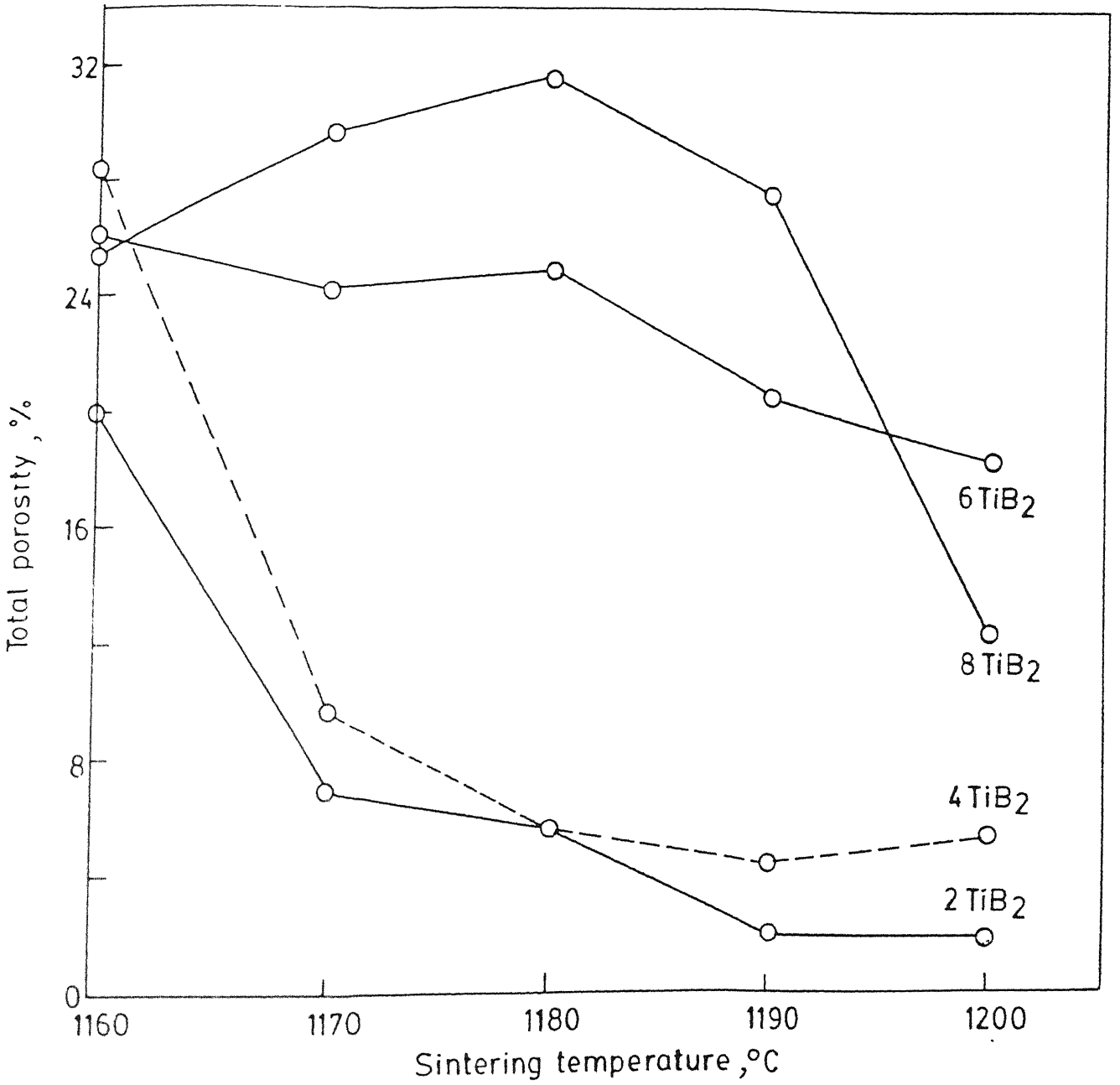

ig 3.11 Total porosity variation of vacuum sintered T42-TiB_2 composites with respect to sintering temperature

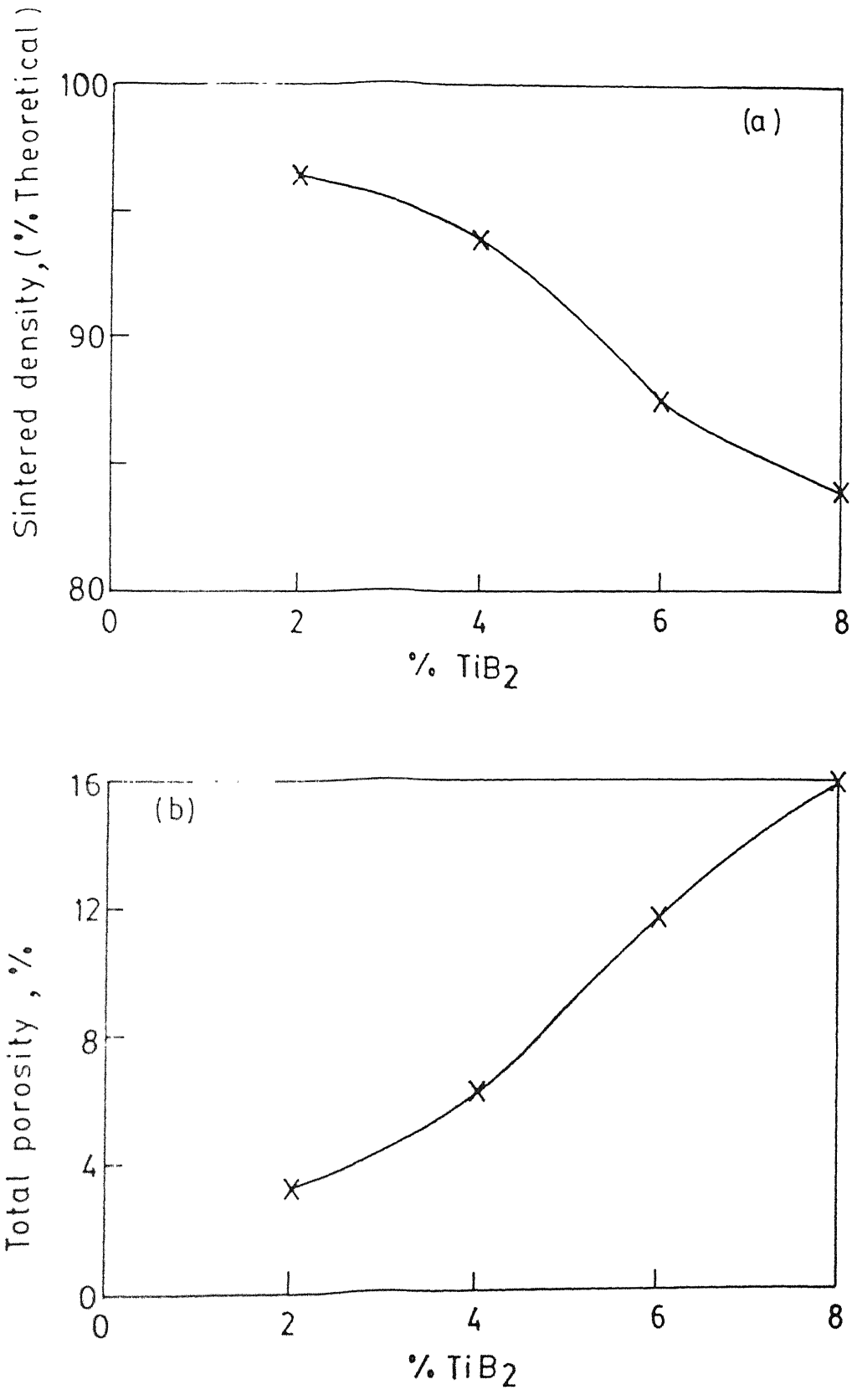

Fig 3.12 Effect of TiB_2 addition on (a) % Theoretical density and (b) Total porosity of hydrogen sintered T 15 HSS (Sintered at 1210°C for 1-5 hrs)

III.2.2. Hardness:

The sintered hardness variation of vacuum sintered TiB_2 containing T15 HSS is shown in Figure 3.9c. The sintered hardness decreased with the increase in TiB_2 content. With the increase in sintering temperature, hardness of 2 and 6 mass % TiB_2 containing composites increased, whereas the reverse is true for 4 and 8 mass % TiB_2 containing composites. T15 HSS composite containing 2 mass % TiB_2 achieved a maximum sintered hardness of 570 HV_{10} after 1220°C sintering. The sintered hardness variation of TiB_2 containing T42 HSS is shown in Figure 3.13. Similar to T15 HSS composites the sintered hardness decreased with the increase in TiB_2 content. Except for 8 mass % TiB_2 containing composites, all other T42-TiB_2 composites showed an increase in hardness with the increase in sintering temperature. T42 HSS composite containing 2 mass % TiB_2 achieved a maximum sintered hardness of 613 HV_{10} after sintering at 1200°C. The hardness variation of hydrogen sintered T15-TiB_2 composites is shown in Figure 3.14. Similar to those for vacuum sintered ones hydrogen sintered T15 HSS composites showed a decreasing trend in hardness with the increase in TiB_2 content, the maximum being for T15-2TiB_2 composite (530 HV_{10}).

Figure 3.15b shows the as sintered and single/triple tempered hardness variation of vacuum sintered T15 HSS with respect to TiB_2 addition. It was noticed that triple tempered hardness was lower than the single tempered

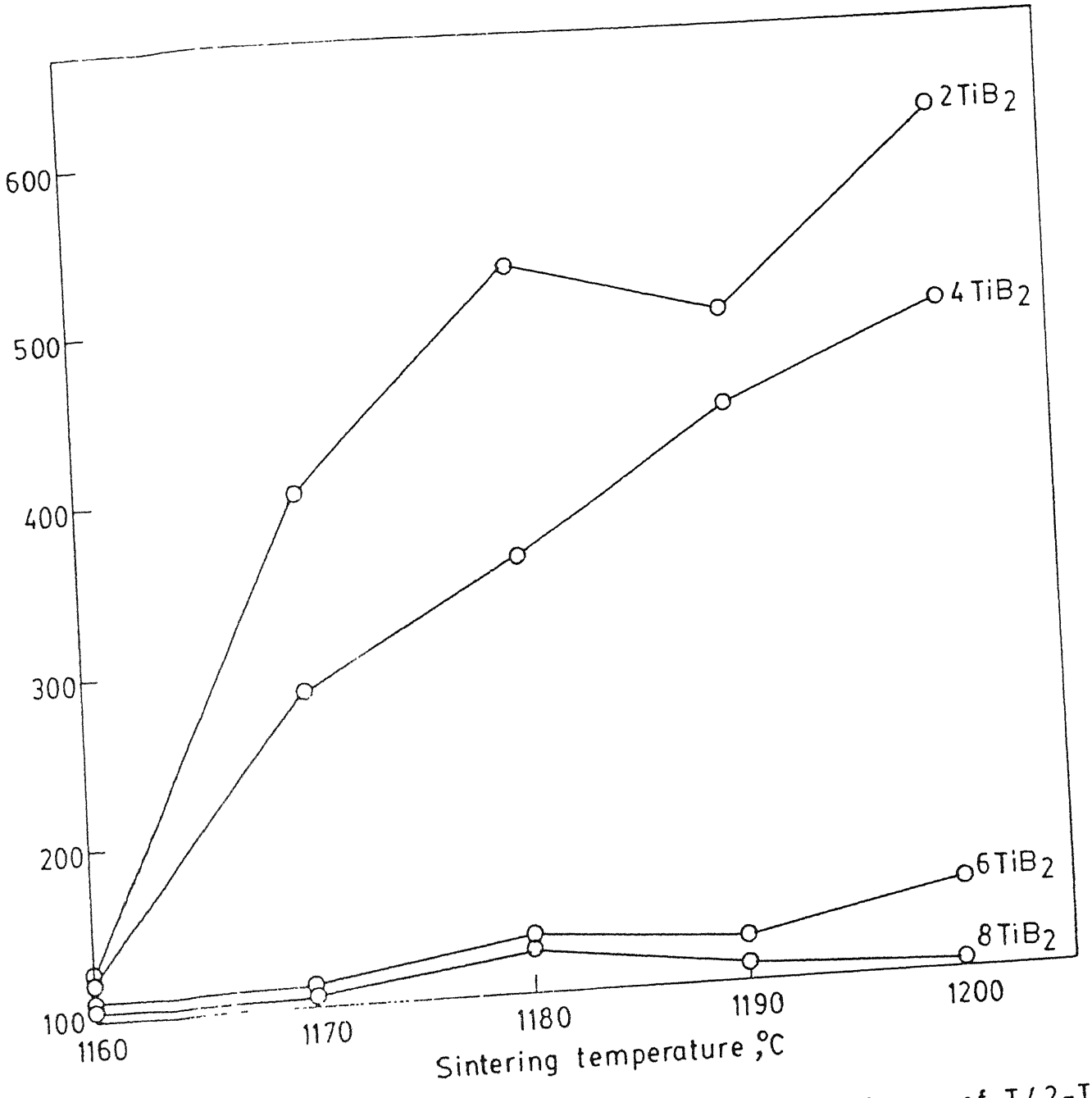

Fig. 3.13 Effect of sintering temperature on vickers hardness of T42-TiB_2 composites

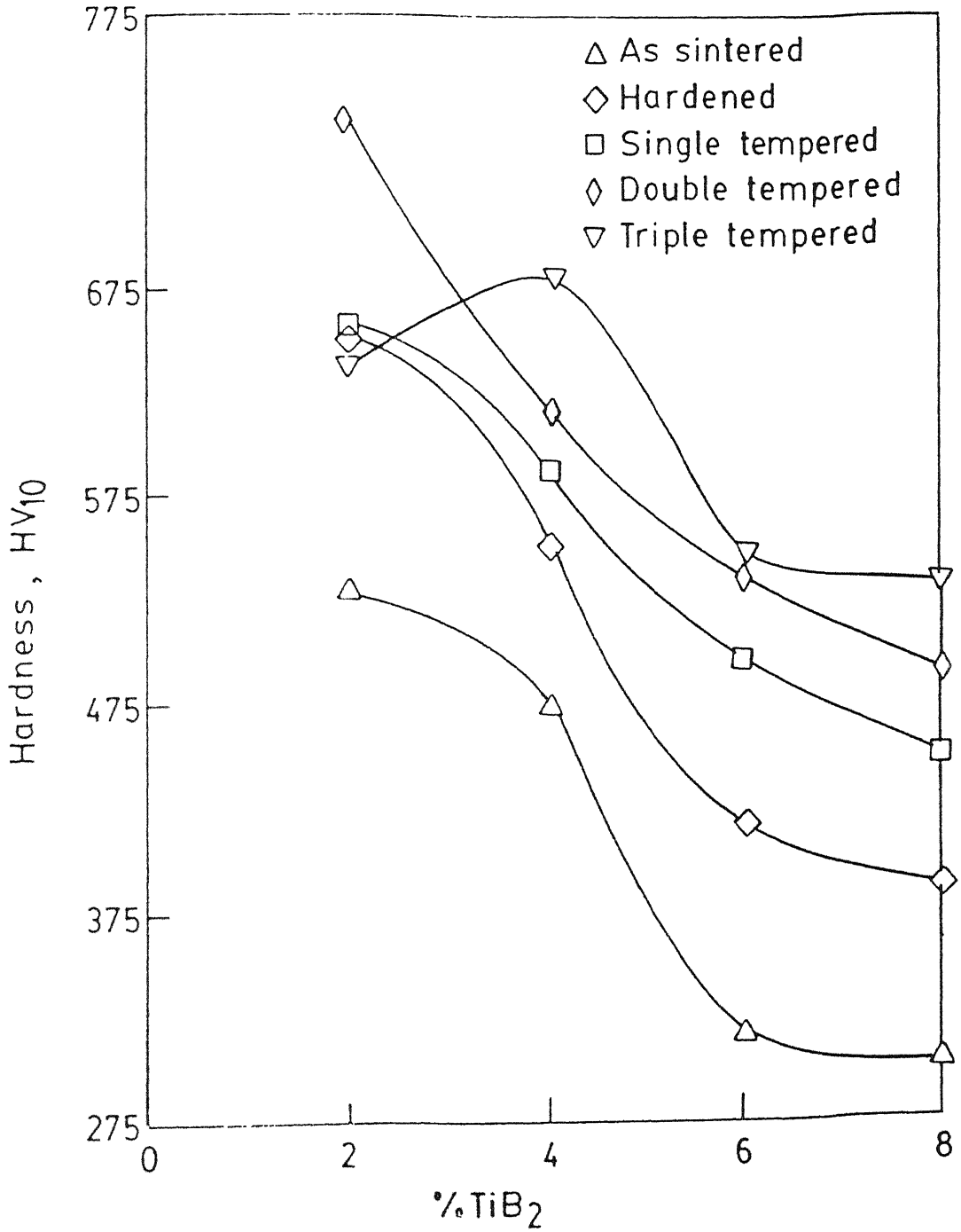

Fig. 3.14 Vickers hardness variation of T 15 - TiB_2 Composites sintered in hydrogen at 1210° for 1.5 hrs.

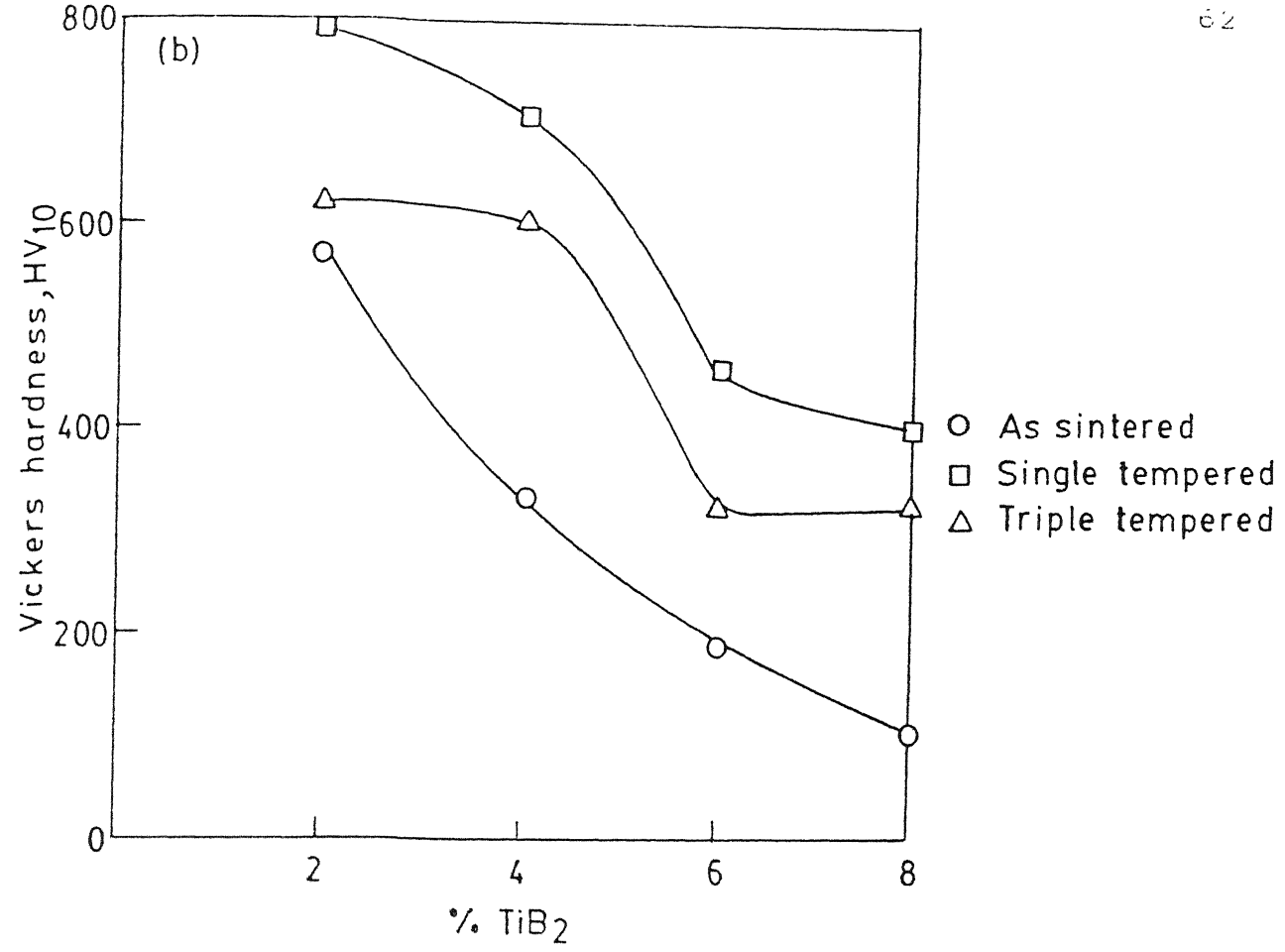

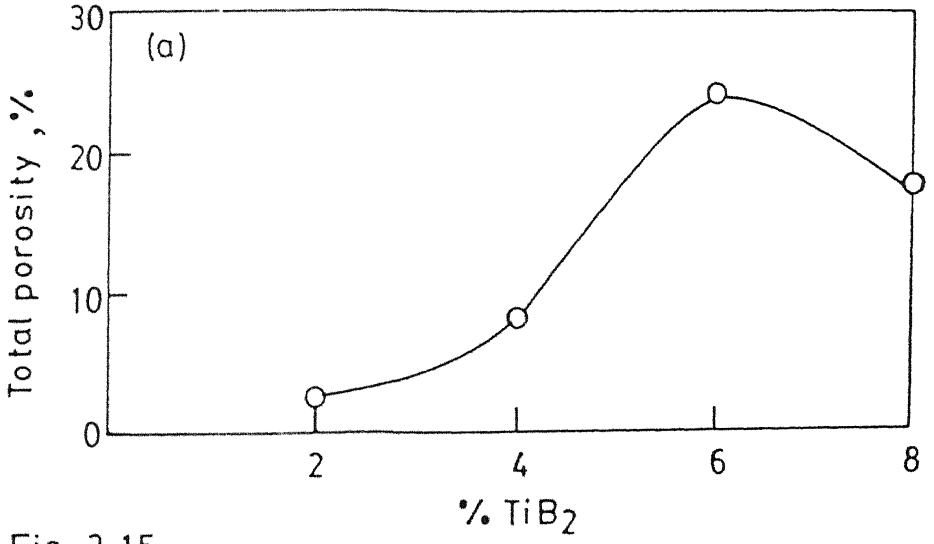

Fig. 3.15

Variation of (a) Total porosity and (b) Vickers hardness of T15 - TiB_2 composites sintered in vaccum at 1220°C for 1.5 hrs

Hardness value of TiB_2 containing T42 HSS could not be determined after heat treatment because all the composites got grossly distorted during hardening. Figure 3.14 shows the as sintered, hardened and tempered hardness variation of hydrogen sintered TiB_2 containing T15 HSS composites. Except for 2 mass % TiB_2 containing composites, all other composites achieved maximum hardness value after triple tempering. 2 mass % TiB_2 containing composites showed a maximum hardness value after double tempering. Hardness in general was found to increase with increase in number of temperings.

III.2.3. Microstructural Analysis:

Figure 3.16 shows optical microstructures of 2 and 6 mass % TiB_2 containing T15 HSS (vacuum sintered at 1220°C) in as sintered and triple tempered conditions. Microstructures reveal the presence of a number of pores indicating the lack of full densification. White primary carbides and dark phase are observed in the microstructure. The dark phase is titanium based phase and white phase corresponds to M_6C type of carbides. This fact was confirmed by EDX analysis [Table III.2]. Figure 3.17 shows optical microstructures of TiB_2 containing T42 HSS sintered at 1190°C. Here also many large pores are observed in the microstructure showing poor densification except 2 mass % TiB_2 containing composites. All the above mentioned phases as in case of T15-TiB_2 composites are also present in T42-TiB_2 HSS.

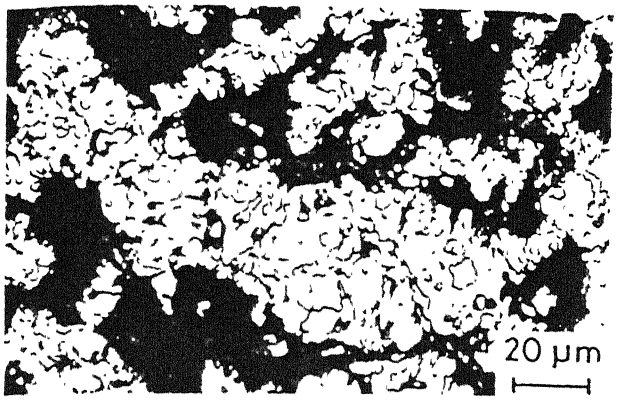

Sintered

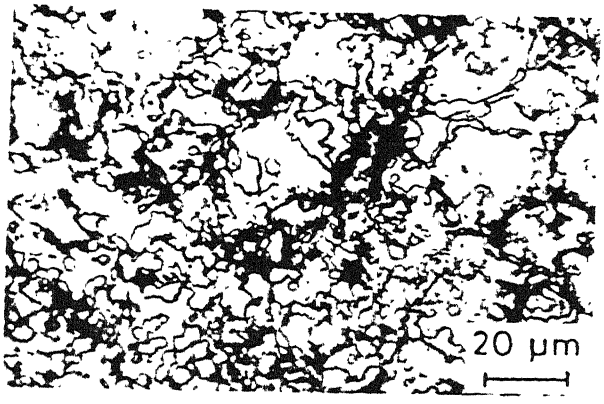

Sintered

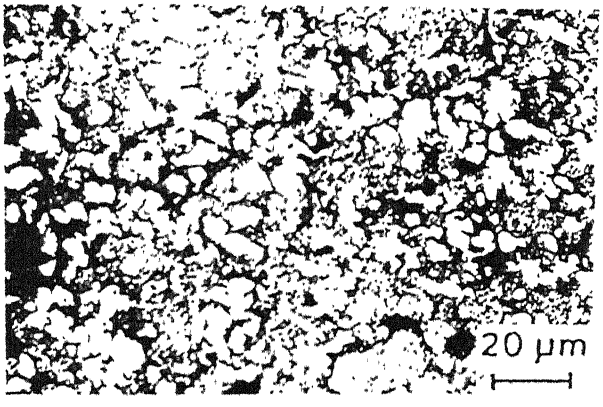

Triple tempered

2% TiB_2

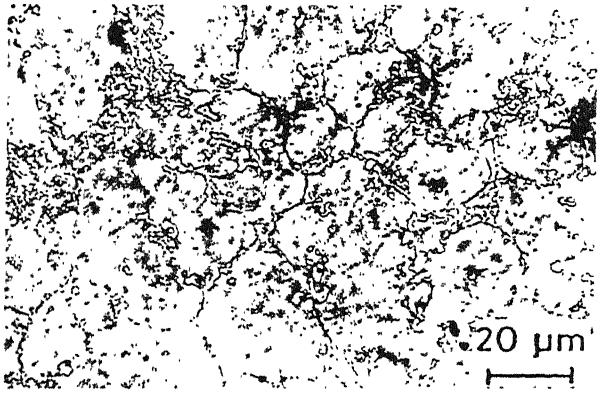

Triple tempered

6% TiB_2

Figure 3.16. Optical microstructures of vacuum sintered T15-TiB_2 composites.

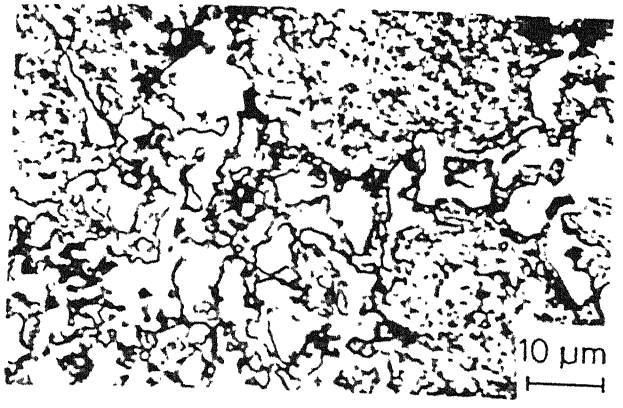

2% TiB_2

4% TiB_2

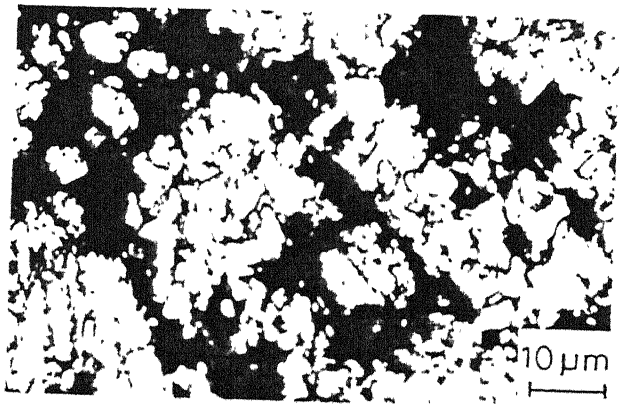

6% TiB_2

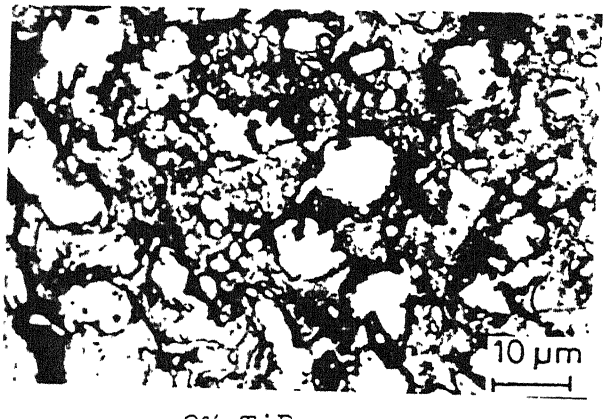

8% TiB_2

Figure 3.17. Optical microstructures of vacuum sintered T42-TiB_2 composites in as-sintered condition.

Table III.2. EDX analysis of various phases in T15-2 TiB_2 and T15-8 TiB_2 triple tempered composites.

HSS grade	Description of phase	Mass % chemical analysis							Assigned phase
		Fe	Cr	Co	Mo	V	W	Ti	
T15-2 TiB_2 (triple tempered)	Matrix	69.82	2.12	6.73	6.19	3.29	10.12	1.73	Matrix
	White phase	32.34	-	4.71	3.91	7.77	39.07	12.29	M_6C type carbide
	Black phase	3.45	-	0.78	2.10	13.53	1.05	79.09	Titanium based phase
T15-8 TiB_2 (triple tempered)	Matrix	85.89	2.74	11.15	0.03	-	0.07	0.12	Matrix
	White phase	24.76	8.31	6.05	8.04	13.46	35.75	3.62	M_6C type carbide
	Black phase	20.87	3.02	3.38	-	13.04	8.04	51.65	Titanium based phase

Figure 3.18 shows the optical and SEM microstructures of 2 and 6 mass % TiB_2 containing composites of T15 HSS (H_2 sintered at 1210°C). Once again confirming the phases as were observed in the case of vacuum sintered ones. The phases observed in the microstructure were M_6C carbide (white), Ti based phase (black) and matrix.

Figures 3.19 and 3.20 show the X-ray mapping analysis of 2 and 6 mass % TiB_2 containing T15 HSS (hydrogen sintered at 1210°C) in triple tempered condition. From the distribution of the elements it is clear that TiB_2 got decomposed and dissolved into the matrix. This was also confirmed by EDX analysis (Table III.2).

III.3. HSS COMPOSITES CONTAINING Ti(C,N):

III.3.1. Densification:

The densification behaviour of T15 HSS containing 0 to 6 mass % Ti(C,N), sintered in hydrogen is shown in Figure 3.21. At 1220°C, T15 straight composition achieved full density. With the exception of 4% Ti(C,N) all other composites could not be fully densified at this temperature. Figure 3.22a shows the effect of Ti(C,N) addition in T15 HSS on sintered density at a constant sintering temperature of 1200°C, while Figure 3.22b shows the optimum sintering temperature required to achieve full density.

Figure 3.23 shows the densification behaviour of T42 HSS composites containing 0 to 6 mass % Ti(C,N). The sintering temperature to achieve full density for T42 straight HSS and its 2 mass % Ti(C,N) containing composites were

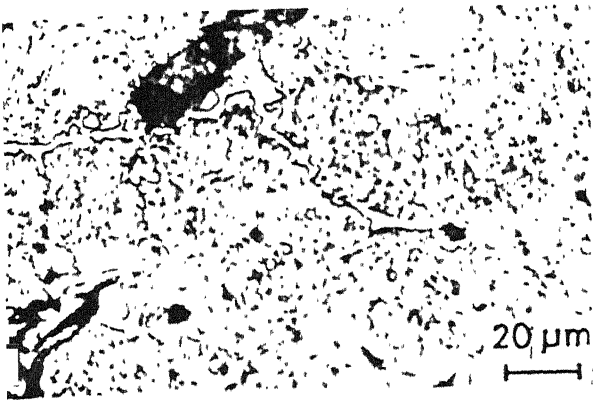

Sintered (optical)

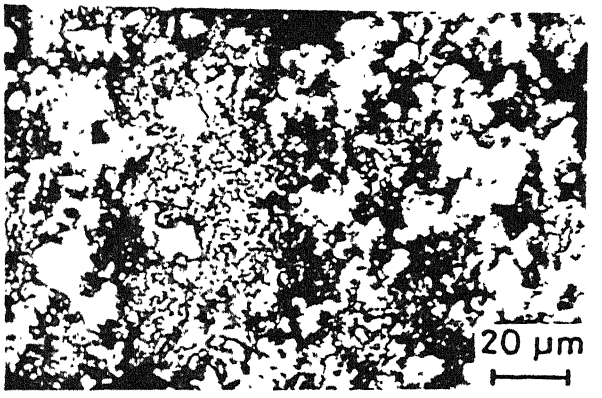

Sintered (optical)

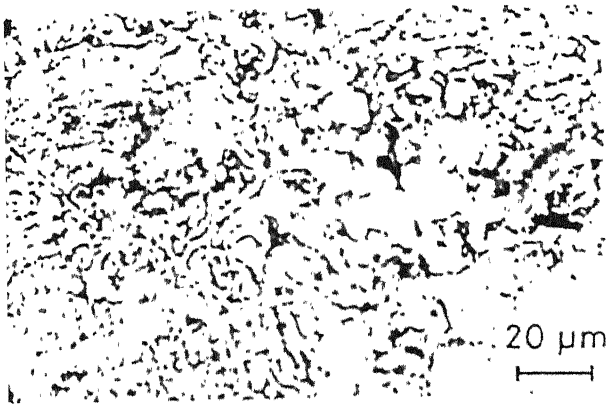

Triple tempered (optical)

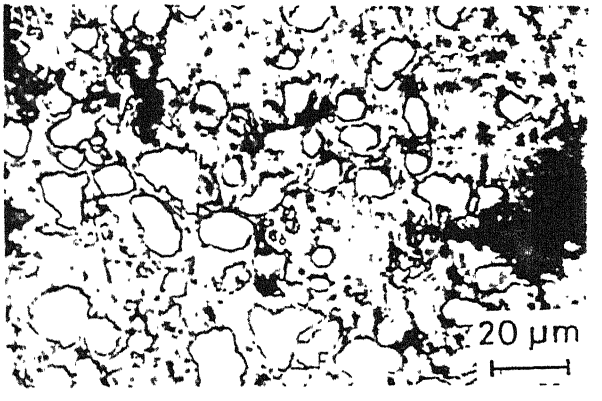

Triple tempered (optical)

Triple tempered (SEM)

2% TiB_2

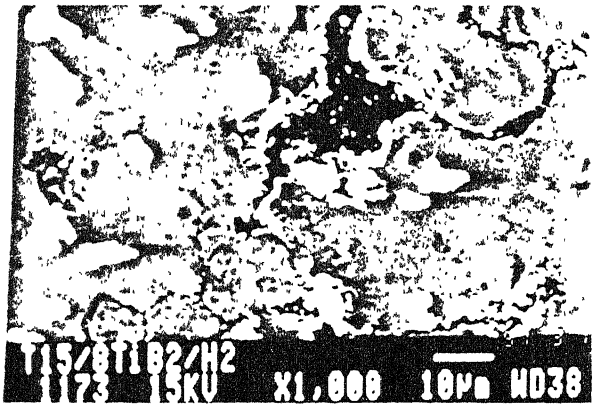

Triple tempered (SEM)

8% TiB_2

Figure 3.18. Optical and SEM microstructures of hydrogen sintered T15-TiB_2 composites.

Image

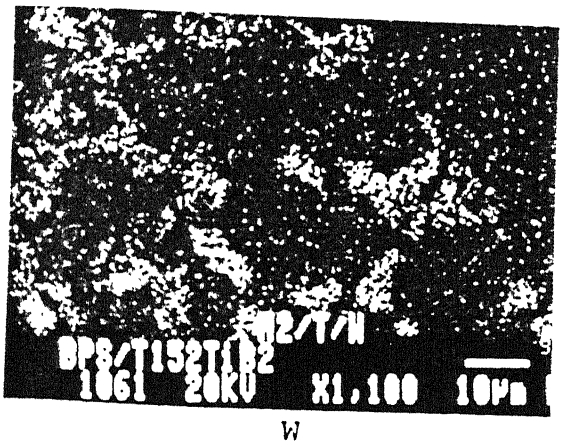

W

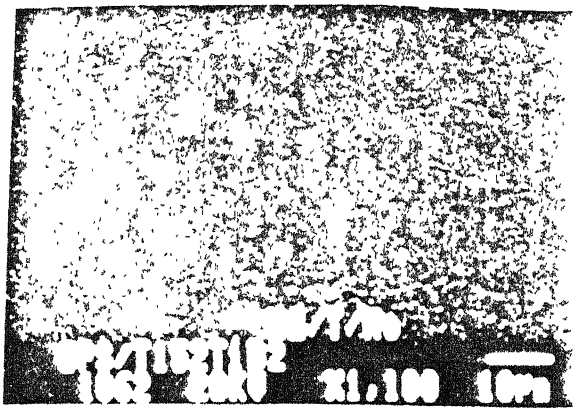

MO

V

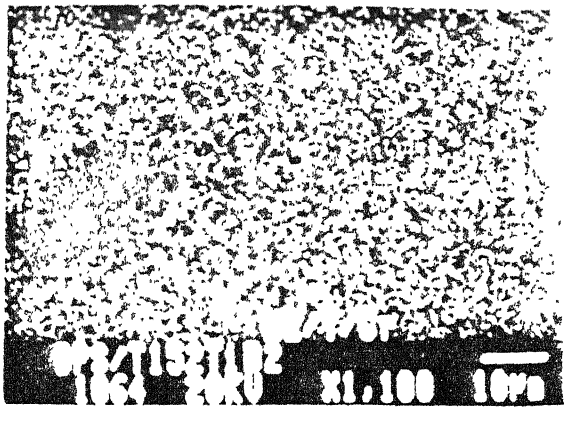

Cr

Co

Fe

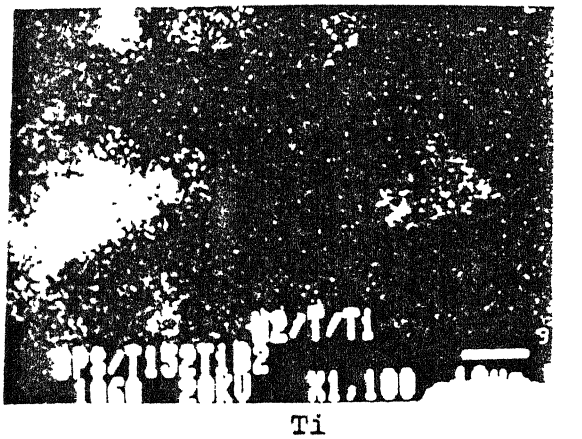

Ti

Figure 3.19. X-ray mapping analysis of triple tempered T15-2TiB$_2$ composite (hydrogen sintered at 1210°C).

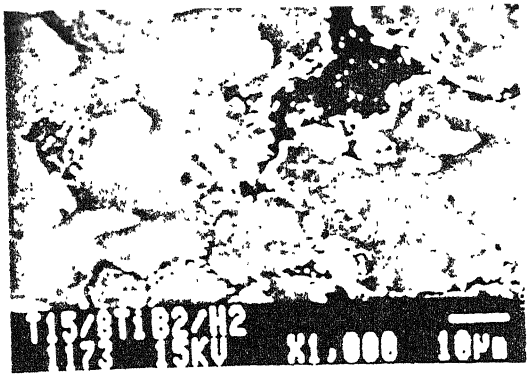

Image

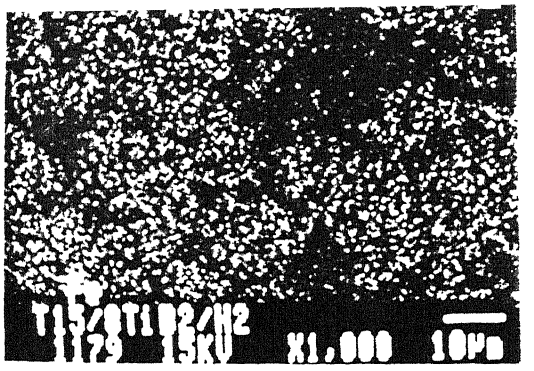

W

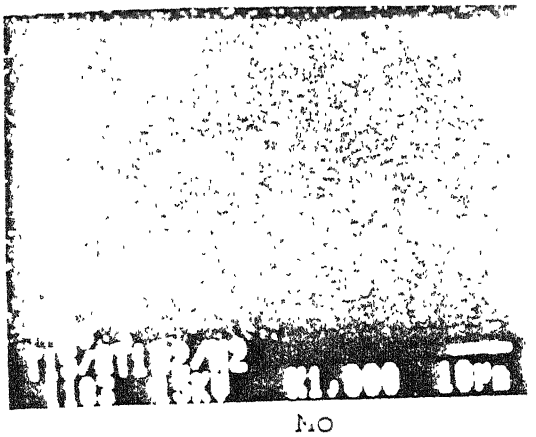

Mo

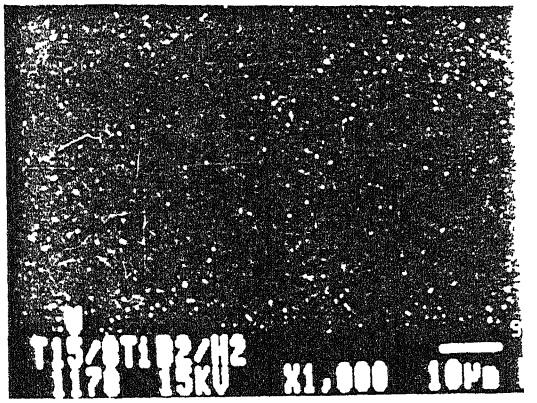

V

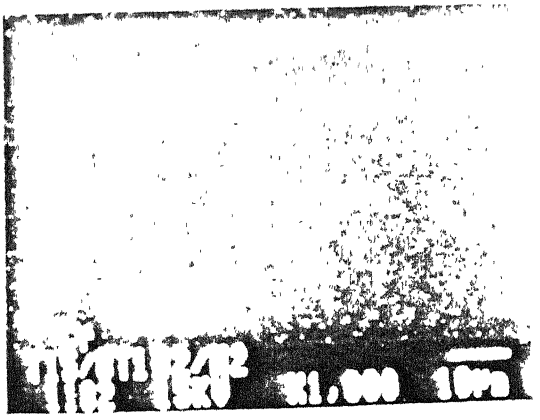

Cr

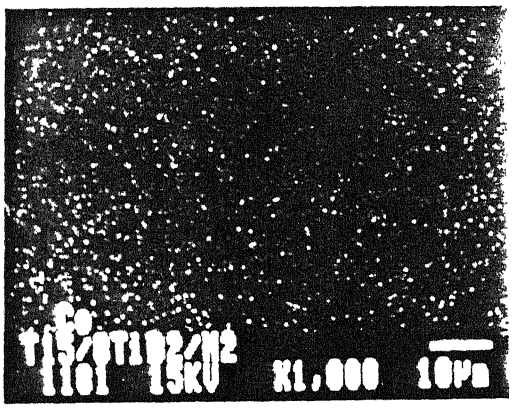

Co

Fe

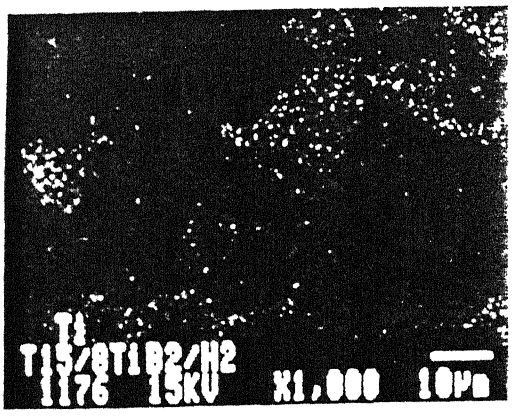

Ti

Figure 3.20. X-ray mapping analysis of triple tempered T15-8TiB_2 composite (hydrogen sintered at 1210^{o}C).

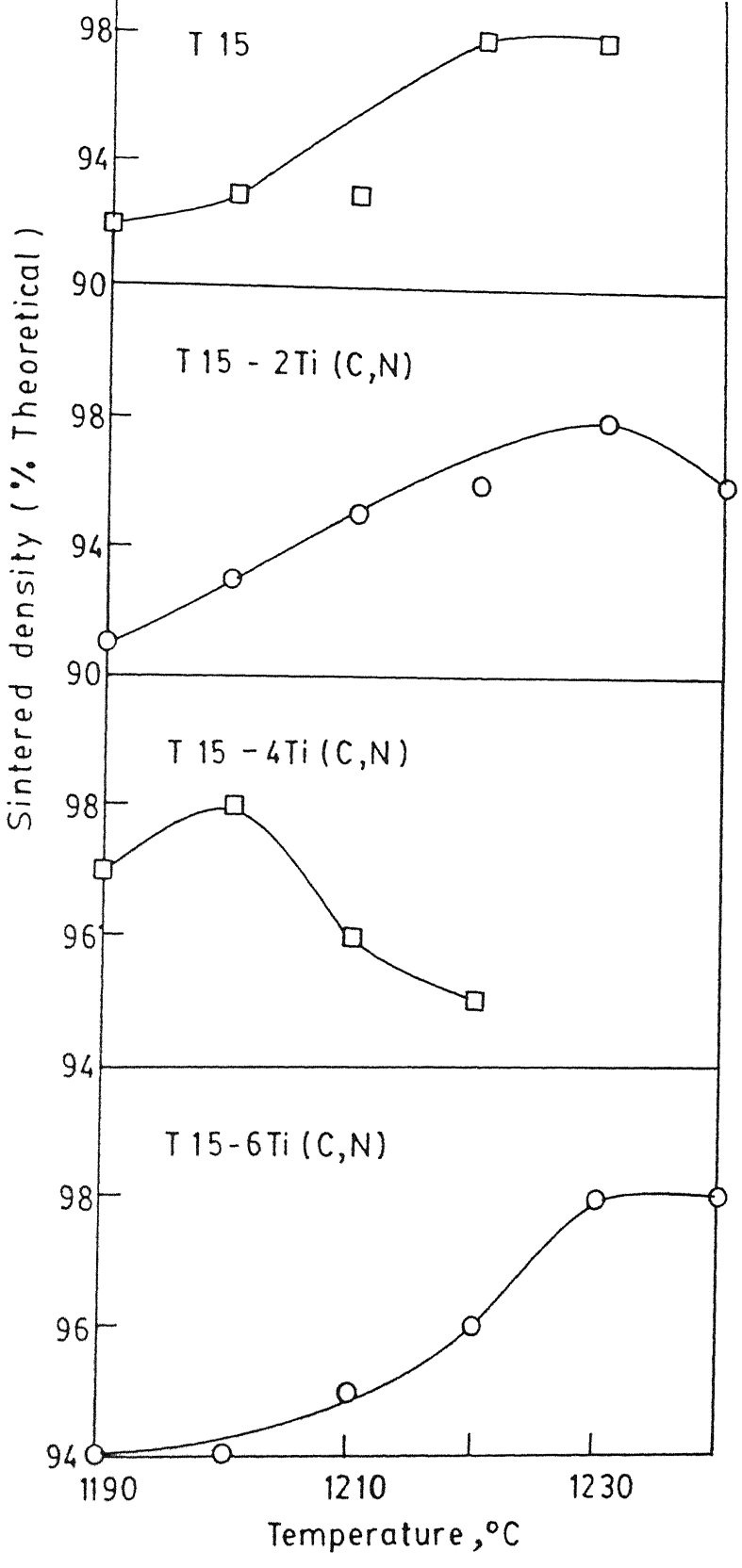

Fig. 3.21 Sintered density variation of T15 -Ti(C,N) composites hydrogen sintered at different temperatures

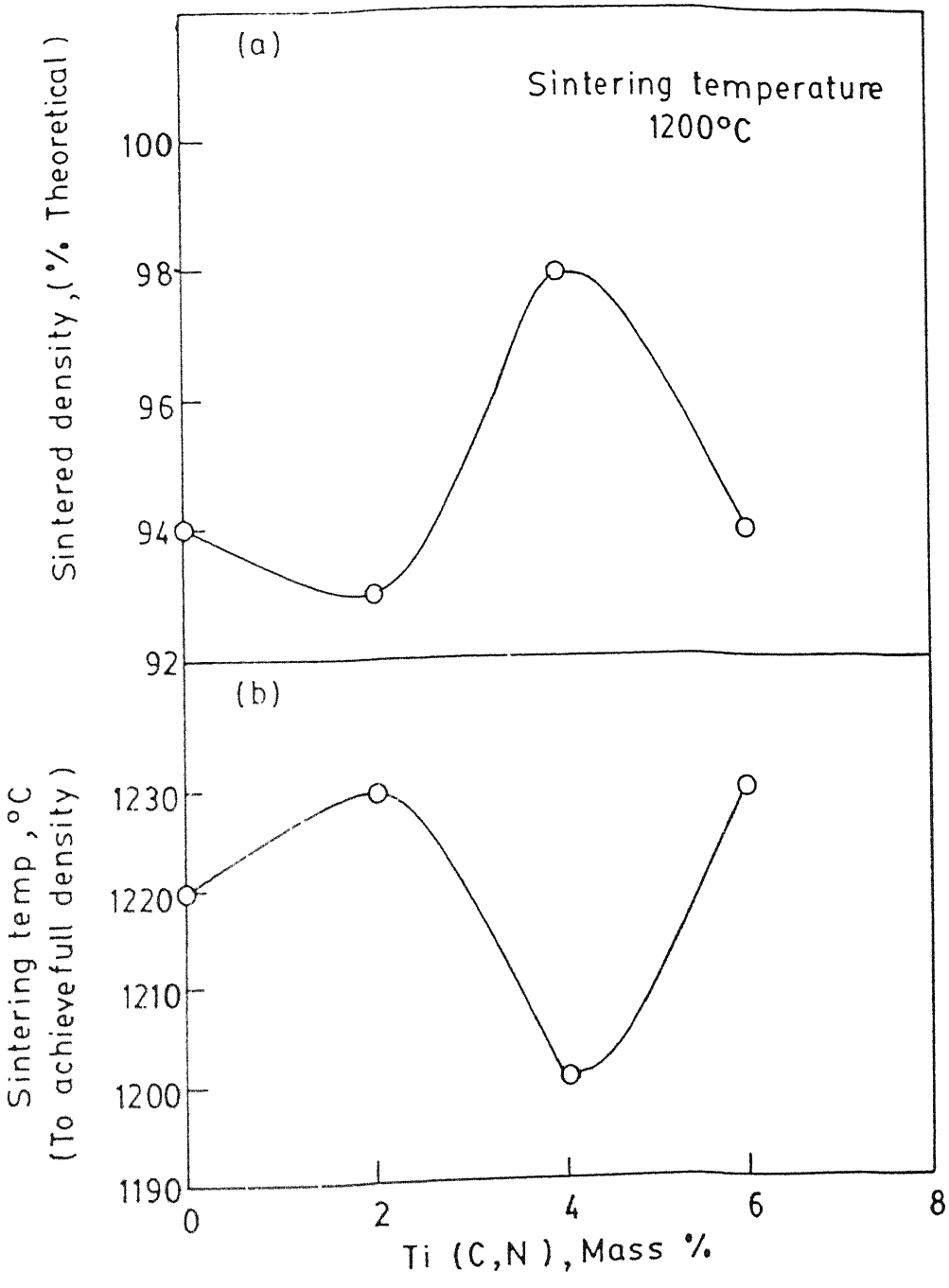

Fig. 3.22 Effect of Ti(C N) addition on (a) Sintered density and (b) Optimum sintering temperature to achieve full density for hydrogen sintered T15 HSS

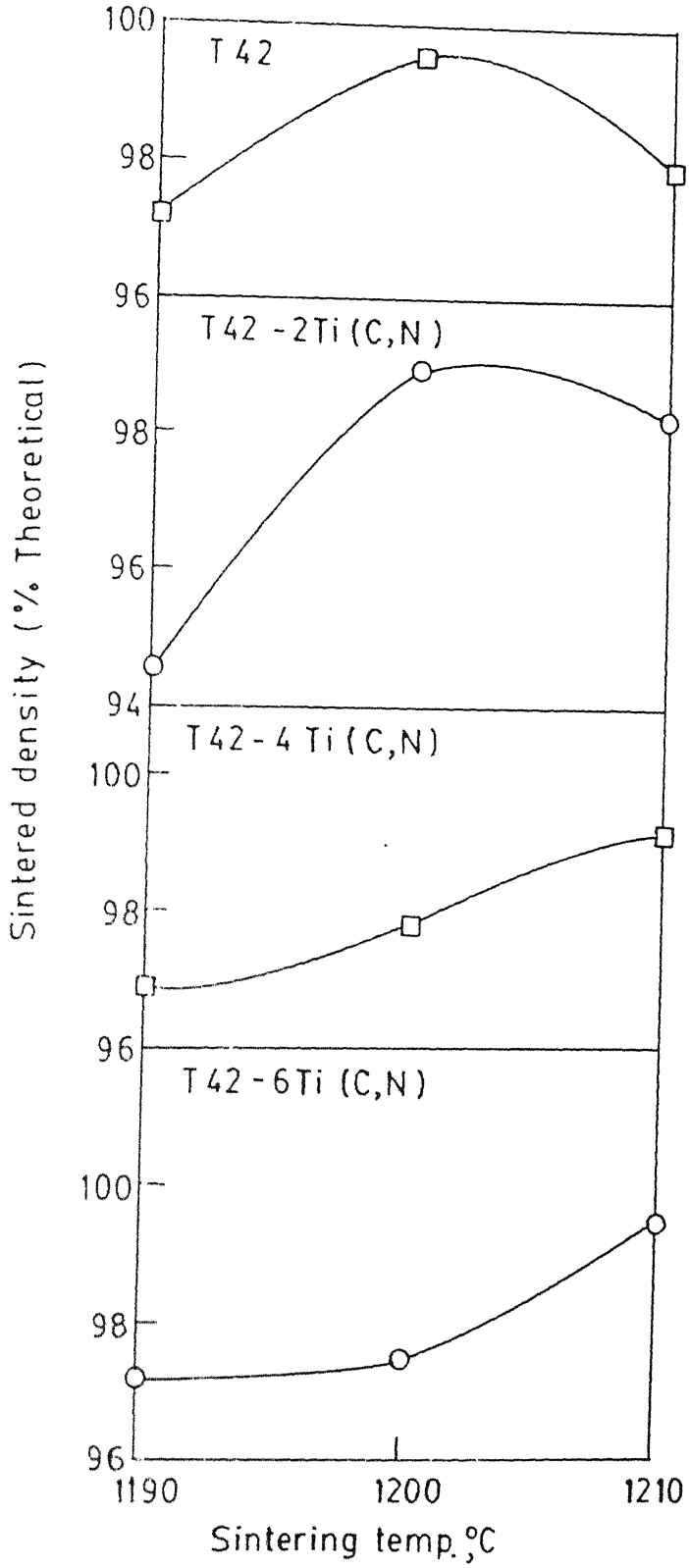

Fig 3.23 Sintered density variation of T42 -Ti (C,N) composites hydrogen sintered at different temperatures.

the same i.e. 1200°C. For the composites containing 4 and 6 mass % Ti(C,N) the sintering temperature to achieve full density was higher than the remaining composites. For any T15 HSS—Ti(C,N) composite, the marginal increase in the sintered density with the increase in sintering temperature was lower than the corresponding T42 HSS based composite.

Figure 3.24 shows the effect of Ti(C,N) addition on the densification behaviour and the optimum sintering temperature to achieve full density for the Ti(C,N) containing T42 HSS composites. The optimum temperature required for attaining full density increased with the increase in Ti(C,N) content [Figure 3.24b].

III.3.2. Hardness:

Figure 3.25 shows the hardness variation of straight T15 HSS and its Ti(C,N) containing composites in as sintered, hardened and tempered conditions. It was noticed that with the increase in Ti(C,N) content the hardness values increased. There was a slight increase in as-sintered hardness with the increase in Ti(C,N) content. However, after tempering, the hardness of straight T15 increased with increase in number of temperings. In case of 2 mass % Ti(C,N) containing composite there was practically no decomposition of martensite, as the hardness was more or less equal to the hardness obtained after hardening. However for 4 and 6 mass % Ti(C,N) containing composites the situation was different such that the tempered hardness was

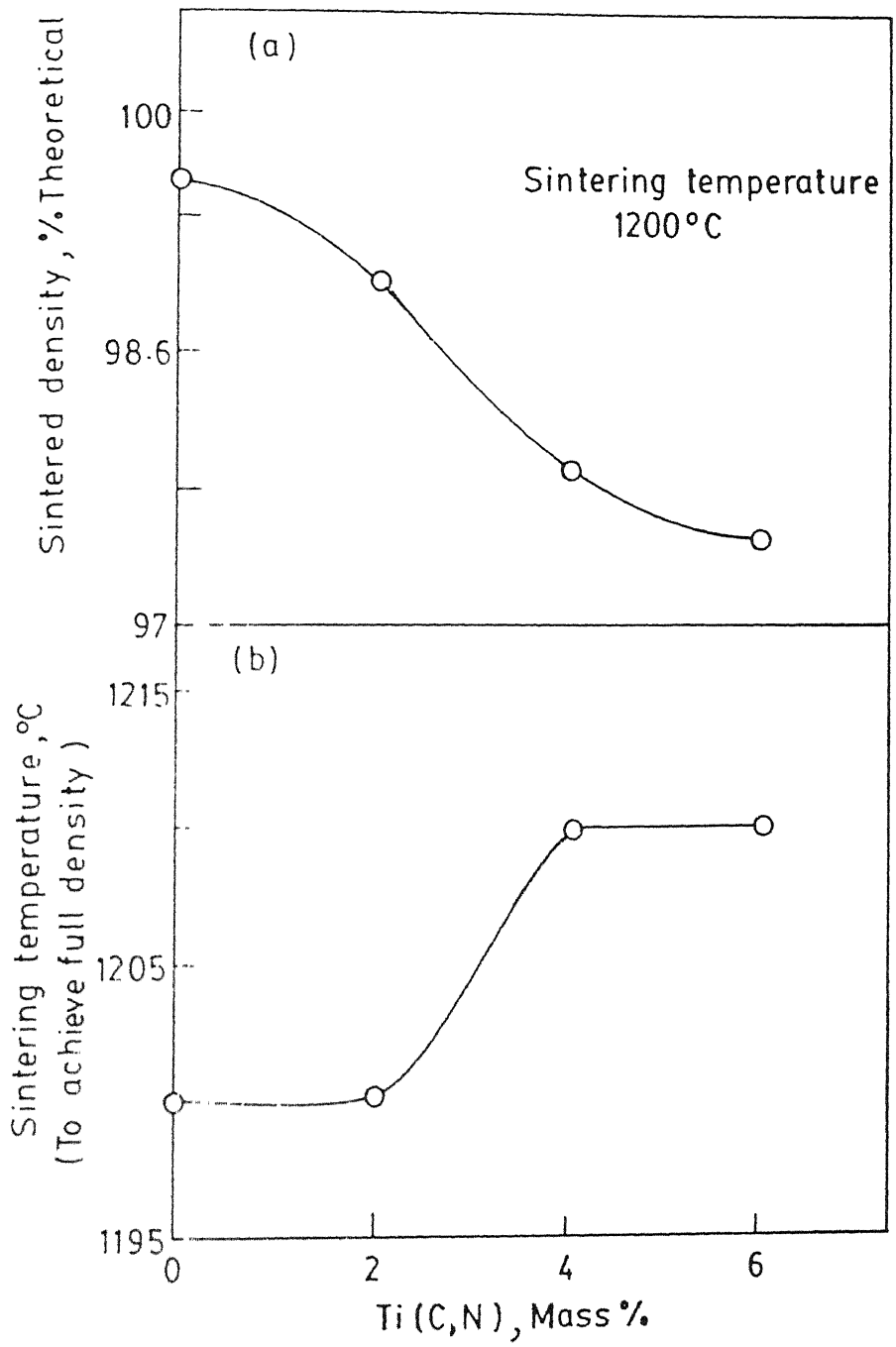

Fig. 3.24 Effect of Ti(C,N) addition on (a) Sintered density and (b) Optimum sintering temperature to achieve full density for hydrogen sintered T42 HSS

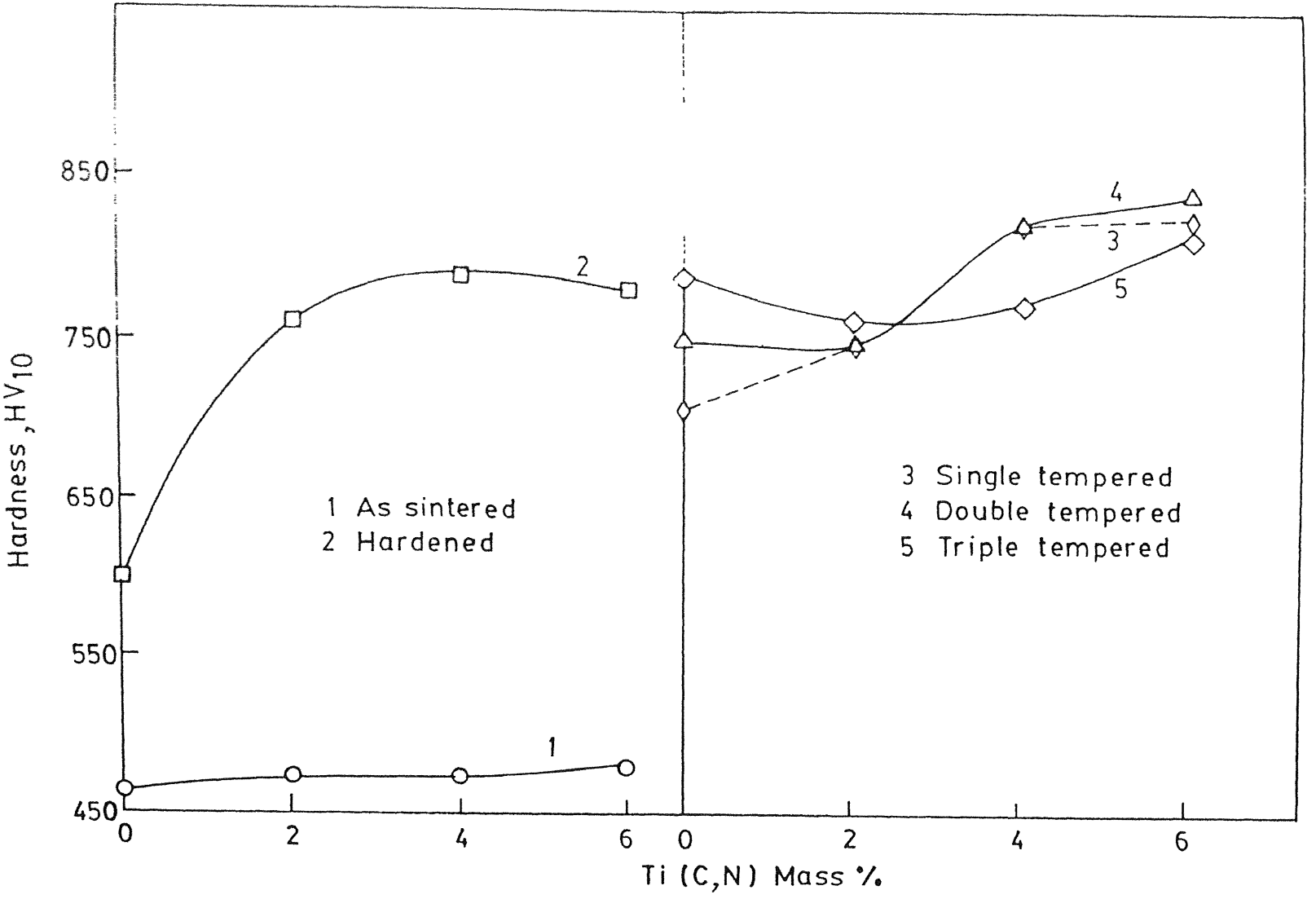

Fig. 3.25 Effect of Ti (C,N) addition on Vickers hardness of T15 HSS after hydrogen sintering and various heat treatments.

slightly greater than hardness achieved after hardening.

Figure 3.26 shows hardness variation of T42 HSS and its Ti(C,N) containing composites in as-sintered, hardened and tempered conditions. The as-sintered hardness of 2 and 4 mass % Ti(C,N) containing composites of T42 HSS was less than that of T42 straight HSS, whereas in case of T42-6Ti(C,N) composite, the as-sintered hardness was higher than the straight T42 HSS. It was noticed that in hardened as well as in tempered conditions hardness of the T42 composites increased with the increase in Ti(C,N) content. It was also noticed that in triple tempered condition all the composites except T15-6Ti(C,N), showed more or less same hardness values. Hardness was found to increase with increase in the number of temperings. The highest hardness obtained was 840 HV_{10} for T15 HSS composite containing 6 mass % Ti(C,N) after double tempering [Figure 3.25] whereas T42 HSS and all of its Ti(C,N) containing composites showed highest hardness values after triple tempering which were more or less same [Figure 3.26].

III.3.3. Transverse Rupture Strength (TRS):

For transverse rupture strength determination, only those composites were selected which showed maximum hardness after tempering. The TRS variation with respect to Ti(C,N) addition of tempered T15 and T42 HSS based composites are shown in Figure 3.27. In case of T15 HSS composites [Figure 3.27a], TRS gradually increased with the

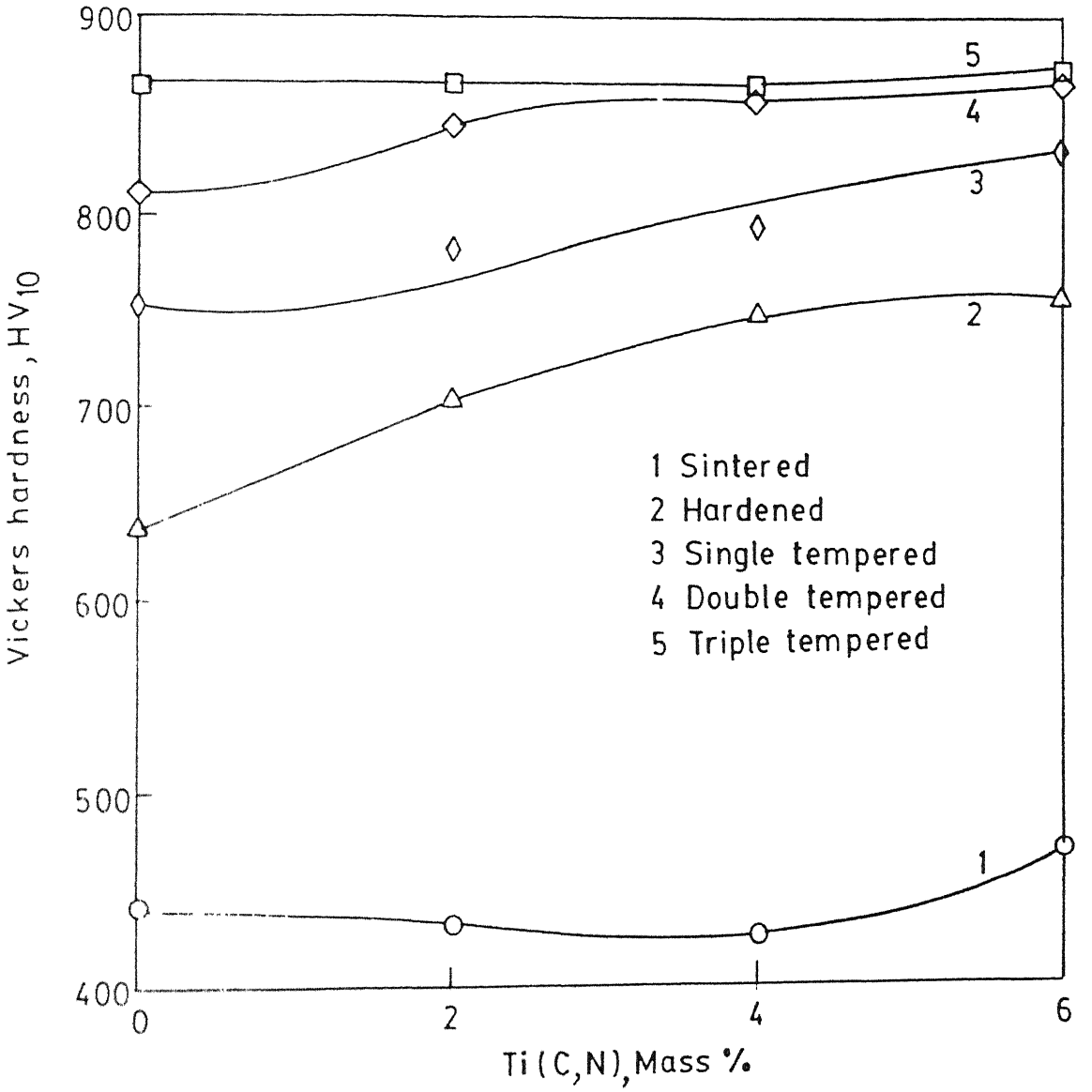

Fig 3 26 Effect of Ti(C,N) addition on Vickers hardness of T42 HSS after hydrogen sintering and various heat treatments

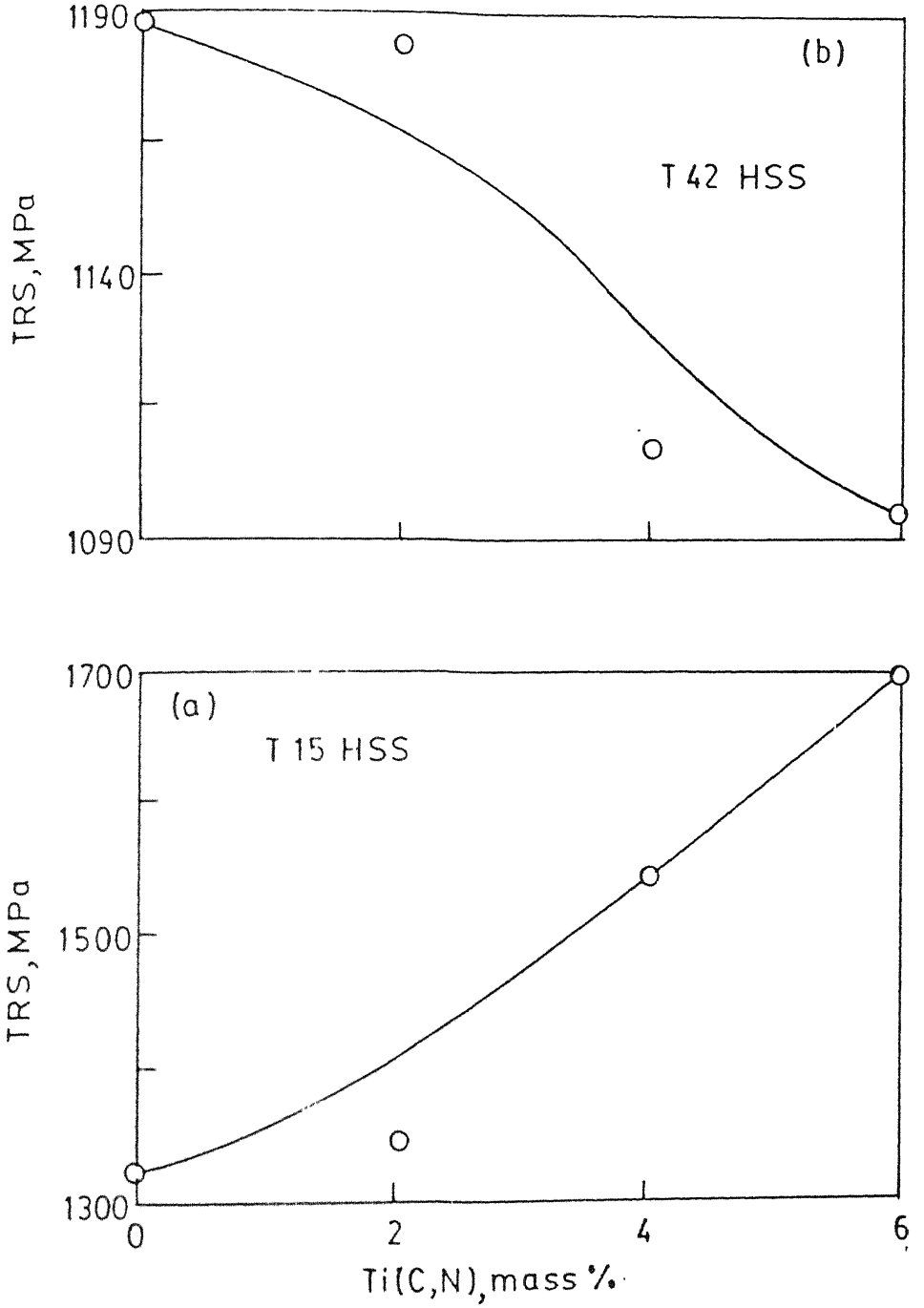

Fig. 3.27 Effect of Ti(C,N) addition on triple tempered TRS after hydrogen sintering (a) T15 HSS and its Ti(C,N) containing composites (b) T42 HSS and its Ti(C,N) containing composites

increase in Ti(C,N) content. Highest TRS value of 1698 MPa was noted for T15-6Ti(C,N) composite. In case of T42 HSS based composites [Figure 3.27b], TRS gradually decreased with the increase in Ti(C,N) content. The value for such composites were lower to those for T15 HSS based composites [Figure 3.27a].

III.3.4. Microstructural Analysis:

Figure 3.28 shows the SEM micrographs of hydrogen sintered straight T15 and T42 HSS and Figures 3.29 and 3.30 show the T15 and T42 HSS based composites containing 6 mass % Ti(C,N) in as sintered, hardened and tempered conditions respectively. The sintered microstructures show very few observable porosity, thus indicating achievement of full density. It consisted of primary carbides over and within the grains. The Ti(C,N) particles at some places got agglomerated particularly in case of composites containing 6 mass % Ti(C,N) [Figures 3.29 and 3.30]. Figures 3.28c and f, 3.29e and 3.30d show different phases present in T15 and T42 HSS as well as their 6 mass % Ti(C,N) containing composites. The phases are marked in the microstructures. From the Figure 3.28c and f and EDX analysis [Table III.3] it is clear that the microstructures of straight T15 and T42 HSS consist of MC and M_6C carbides embeded in the matrix. On the other hand Figures 3.29e and 3.30d and EDX analysis [Table III.3] show that microstructures of 6 mass % Ti(C,N) containing T15 and T42 HSS composites consist of three phases viz.

(a) Sintered

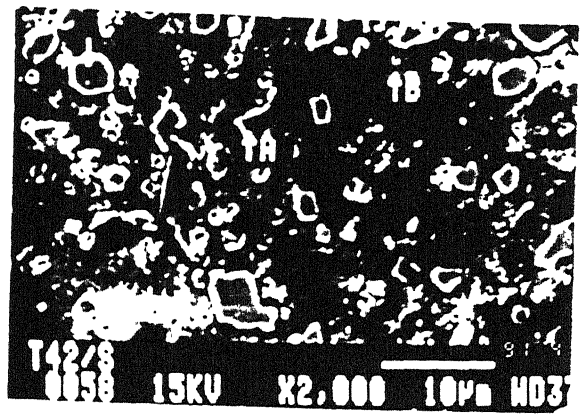

(d) Sintered

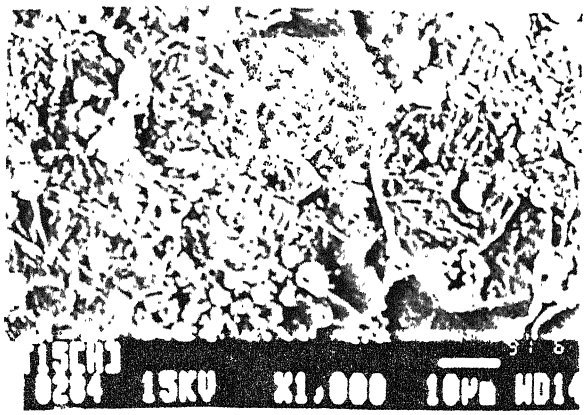

(b) Hardened

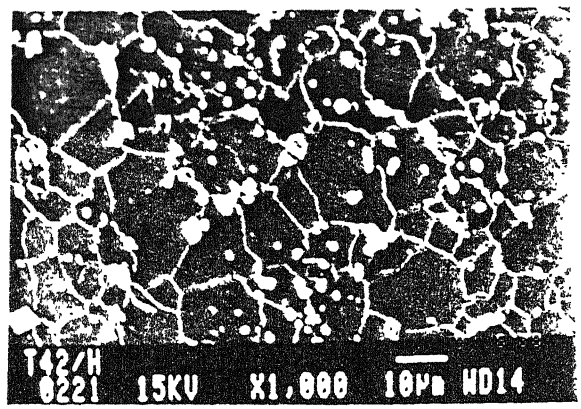

(e) Hardened

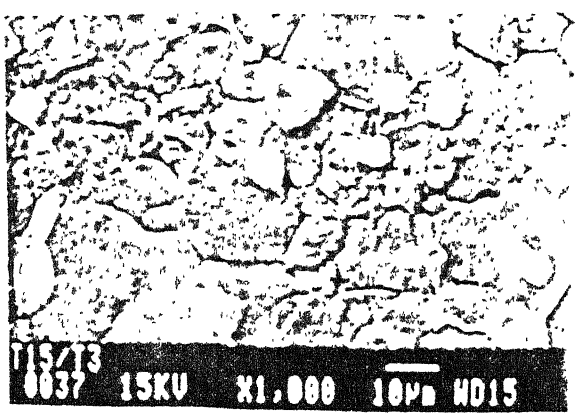

(c) Triple tempered

T15

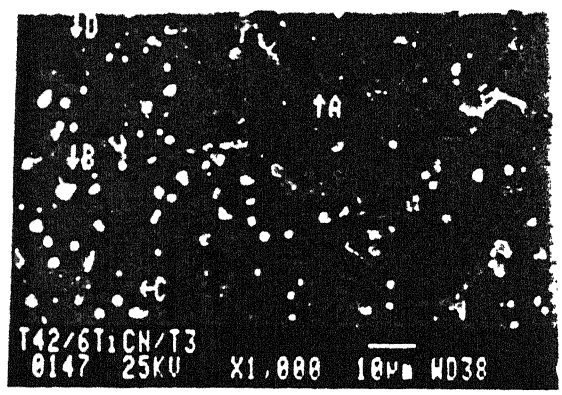

(f) Triple tempered

T42

Figure 3.28. SEM microstructures of T15 and T42 HSS in sintered and heat treated conditions.

(a) Sintered

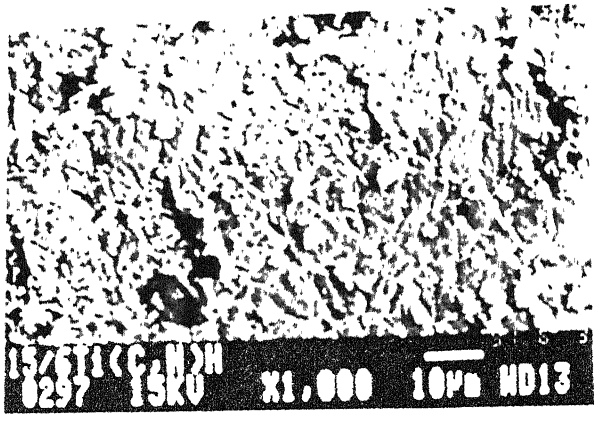

(b) Hardened

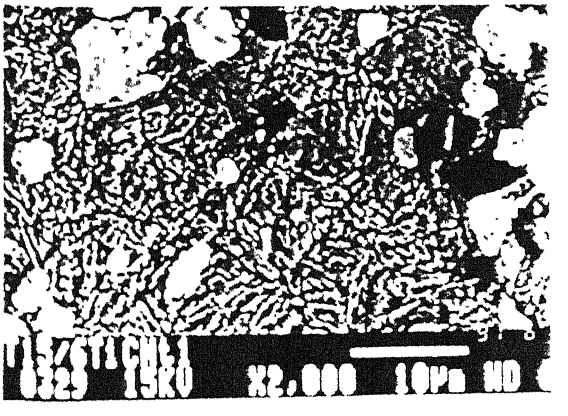

(c) Single tempered

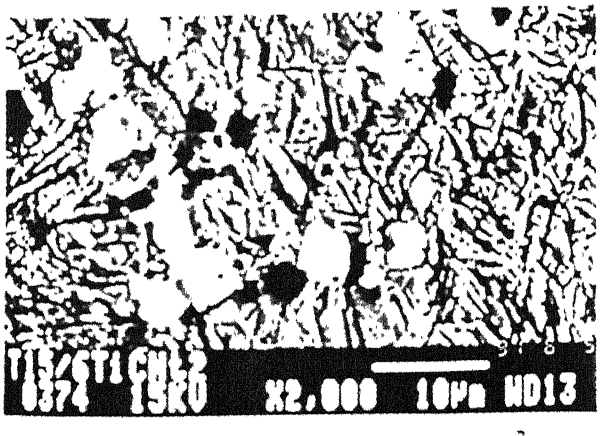

(d) Double tempered

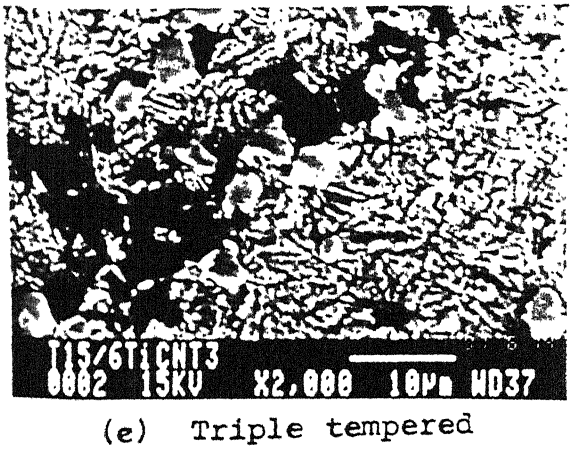

(e) Triple tempered

Figure 3.29. SEM microstructures T15-6 Ti(C,N) composite in sintered and heat treated conditions.

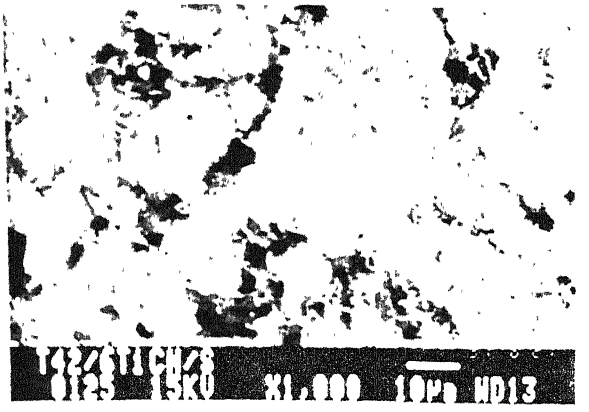

(a) Sintered

(b) Hardened

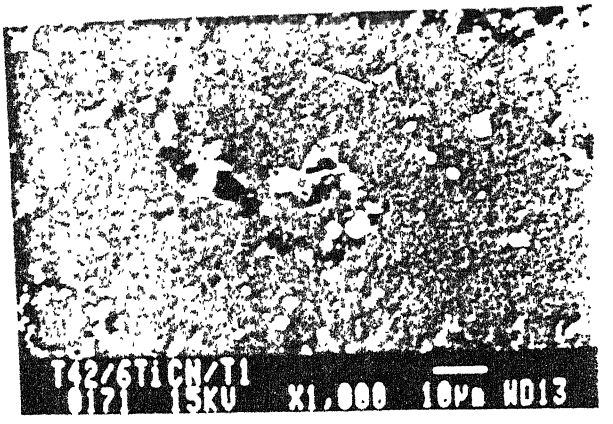

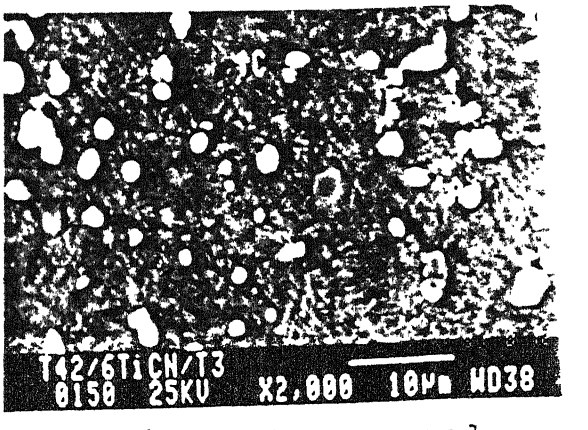

(c) Single tempered

(d) Triple tempered

Figure 3.30. SEM microstructures of T42-6 Ti(C,N) composite in sintered and heat treated conditions.

Table III.3. EDX analysis of various phases in T15 and T42 HSS and their 6 mass % Ti(C,N) containing composites.

HSS grade	Description of phase	Mass % chemical analysis							Assigned phase
		Fe	Cr	Co	Mo	V	W	Ti	
T15 (triple tempered)	Matrix (A)	82.36	5.10	8.80	0.03	1.12	2.58	-	Matrix
	Grey phase (B)	3.15	11.99	0.93	0.70	53.39	29.84	-	MC carbide
	White phase (C)	36.12	3.29	5.12	0.72	6.10	48.56	-	M_6C carbide
T15-6Ti(C,N) (triple tempered)	Matrix (C,D)	82.56	4.83	9.20	-	1.20	2.14	0.25	Matrix
	Grey phase (A)	31.32	8.83	3.37	1.07	27.00	24.09	4.32	MC carbide
	Black phase (B)	1.48	0.31	0.43	-	13.64	2.05	82.09	Ti(C,N) particle
T42 (triple tempered)	Matrix (C)	73.83	4.65	11.23	1.29	1.24	7.78	-	Matrix
	White phase (B)	29.05	4.05	5.61	7.02	3.00	51.27	-	M_6C carbide
	Grey phase (A)	4.42	9.12	2.36	0.91	55.06	28.13	-	MC carbide
T42-6Ti(C,N) (triple tempered)	Matrix (A,C)	60.18	1.76	11.54	2.06	7.21	17.23	0.02	Matrix
	White phase (B)	25.10	4.04	4.52	6.07	2.80	56.95	0.44	M_6C carbide
	Black phase (D)	17.70	1.77	3.17	0.43	1.13	7.95	67.85	Ti(C,N) particle

white (MC carbide), black (Ti(C,N) particle) and the matrix. On the basis of EDX analysis the stability of the Ti(C,N) particles could be gauged as matrix was practically free from titanium atoms.

Figure 3.31 show the X-ray mapping analysis of T15 based composite containing 6 mass % Ti(C,N) which show the distribution of elements in different phases in the structure and as well as confirm the stability of Ti(C,N) particles showing practically titanium free matrix.

Figure 3.32 shows the SEM fractographs taken on the fracture surfaces of the broken TRS test pieces of T15 and T42 HSS and their 6 mass % Ti(C,N) containing composites. The fracture in all the cases appeared to be quasi cleavage in nature showing the features of both ductile and brittle natures. The crack propagated in the same manner as were in the case of vacuum sintered T15 and T42 HSS explained in Chapter IV.2.2.

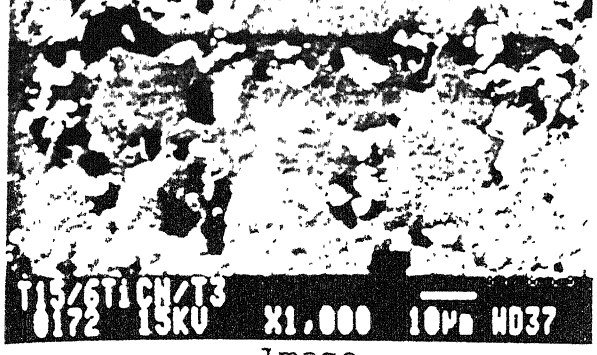

Image

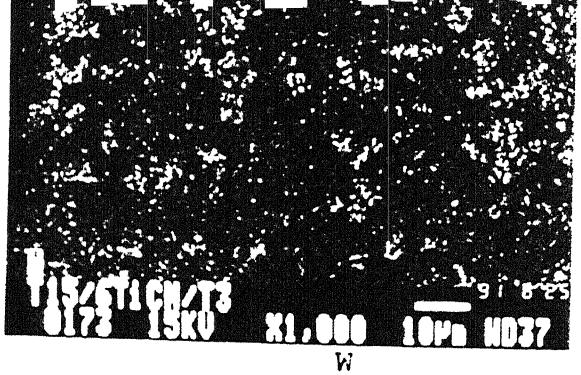

W

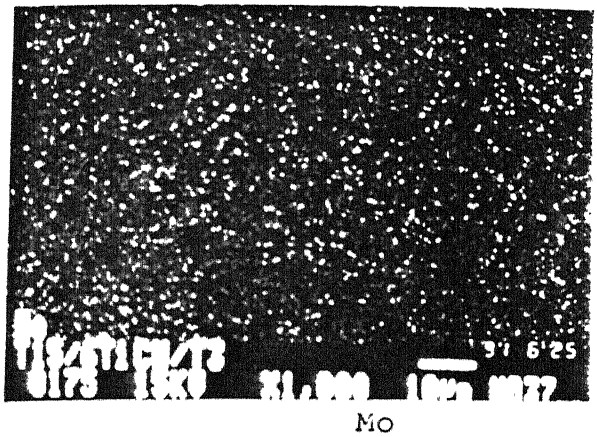

Mo

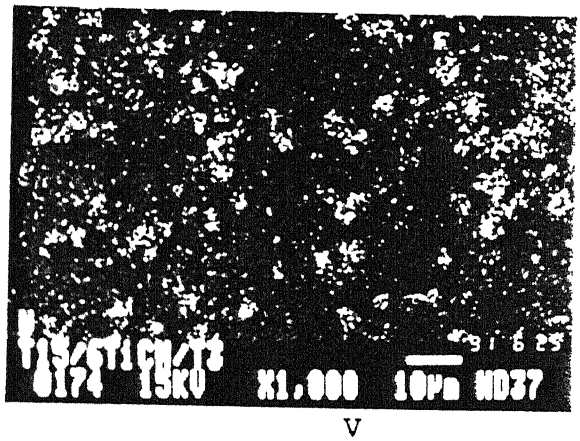

V

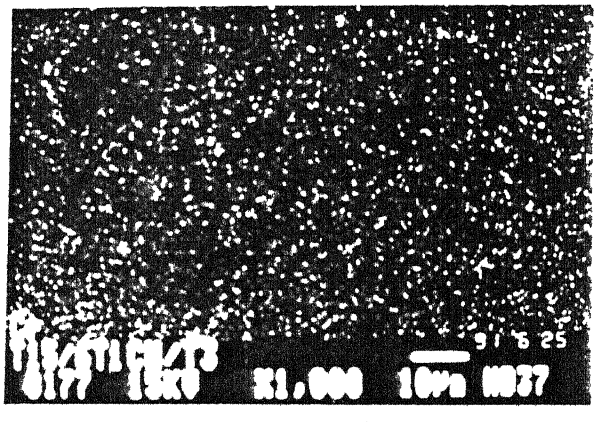

Cr

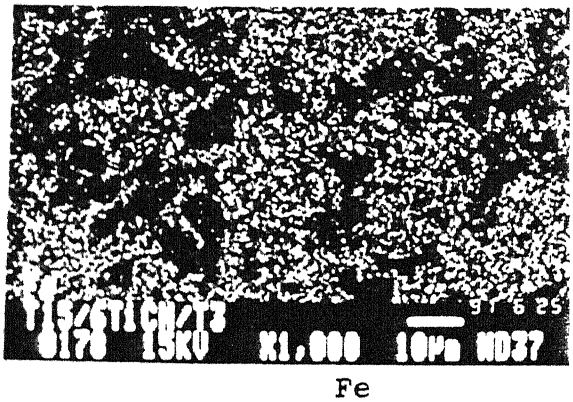

Fe

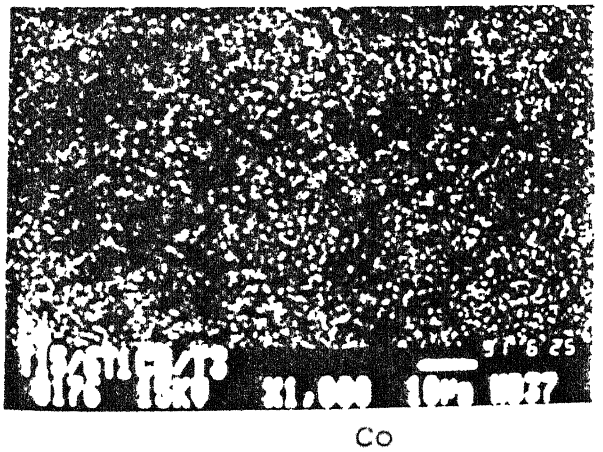

Co

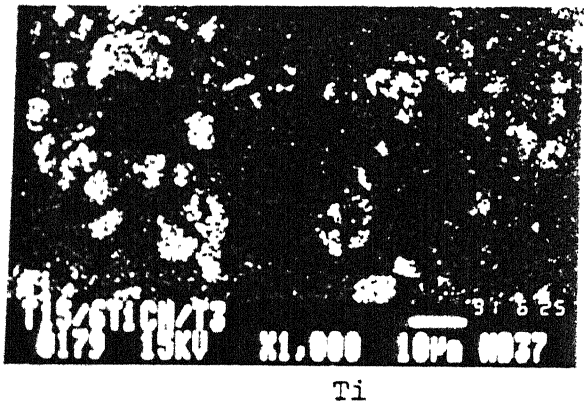

Ti

Figure 3.31. X-ray mapping analysis of hydrogen sintered a triple tempered T15-6Ti(C,N) composite.

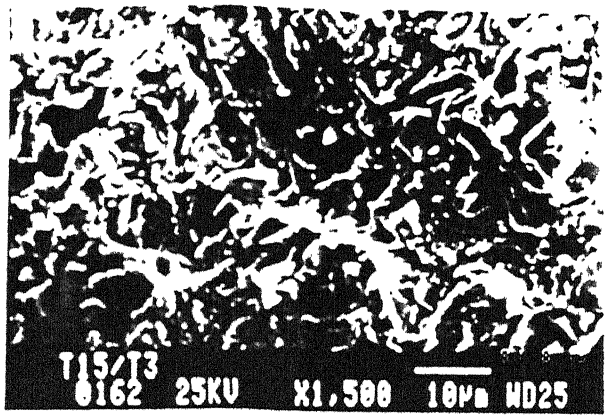

T15

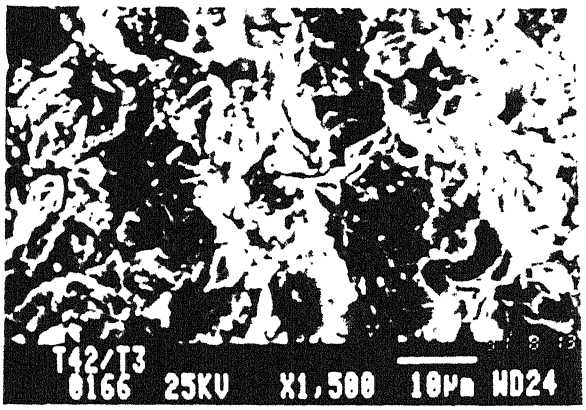

T42

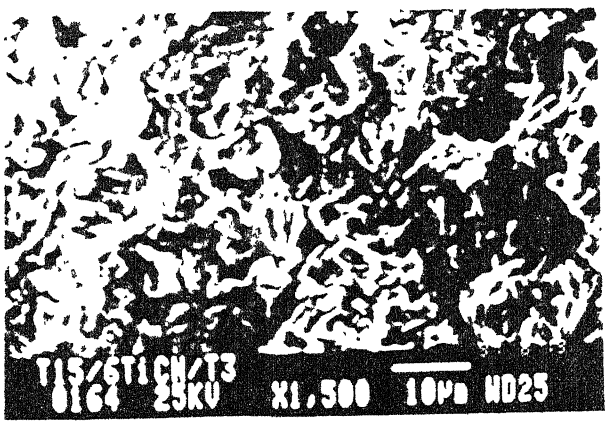

T15-6 Ti(C,N)

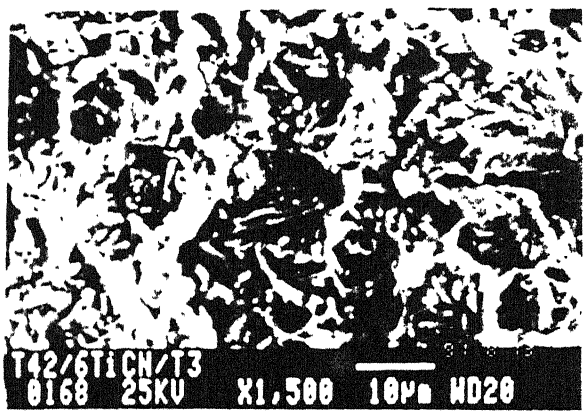

T42-6 Ti(C,N)

Figure 3.32. SEM fractographs of T15 and T42 HSS and their 6 mass % Ti(C,N) containing composites.

CHAPTER IV

DISCUSSION

IV.1. INTRODUCTION:

The conventionally produced high speed steels lie within the range of 2.6 to 2.9 atomic % carbon and 9.3-15 atomic % carbide formers [1]. The collective atomic percent of W and Mo (or tungsten equivalent) varies only slightly from specification to specification in HSS and these two elements perform similar functions and more or less interchange on an atomic basis. The P/M route enables to extend the range and variety of alloying element addition to a large extent. The major differences in various grades of high speed steel emerge due to changes in carbon, vanadium and cobalt present. The normal restrictions on composition of conventional I/M HSS is relaxed in the case of P/M grades. A much higher vanadium and cobalt content can be promoted in P/M high speed steels as the undesirable effects of these elements on the forging behaviour of ingot material are eliminated [1, 45]. Balance carbon, 'cb', as suggested by Steven [62] and balance carbon difference, ΔC [50], is an important indicator for any HSS as these indicate whether the carbon content is in stoichiometric value to accommodate all the carbide formers or not. cb and ΔC are calculated from the following formula:

Balance carbon, cb = 0.033 W + 0.063 Mo + 0.06 Cr + 0.2 V

Balance carbon difference, ΔC = Cb - Ca

where Ca = actual carbon in composition.

A positive ΔC value indicates that sufficient carbon is not present to satisfy all the carbide formers as well as martensitic transformation. A negative ΔC value would, on the other hand, ensure that the carbon requirement of all the carbide formers is satisfied and sufficient carbon is available for the martensitic transformation of the matrix. In such a case, the requisite hardness value is achieved on the sacrifice of the toughness value.

The carbide phase present in HSS depends vitally on the carbon content. If the amount of carbon is very low and the tungsten and/or molybdenum content is high, an intermetallic compound M_3R_2 (Fe_3Mo_2 or Fe_3W_2) [63] may form.

In many HSS increasing carbon content leads to progressive appearance of M_2C carbides at the expence of M_6C and MC carbides [64]. Raising the carbon level in HSS containing $M_{23}C_6$ may result in the formation of M_7C_3, at the cost of $M_{23}C_6$ [65]. As far as role of carbon on the solidus temperature is concerned, an increase in 1% added carbon in HSS, lowers the latter by a factor of 111°C [1]. This means that higher the carbon content, the closer the solidus temperature will approach the upper limit of the heat treatment range and greater the risk of incipient melting in hardening.

The main effect of vanadium addition in HSS is to produce very hard vanadium carbide (MC) which is important in promoting abrasion resistance. It is generally considered that each 1% vanadium addition requires an additional carbon of 0.25%.

Cobalt addition in HSS gives improved red hardness and enables higher cutting speeds to be used. Its overall effect can be summarised as follows [45, 54-60]:

(a) Cobalt does not form carbides, but remains in solution in the matrix. The resultant solution hardening is less affected by an increase in temperature.

(b) Cobalt slows down the $\alpha - \gamma$ transformation and increases the transformation temperature.

(c) It accelerates the decomposition of austenite and increases the critical cooling rate.

(d) Cobalt delays the precipitation of carbides from martensite during tempering and retards carbide coarsening, which contributes in high red hardness. Moreover, by slowing down the diffusion of carbide forming elements, it encourages the formation of a fine, well dispersed carbide precipitate wnich increases wear resistance.

(e) Cobalt slows down grain growth. Thus the solutionising temperature can be raised and also the content of elements dissolved in austenite thereby increased.

(f) Cobalt improves the thermal conductivity and this

entails the use of higher cutting speed as the heat generated at the tool-tip is conducted away more effectively.

In summary, the two grades of HSS viz. T15 and T42 studied in the present investigation have similar W-equivalents and differs as regards to the cobalt and vanadium content. T42 grade has higher cobalt content (10%) as compared to T15 grade (5%), whereas T15 has higher vanadium content (5%) as compared to T42 (3%). To match with vanadium contents, carbon content in T15 is comparatively higher (1.5%) as compared to that for T42 (1.3%).

IV.2. T15 AND T42 GRADE HSS:

IV.2.1. Densification:

The densification process in the present studies can be related only to the sintering temperature, and sintering atmosphere since all the green compacts contain a constant green porosity level of 24-26% for any given grade of HSS. The sintered density of T15 HSS in case of either vacuum or hydrogen sintering (Figures 3.1a and 3.21 respectively) increased with the increase in the sintering temperature till the optimum full density ($\geq$98% Th.) was achieved. It was observed that temperature required for full densification in case of vacuum sintering (1270^{o}C) was higher than hydrogen atmosphere sintering (1220^{o}C). Microstructure corresponding to optimum sintering temperature in both the

cases viz. vacuum or hydrogen sintering consisted of fine and uniformly distributed carbides and matrix grains [Figures 3.4a, b and 3.28]. The slight decrease in sintered density for vacuum sintered samples [Figure 3.1] beyond the optimum sintering temperature is attributed to the emergence of solidification pores [17]. On the other hand sintered density remained constant beyond the optimum temperature in case of hydrogen sintered sample [Figure 3.21].

T42 HSS also showed a densification behaviour similar to T15 HSS. However, the densification behaviour was better in case of T42 HSS as compared to T15 HSS. The optimum sintering temperature to achieve full density for T15 HSS was 1270°C as compared to 1230°C for T42 HSS for vacuum sintered samples and for hydrogen sintered samples it was 1220°C and 1200°C respectively. T15 even having higher carbon content than that of T42 HSS, required a relatively higher sintering temperature mainly because of its relatively high W, V and less Mo contents. It is well known that Mo reduces the solidus temperature of the steel more than W [1, 6]. The effect of vanadium in HSS is to shift the phase boundaries more towards the right i.e. equivalent to a decrease in the carbon content [1, 6, 49]. From the above fact, it can be concluded that the solidus temperature for T15 is higher than that for T42 HSS. Similar conclusion can be arrived from the 'balance carbon difference' [50] between the two grades as discussed in the previous section. From the balance carbon difference, ΔC, calculated from the

powder compositions given in Section II.1, it is seen that T15 has a balance carbon difference, ΔC equal to 0.061 as compared to ΔC of -0.091 for T42 grade HSS. This indicates that the matrix carbon content (assuming that all the carbide forming elements are tied up) is higher for T42 HSS as compared to the T15 HSS. Consequently, the solidus temperature of T42 HSS is lower than T15 HSS. This explains the higher optimum sintering temperature for T15 as compared to T42 HSS in order to produce a full density product.

As far the sintering atmosphere is concerned, hydrogen sintered HSS requires a lower sintering temperature to achieve full density than vacuum sintered HSS. It was noticed that in case of T15 HSS, a temperature difference of 50°C lies between vacuum and hydrogen sintering for achieving equivalent density. However in case of T42 HSS this difference was only 30°C. The lower temperature requirement for nearly full densification in case of hydrogen sintering can be attributed to the fact that it has a good thermal conductivity and during sintering each fresh oxide surface of metal immediately gets reduced by hydrogen gas [17].

IV.2.2. Heat Treatment, Mechanical Properties and Microstructural Aspects:

High speed steels are always used after a suitable heat treatment which include transformation annealing/stress relieving, austenitizing and hardening followed by multiple tempering. The heat treatment parameters dictate the end

property and are selected in consonance with the intended steel application.

From the present DTA test result (Figure 3.3) it can be seen that the AC_m temperature for T42 HSS is $10^{\circ}C$ higher as compared to that of T15 HSS. This may be attributed to the relatively higher cobalt content of T42 as compared to T15. In the annealed condition, the total cobalt content in the steel particularly remains in the ferrite and most carbide forming elements are tied up in the form of carbides which remain undissolved [5]. Cobalt is known to increase the $\alpha - \gamma$ transformation temperature [45] which results in higher AC_m temperature for T42 HSS. The selection of the transformation annealing hold temperature of $900^{\circ}C$ and $760^{\circ}C$ for both the grades of T15 and T42 HSS is thus justified in view of a rather little difference between the transformation temperatures.

The higher hardness values of T42 HSS after ~~sim~~temp-ering [Figures 3.2b and 3.2c] as compared to T15 HSS [Figures 3.1b and 3.2b]were due to high cobalt content in T42 HSS. Cobalt enhances the diffusivity of carbon by which greater precipitation of alloy carbides from the retained austenite occurs in cobalt containing HSS. As a result, the carbon content of the remaining austenite decreases thereby increasing the M_s temperature. It becomes possible for the remaining austenite to get transformed to martensite during cooling after subsequent tempering. Cobalt containing steels, thus have less amount of retained austenite as compared to

the non-cobalt bearing grades.

During tempering, cobalt in HSS promotes greater precipitation of W and Mo from martensite as finely dispersed secondary carbides. This enhances precipitation hardening and increases the secondary hardness [1, 45, 51, 52].

The higher triple tempered hardness of T42 HSS in comparison to that of T15 HSS is once again attributed to the higher cobalt content in the matrix. The combined effect of cobalt in strengthening the matrix and the dispersion strengthening due to the presence of very fine stable carbide precipitates which restrict the dislocation motion results in a relatively higher triple tempered hardness for T42 HSS. It is also known, that cobalt decrease the stability of retained austenite during tempering in addition to the solid solution strengthening of the matrix [45, 54-58]. It is obvious that the precipitated carbides in a concentrated solid solution hardened matrix would result in a stronger alloy as compared to similar precipitates in a lean solid solutions. Similarly, carbide precipitates in a fine grained matrix would impart further strengthening than that in coarse grained HSS with equivalent amount and type of precipitates. As is well known, cobalt increases the dislocation density and retards the recovery of the dislocation substructure, so that the number of nucleation sites for the subsequent precipitation of carbides are increased.

A relatively lower triple tempered TRS value of T42 HSS (for either vacuum or hydrogen sintering) as compared

to that of T15 HSS may be attributed to the relatively larger cobalt content of T42 HSS [45, 53, 59]. Cobalt induces very fine dislocation nucleated precipitates of alloy carbides both in retained austenite and martensite leading to retention of dislocation substructure as explained earlier. In addition to this, a high cobalt content strongly reduces the retained austenite values reducing the softer constituent content in the microstructure. Due to the above reasons, the TRS value of T42 HSS is relatively low.

The fracture surface of the triple tempered TRS test specimens, for either vacuum or hydrogen sintering [Figures 3.6 and 3.32], show a quasi-cleavage fracture which combines the features of both ductile and brittle natures. The origin of the main crack is not very clear from the fractographs. After the main crack has been initiated, the presence of divergent secondary cracks could be seen.

The triple tempered TRS and hardness values in case of vacuum sintered T15 and T42 HSS were found to be higher than those of hydrogen sintered specimens due to the fact that in case of hydrogen sintering, there were always some closed porosity associated with the compacts due to the entrapment of gases, which reduced the TRS and hardness values.

The microstructural studies reveal that as sintering temperature approached the optimum, there was a decrease in the pore size as well as in its volume fraction. At such a sintering temperature, the microstructures were well developed

[Figure 3.4a, b and 3.4d, e] with fine grain matrix, carbides and few isolated pores. Coarsening of the carbides as well as grains occurred when the sintering temperature was higher than the optimum. At the optimum sintering temperature MC and M_6C carbides were found to precipitate inside the grains as well as along the grain boundaries in both the cases of vacuum or hydrogen sintering. During transformation annealing, the austenite grains get refined in addition to stress relieving [61]. Such a control during annealing helps in the achievement of uniform microstructure after hardening and triple tempering. During austenitizing, dissolution of various carbides in the matrix is brought about. Its sequence [1, 5] is such that the chromium rich carbides ($M_{23}C_6$) dissolve first followed by tungsten-molybdenum rich double carbide (M_6C). The refractory vanadium rich carbide (MC) is the last to dissolve. Correspondingly, the primary carbide content after quenching is lowered. During triple tempering, these dissolved carbides reprecipitate and the total carbide content again increases in addition to some coarsening associated with the increase in the carbide growth kinetics.

The findings of SEM study [Figures 3.5 and 3.28] for T15 and T42 HSS (vacuum or hydrogen sintered) confirm the different phases present in the structure. In case of vacuum sintered samples, the type of the primary carbides can be distinguished from the phase contrast. M_6C carbide appears white as compared to the MC carbide which is greyish

in colour due to difference in their compositions. The EDX analysis results (Table III.1) also confirm this finding. The chromium rich carbides were of submicron size and could be resolved at a magnification above 5000X. In case of hydrogen sintered samples different types of carbide could only be distinguished by EDX analysis (Table III.3). Colour contrast of different carbides was not very prominant to be distinguished under the microscope. For further confirmation of different phases, X-ray mapping analysis was done for vacuum sintered samples to see the distribution of various elements in respective phases [Figures 3.7 and 3.8]. It was found that the cobalt concentration in the matrix was more in case of T42 HSS than T15 HSS. On the other hand vanadium concentration was more in T15 HSS than T42 HSS confirming the present investigation.

IV.3. HSS CONTAINING COMPOSITES:

IV.3.1. Densification:

In any metal-ceramic particulate composites similar and dissimilar powder surfaces are in contact with the consequence that the atomic and defects migrations along and across the dissimilar contacts are greatly modified. As the second phase ceramic particles are harder than the metal matrix, the densification of the composite would be reduced [67-73]. This effect is attributed to the constriction of the diffusion cross-section for the lattice or grain boundary

diffusion of matrix atoms [69], as well as the inhibition of dislocation motion by the dispersoids [68, 71, 72] provided the hard ceramic phase does not decompose or react with the matrix. It is worth noting that supersolidus sintering occurs at a fairly high temperature (>0.89 T_m) and for a considerable amount of time, in case of HSS and hence, the role of solid state sintering could not be ignored. As sintering progresses in such particulate composites, there would be all probability of diffusion barriers thus inhibiting the densification kinetics.

In the presently selected HSS composites enriched with TiB_2, major part of the densification during liquid phase sintering occurs by the rearrangement of the particles, where the amount of liquid phase at sintering temperature plays an important role. The liquid formation is associated with the melting of fine particles preferentially along the surfaces of the large powder particles and also along the grain boundary within the particles. The presence of TiB_2 particles in the composites, restrict the particle rearrangement and grain growth stage required for densification during sintering. Such a feature becomes more prominent with increased content of the refractory compounds in the composite. As a result of which full density could not be achieved for composites containing more than 2 mass % TiB_2 [Figures 3.9 and 3.10]. The increase in sintered porosity of the composites with increase in TiB_2 content can be attributed to rather poor wettability of TiB_2 particles with

the HSS melt during supersolidus sintering. Better densification behaviour in case of vacuum sintered composites is due to the fact that vacuum atmosphere exhibit better wettability than hydrogen [Figures 3.9, 3.10 and 3.12]. In the present study hydrogen sintered composites achieved an equivalent density at a temperature less than that of vacuum sintered ones, the cause of which was explained earlier.

As the cobalt content in T42 HSS is about two times than that of T15 HSS, hence better sinterability of T42-TiB_2 composites than that of T15-TiB_2 composites may be attributed to the fact that TiB_2 has better wettability for cobalt rich melt than that for iron rich melt [73, 74]. A detailed justification from the electronic structure viewpoint has been presented by Upadhyaya [75].

IV.3.1. Mechanical Properties and Microstructural Aspects:

In the present investigation the better hardness values in as sintered and tempered condition of T15 and T42 HSS as compared to their TiB_2 containing composites can be attributed to the better densification behaviour of the formers [Figures 3.1, 3.2, 3.14 and 3.15]. For equivalent density samples, vacuum sintered ones show better hardness values than hydrogen sintered ones due to the absence of closed porosity, which is a common feature encountered in hydrogen sintering [Figures 3.15b and 3.14]. It has been reported by Peterson [76] that a eutectic reaction takes

place between iron and boron at 1160°C and also there is a decomposition of TiB_2 at elevated temperature so as to form a series of complex borides with iron [77]. Consequently there is a decrease in hardness value for the T15 and T42 composites containing TiB_2.

From the qualitative microstructural analysis it is clear that coarse titanium based phase obtained after decomposition of TiB_2 in the composites during sintering results in a loss in the hardness [Figure 3.18]. The MC type primary carbide (VC) appears to get alloyed with decomposed titanium from the TiB_2. This was confirmed by the presence of vanadium in titanium rich phase as seen from EDX and X-ray mapping analysis [Table III.2; Figures 3.19 and 3.20]. The fine secondary MC carbide obtained after tempering could not be resolved under the microscope.

IV.4. Ti(C,N) CONTAINING COMPOSITES:

IV.4.1. Densification:

The presence of Ti(C,N) particles in the composites, restricts the particle rearrangement and grain growth stage required for densification during sintering. Such a feature becomes more prominent with increased content of the Ti(C,N) particle in the composite. It, therefore, becomes necessary to employ higher and higher sintering temperature in order to make the melt less viscous and also to increase the liquid phase amount effectively. The densification behaviour with respect to sintering temperature observed for

Ti(C,N) containing composites studied presently supports the above conclusions [Figures 3.21 and 3.23]. The optimum sintering temperature for achieving full density (≥98% Theoretical) increases for the Ti(C,N) rich composites [Figures 3.22b and 3.24b], the exception being T15-4Ti(C,N) composite which densified at a temperature much lower than that required by other T15 composites. The wettability behaviour of Ti(C,N) with Fe or Co follows the same trend as that of TiC with Fe or Co. From the work of Kar and Upadhyaya [79] it was found that T42-TiC composites show better sinterability than T15-TiC composites. Present investigation also confirms the similar trend.

IV.4.7. Mechanical Properties and Microstructural Aspects:

The strengthening mechanism in metal-matrix particulate composites are complex. Various related mechanisms in strengthening are (1) coherency strain, (ii) strengthening where dislocation movements are easily blocked by the dispersoid particles(Orowan mechanism) and other modified models [78], (iii) indirect strengthening, where dispersed particles stabilize the grain size and the dislocation substructure and (iv) direct strengthening by load sharing ability by strong ceramic particles. Apart from this, interfacial energy, stored energy, particles morphology are also responsible in contributing to strength. It is also true that all the mechanisms do not necessarily operate for all particulate composites. In the present investigation,

exclusive role of the Orowan strengthening mechanism is ruled out owing to the coarser size of the dispersoids and moreover apart from the tendency to agglomerate, their distribution may not be perfectly uniform in the powder premixes. However, such a role does exist during secondary precipitated hardening, where the carbide particles are small in size. It is expected that Ti(C,N) addition if properly bonded with the HSS matrix would more or less behave similarly to the primary MC carbides. With the increase in the refractory compound content in the HSS matrix, the need for higher sintering temperatures for full density is justifiable.

From the present investigation, it can be seen that hardness of sintered composites does not vary significantly with Ti(C,N) content, however, after heat treatment this is not so [Figures 3.25 and 3.26]. Results of Kar and Upadhyaya [78] establish that the sintered hardness of TiC containing composites increases with dispersoids content in T15 HSS, whereas the reverse is true in TiN containing composites. The present results of negligible variation of sintered hardness is therefore logical. Hardness was found to increase after hardening for T15 and its Ti(C,N) containing composites due to the formation of martensite. It was found that after the single tempering there was not much increase in hardness or 2 mass % Ti(C,N) containing composite . However in case of T15 straight HSS and its composites containing more than 2 mass % Ti(C,N) show a

considerable amount of increase in hardness after single tempering. In case of 2 mass % Ti(C,N) containing T15 HSS, martensite could not be tempered in the subsequent tempering operation. For other composites containing more than 2 mass % Ti(C,N) hardness was not found to increase after further tempering, probably due to the fact that secondary carbides were absent.

In case of T42 HSS and its Ti(C,N) containing composites hardness was found to increase with the number of temperings and in general all T42 HSS and its Ti(C,N) containing composites show better hardness compared to T15 HSS and its Ti(C,N) containing composites. This may be due to the fact that T42 HSS contains higher amount of Co (10%) as compared to T15 (5%) which strengthens the matrix and causes dispersion strengthening due to the presence of very fine stable carbides by the same mechanism as discussed in Section IV.1.1. Moreover carbide and grain coarsening were found to occur in case of T15 and its Ti(C,N) containing composites as compared to T42 HSS and its Ti(C,N) containing composites. In addition it is worthwhile to mention that the optimum sintering temperature for T15 HSS (1220^{o}C) was higher than that for T42 HSS (1200^{o}C), which also attributes in some degree of grain coarsening of the former.

The results by Kar and Upadhyaya [47, 48] on T15 or T42 HSS based composites cannot be compared directly with the present results, as their sinterings were carried out in vacuum. However, the present results show that the

qualitative trend of the role of Ti(C,N) on T15 is similar to the results of T15-TiC composites [79] such that the TRS value increases with increase in the dispersoid content till 6 mass %. On the other hand results of T42-Ti(C,N) composites show that the TRS decreases uniformly with the increase in the Ti(C,N) content (1182 to 1095 MPa), which is in contrast with the results of Kar [48] where TiC or TiN dispersoids revealed a maximum TRS in 2 to 4 mass % dispersoid containing composites.

CHAPTER V

CONCLUSIONS

Based on the detailed studies on the sintering behaviour of the T15 and T42 HSS based composites and their properties, the following conclusions can be made:

1. The respective temperatures required to achieve full density for vacuum sintered T15 (1270°C) and T42 (1230°C) HSS were higher than hydrogen sintered T15 (1220°C) and T42 (1200°C) HSS. This may be attributed to the better thermal conductivity of hydrogen than vacuum. Moreover in hydrogen sintering each oxide surface of metal got reduced, which increased the sinterability.

2. The maximum hardness for hydrogen and vacuum sintered HSS was obtained after triple tempering. Triple tempered hardness values of vacuum sintered T15 and T42 HSS were higher as compared to hydrogen sintered ones. Vacuum sintered T42 HSS showed the highest value.

3. The optimum sintering temperature (for achieving maximum density) increased with increase in TiB_2 content in the composites based on T15 and T42 HSS. Due to the poor wettability of TiB_2 with Fe, except 2 mass % TiB_2 containing composite no other composite could achieve full density ($\geq$98% of theoretical).

4. Relatively poor hardness values of TiB_2 containing composites of either T15 or T42 HSS as compared to their respective straight grades were due to the fact that TiB_2 decomposed at sintering temperature and formed a series of complex borides with iron.

5. TiB_2 containing composites based on either T15 or T42 HSS showed the presence of M_6C carbide, a titanium based dark phase and matrix in the microstructure.

6. The optimum sintering temperature (for achieving full density) increased with increase in Ti(C,N) content in the HSS composites.

7. T15-6 Ti(C,N) composite gave the best combination of mechanical properties like hardness and TRS.

8. M_6C carbide, Ti(C,N) particle and matrix were observed in the microstructures of T15-Ti(C,N) composites, whereas T42-Ti(C,N) composites contained M_6C carbide, Ti(C,N) particle and matrix.

REFERENCES

1. G. Boyle, "High Speed Steels", Butterworths, London, 1988.

2. W.E. Henderer and B.F. von Turkovich, "New Developments in the Processing and Properties of HSS Tool Steels", Ed. M.G.H. Wells and L.W. Lherbier, The Metals Soc. of AIME, New York, 1980, p. 13.

3. "Metals Handbook", Vol. 6, 9th Ed., ASM, Metals Park, Ohio, 1988, pp. 51-59.

4. "Metals Handbook", Vol. 7, 9th Ed., ASM, Metals Park, Ohio, 1989, pp. 784-786.

5. P. Payson, "The Metallurgy of Tool Steels", John Wiley and Sons, New York, 1962.

6. J.F. Gill, "Tool Steels", ASM, Metals Park, Ohio, 1944, pp. 494-529.

7. F.A. Kirk, Metals Technology, May 1977, pp. 233-239.

8. T. Malkiewicz et al., Journal Iron Steel Inst., Vol. 193, 1959, p. 25.

9. G.A. Roberts and R.A. Cary, "Tool Steels", 4th Ed., ASM, Metals Park, Ohio, 1980, pp. 647-664.

10. T. Mukherjee, "Materials for Metal Cutting", Proceedings of the Conference jointly sponsored by BISRA, Corporate Laboratories of BSC and ISI, held on 14-16 April, 1971, London, 1970, pp. 80-96.

11. P.K. Kar and G.S. Upadhyaya, Powder Metallurgy International, Vol. 22, No. 1, 1990, pp. 23-26.

12. K. Richter, P.E.H. Mayer, G. Jangg and G. Weissmann, "Modern Developments in Powder Metallurgy", Vol. 8, Ed. H. Hausner and W.E. Smith, Metal Powder Industries Federation (MPIF), Princeton, 1974, pp. 1-18.

13. K.J. Carston and J.J. Dunkley, Proceedings of Vth International Conference on Powder Metallurgy, Vol. 1, Czechoslovak Socialist Republic, 1978.

14. M. Santos, I.M. Martins, M.M. Oliveira and H. Carvalhinhos, Paper presented at the conference "Tribology Trends in the 90's", Organised by Instituto Superior Tecnico, May 1988, Lisbon, Portugal.

15. C.S. Wright, J.D. Bolton, M.M. Rebbeck and A.S. Wronski, "Proceedings First International High Speed Steel Conference", Ed. G. Hackl and B. Hribernik, Montanuniversitat, Leoben, 1990, pp. 93-98.

16. W.B. Kent, "Processing and Properties of High Speed Tool Steels", Ed. M.G.H. Wells and L.W. Lherbier, The Metallurgical Society of AIME, New York, 1980, pp. 159-166.

17. R.M. German, International Journal of Powder Metallurgy, Vol. 26, No. 1, 1990, pp. 23-34.

18. L. Gamba and J.A. Lund, International Journal of Powder Metallurgy, Vol. 8, No. 3, 1972, pp. 131-140.

19. S. Takajo and K. Kitta, In "Sintering-85", Ed. G.C. Kuczynski, D.F. Uskokovic, H. Palmer and M.M. Ristic, Plenum Press, New York, 1987, pp. 189-195.

20. K.M. Kulkarni, In "Sintering of Multi Phase Metal and Ceramic Systems", Ed. G.S. Upadhyaya, Sc. Tech. Publications, Vaduz, 1990, pp. 223-234.

21. K.M. Kulkarni, "Modern Developments in Powder Metallurgy", Vol. 19, Ed. P.U. Gummeson and D.A. Gustafson, MPIF, Princeton, 1988, pp. 329-344.

22. G. Grimes, L. Berglin and M. Sporrong, Paper presented at the 1984 Powder Metallurgy Conference, June 17-22, Toronto, MPIF, Princeton, 1984.

23. K.H. Prima, U. Martinez and J.J. Urcola, Powder Metallurgy, Vol. 32, No. 4, 1989, pp. 291-299.

24. I.H. Moon, S.D. Oh and I.S. Ahn, "Modern Developments in Powder Metallurgy", Vol. 17, Ed. E.N. Aqua and C.I. Whitman, MPIF, Princeton, 1985, pp. 441-450.

25. C. Smart, I.H. Reed and P.R. Brewin, Paper presented at the 1979 Powder Metallurgy group meeting, Inst. of Metals, London, 22-24 Oct., 1979.

26. R. Wahling, I. Reiss and W.J. Huppmann, Powder Metallurgy, Vol. 29, No. 1, 1986, pp. 53-56.

27. A.H. Klein, R. Oberacker and F. Thurmmler, Metal Powder Report, Vol. 39, 1984, p. 335.

28. K.M. Kulkarni, A. Ashurst and M. Svilar, "Modern Developments in Powder Metallurgy", Vol. 12-14, Ed. H.H. Hausner, H.W. Antes and G.D. Smith, MPIF, Princeton, 1981, pp. 93-100.

29. W.J.C. Price, M.M. Rebbeck, A.S. Wronski and S.A. Amen, Powder Metallurgy, Vol. 28, No. 1, 1985, pp. 1-6.

30. "Metals Handbook", Vol. 7, 9th Ed., ASM, Metals Park, Ohio, pp. 370-379.

31. J.D. Bolton, In Proceedings "Colloquium: Controlling the Properties of Powder Metallurgy Parts through Their Microstructure", Paris, 19-21 March, 1990, Organised by Societe Francaise De Metallurgie, Paris, Paper No. 15.

32. F. Thummler, R. Oberacker and R. Klausmann, "Modern Developments in Powder Metallurgy", Vol. 30, Ed. P.U. Gummeson and D.A. Gustafson, MPIF, Princeton, 1988, pp. 431-441.

33. P. Beiss, R. Wahling and D. Duda, "Modern Developments in Powder Metallurgy", Vol. 17, Ed. E.N. Aqua and C.I. Whitmann, MPIF, Princeton, 1985, pp. 331-357.

34. I. Hellmann and H. Wisell, Paper presented in SEMPS, P/M-78, June 1978, Vol. 1, Stockholm.

35. H. Brandis, E. Haberling and H.H. Weigand, "Processing and Properties of High Speed Tool Steels", Ed. M.G.H. Wells and L.W. Lherbier, The Metallurgical Society of AIME, New York, 1980, pp. 1-18.

36. G.A. Roberts and R.A. Cary, "Tool Steels", 4th Ed., ASM, Ohio, 1980, pp. 691-699.

37. R.A. Lueeney, R.E. Masters, R.J. Beltz and J.D. Lankoff, "Modern Developments in Powder Metallurgy", Vol. 20, Ed. P.U. Gummeson and D.A. Gustafson, MPIF, Princeton, 1988, pp. 409-420.

38. T. Arai and N. Komatsu, Tetsu-to-Hagane, Vol. 61, No. 2, 1975, pp. 241-250 (H.B. Translation No. 9406).

39. F.G. Wilson and P.W. Jackson, Powder Metallurgy, Vol. 16, No. 12, 1973, pp. 257-276.

40. G.G. Kiparisov, G.A. Meerson, V.S. Panov, M.M. Smirnova and A.F. Fokina, Soviet P/M and Metal Ceramics, Jan. 1977, pp. 31-36.

41. I.M. Martins, M.M. Oliveira and H. Carvalhinhos, In Proceedings "Colloquium: Controlling the Properties of Powder Metallurgy Parts through Their Microstructures", Paris, 19-21 March, 1990, Organised by Societie Francaise De Metallurgie, Paris, Paper No. 15.

42. K. Laenhoter, J.W. Bouwman and F. Bless, in "Proceedings First International High Speed Steel Conference", Ed. G. Hackl and B. Hribernik, Montanuniversitat. Leoben.

43. H. Altena, ibid, pp. 212-223.

44. Private communications, British India Steels, Ahmedabad, India.

45. Yu. Geller, "Tool Steels", MIR Publishers, Moscow, 1978, pp. 440-455.

46. J. Arthur, J. Inst. of Metals, 84 (1956), pp. 327.

47. "Liquid Phase Sintering and Heat Treatment of T15 Grade PM High Speed Steel", Metal Powder Report, Vol. 45, No. 12, 1990, pp. 841-843 and Trans. PMAI, Vol. 17, 1990, pp. 25-32.

48. Ph.D. Thesis of Kar, Department of Metallurgical Engg., I.I.T. Kanpur, 1990.

49. J.O. Lord, "Alloy Systems - An Introductory Text", Pitman, New York, 1949, pp. 253.

50. S. Ni and S. Wang, In "Proceedings of the Ist International HSS Conference", Ed. G. Hackl and B. Hribernick, Montanuniversitat, Leoben, 1990, pp. 438-446.

51. R.S. Irani, C.S. Wright and A.S. Wronski, J. Mat. Sc. Letters, Vol. 1, 1982, pp. 318-320.

52. C.S. Wright and R.S. Irani, J. Mat. Science, Vol. 19, 1984, pp. 3389-3398.

53. P. Leckie-Ewing, Iron Age, Dec. 1950, pp. 115-118.

54. V.K. Chandhok, J.P. Hirth and E.J. Dulis, Trans. ASM, Vol. 56, 1963, pp. 677-692.

55. V.K. Chandhok, J.P. Hirth and E.J. Dulis, Trans. AIME, Vol. 224, 1962, pp. 858-864

56. M. Ubrain, Cobalt, No. 12, 1961, pp. 1-14.

57. L. Habraken and D. Coutsouradis, Cobalt, No. 12, 1965, pp. 1-15.

58. A. Magnee, J.M. Drapier, J. Dumont, D. Coutsouradis and L. Habraken, "Cobalt Containing High Strength Steels", Centre D'Information Ducobalt, Brussels, 1974.

59. J.H. Woodhead and A.G. Quarrell, "The Role of Carbides in Low Alloy and Creep Resisting Steels", Published by Climax Molybdenum Company Ltd., London.

60. R.W.K. Honeycombe, "Metallurgical Developments in High Alloy Steels", ISI Special Report No. 86, ISI, London 1964.

61. A. Basu, B.K. Ghosh, S. Jana and S.C. Dasgupta, Metals Technology, Vol. 7, No. 4, 1980, pp. 151-158.

62. G. Steven et.al., Trans. ASM, Vol. 57, 1964, pp. 925-948.

63. D.J. Blickwede et.al., Trans. ASM, 1950, 42, 1162.

64. G. Steven et.al., Trans. ASM, 1969, 62, 180.

65. G. Steven et.al., ASM, 1964, 57, 925.

66. T.K. Jones and T. Mukherjee, JISI, 1970, 208, 90-92.

67. M.H. Tikkanen, B.O. Rossel and O. Wiberg, Powder Met., Vol. 10, 1962, pp. 49.

68. M.H. Tikkanen, Physics of Sintering, Vol. 1, J. 1, 1969.

69. B.N. Singh and D.H. Houseman, Powder Met. Int., Vol. 3, 1971, pp. 1.

70. F.V. Lanel, G.S. Ansell and D.P. Borron, Met. Trans., Vol. 1, 1970, pp. 1772.

71. F.V. Lanel, Physics of Sintering, Vol. 4, 1972, pp. 1.

72. J. Berly, F.V. Lanel and G.S. Ansell, Trans. Met. Soc., AIME, Vol. 230, 1964, pp. 1641.

73. G.V. Samsonov, A.D. Panasyk and H.S. Borivikova, In "Wettability and Surface Properties of Metals and Solid Bodies" (in Russian), Neukova Dumka, Kiev, 1972, p. 99.

74. V.I. Dumonov, A.E. Goybunov and G.M. Kondretenko, ibid, p. 102.

75. G.S. Upadhyaya, In "Sintered Metal Ceramic Composites", Ed. G.S. Upadhyaya, Elsevier, Amsterdam, 1984, p. 41.

76. B. Yu Turiditskii, V.A. Pesin and S.S. Ordan'yan, Change in fine structure of the titanium diboride occurring during sintering of a TiB_2-Fe(Mo) cermet, Sov. Powder Metal. Met. Ceram., 21 (1982), pp. 280-282.

77. I.I. Iskoldskii and L.P. Bogorodskaya, Zhurnal Prikl Khimii, Vol. 30, 1957, pp. 177-185.

78. G.S. Ansell, In "Oxide Dispersion Strengthening", Ed. G.S. Ansell et.al., Gordon and Breach Sc. Pub. Inc., New York, 1968, p. 61.

79. P.K. Kar and G.S. Upadhyaya, In "Novel liquid phase sintered high speed steels", In "Proceedings of First International High Speed Steel Conference", Ed. H. Hackl and B. Hribernick, Montan-universitat, Leoben, Austria, 1990, pp. 477-485.

80. S.S. Kiparisov and G.A. Libenson, Powder Metallurgy (in Russian), Metallurgiya, Moscow (1972).

81. N. Uchida and H. Nakamura, Proceedings of 12th Int. Plansee Seminar, May 1989, Reutte, Austria, Vol. 2, Metallwerk Plansee, Reutte, 1989, p. 541.

82. C.S. Wright, A.S. Wronski and M.M. Rebbock, Metals Technology, Vol. 11, May 1984, pp. 181-188.

83. I. Kvasnicka, Powder Metallurgy, Vol. 26, No. 3, 1983, pp. 145-148.